Scientific Papers of
the Institute of Electrical Power Engineering of
the Wrocław University of Technology

PRESENT PROBLEMS OF POWER SYSTEM CONTROL

3

Wrocław 2013

Printed in the camera ready form

Institute of Electrical Power Engineering
Wrocław University of Technology
Wybrzeże Wyspiańskiego 27, 50-370 Wrocław, Poland
phone: +48 71 320 26 55, fax: +48 71 320 26 56
www: http://www.ie.pwr.wroc.pl/; e-mail: Inst.Energ@pwr.wroc.pl

OFICYNA WYDAWNICZA POLITECHNIKI WROCŁAWSKIEJ
Wybrzeże Wyspiańskiego 27, 50-370 Wrocław
http://www.oficyna.pwr.wroc.pl
e-mail: oficwyd@pwr.wroc.pl
zamawianie.ksiazek@pwr.wroc.pl

ISSN 2084-2201

Drukarnia Oficyny Wydawniczej Politechniki Wrocławskiej. Order No. 295/2013.

CONTENTS

protective relaying,
differential protection,
Alpha Plane principle

Bogdan KASZTENNY*, Gabriel BENMOUYAL*,
Héctor J. ALTUVE*, Normann FISCHER*

TUTORIAL ON OPERATING CHARACTERISTICS OF MICROPROCESSOR-BASED MULTITERMINAL LINE CURRENT DIFFERENTIAL RELAYS

Line current differential (87L) protection schemes face extra challenges compared with other forms of differential protection, in addition to the traditional requirements of sensitivity, speed, and immunity to current transformer saturation. Some of these challenges include data communication, alignment, and security; line charging current; and limited communications bandwidth.

To address these challenges, microprocessor-based 87L relays apply elaborate operating characteristics, which are often different than a traditional percentage differential characteristic used for bus or transformer protection. These sophisticated elements may include adaptive restraining terms, apply an Alpha Plane, use external fault detection logic for extra security, and so on.

While these operating characteristics provide for better performance, they create the following challenges for users:

- Understanding how the 87L elements make the trip decision.
- Understanding the impact of 87L settings on sensitivity and security, as well as grasping the relationship between the traditional percentage differential characteristic and the various 87L operating characteristics.
- Having the ability to transfer settings between different 87L operating characteristics while keeping a similar balance between security and dependability.
- Testing the 87L operating characteristics.

These issues become particularly significant in applications involving more than two currents in the line protection zone (multiterminal lines) and lines terminated on dual-breaker buses.

This paper is a tutorial on this relatively new protection topic and offers answers to the outlined challenges.

* Schweitzer Engineering Laboratories, Inc.

1. INTRODUCTION

The current differential principle is the most powerful short-circuit protection method. Responding to all currents bounding the zone of protection, the principle has a very high potential for both sensitivity (effectively, it sees the fault current at the place of an internal fault) and security (effectively, it sees an external fault current flowing in and out of the protection zone). Also, differential protection is typically easy to apply because it does not require elaborate short-circuit studies and settings calculations.

In its application to power lines, the principle is little or not affected by weak terminals, series compensation, changing short-circuit levels, current inversion, power swings, nonstandard short-circuit current sources, and many other issues relevant for protection techniques based on measurements from a single line terminal [1].

Differential protection applied to buses, transformers, generators, or motors is well-researched and belongs to a mature field of protective relaying. In contrast, microprocessor-based 87L schemes began to be commonly applied less than 15 years ago and belong to a relatively new field with only the second generation of relays available in the market.

Each type of differential protection faces its own unique challenges. Transformer differential protection must deal with fictitious differential signals caused by magnetizing inrush conditions while striving for fast operation and sensitivity to turn-to-turn faults, for example. Line current differential protection is no exception. Its challenges include the requirement of high sensitivity, current alignment issues, security under current transformer (CT) saturation, line charging current, limited bandwidth channels, channel impairments, and failure modes, to mention the key challenges.

Present 87L elements are sophisticated and adaptive in order to maintain the simplicity of application inherent in the differential principle itself, while addressing challenges related to applications to power lines.

This paper is a tutorial on the operating characteristics of 87L elements. We focus on practical implementations actually available in present 87L relays.

We start with an overview of challenges inherent in 87L applications and then review the two main implementations in great detail – the percentage differential and the Alpha Plane differential elements. We highlight their similarities and differences as well as relative strengths. Other operating principles exist, but they are either theoretical or not commonly used and are not covered in this paper.

We follow with a description of a generalized Alpha Plane principle that merges the two-restraint Alpha Plane and multiterminal percentage differential approaches, allowing us to benefit from the relative strengths of each.

Next, we focus on solutions to three challenges of 87L protection: security under external faults and CT saturation, security under current alignment errors, and line charging currents.

Finally, we discuss the high adaptivity of 87L elements, which results from addressing the challenges, and the impact of that adaptivity on settings selection and testing.

This tutorial provides in-depth coverage of the topic with specific equations and numerical examples using steady-state values, as well as waveforms from transient simulation studies.

We assume the reader has a background in differential protection in general, as well as in line protection requirements and general principles. We also assume the reader has basic knowledge of signal processing methods used in microprocessor-based relays, such as Fourier or cosine filtering. The references provide the required background knowledge and allow for further reading to explore some of the topics in greater detail.

The goal of this paper is to contribute to the better understanding of microprocessor-based 87L relays and bring appreciation to the advancements achieved by relay designers and application engineers over the last decade.

2. CHALLENGES OF LINE CURRENT DIFFERENTIAL PROTECTION

Line current differential applications create several new challenges in addition to the general considerations applicable to bus, transformer, generator, and other forms of differential protection. These challenges stem from the fact that a power line is not a contained piece of apparatus, like a bus or a power transformer, but stretches across a distance. The following subsections elaborate on specific issues resulting from the size of lines as protected elements.

2.1. SENSITIVITY REQUIREMENTS

Short circuits on power lines can happen under a variety of conditions, including high soil resistivity increasing the tower grounding resistance, contact with trees and other objects, isolator flashover due to contamination, ionization of air due to fires in the vegetation along the right of way, and impact of wind, to name the most common factors.

Grounding of power line towers is less effective than substation grounding, and power lines are not surrounded with many solidly grounded objects. As a result, short circuits on power lines can be accompanied by relatively high fault resistance, particularly for single-line-to-ground faults.

High-resistance line faults draw limited currents and do not normally impact the power system from the dynamic stability and equipment damage points of view. However, power lines are located in public space, and as such, short circuits on power lines can contribute to secondary effects (such as human safety issues and property damage) if not detected with adequate sensitivity and speed.

Therefore, the sensitivity of 87L protection is an important consideration.

2.2. LINE CHARGING CURRENT

Long transmission lines and cables can draw a substantial amount of charging current. The line charging current is not measured by the 87L scheme as an input and therefore appears as a fictitious differential signal, jeopardizing security.

Line energization is the most demanding scenario when considering the line charging current.

First, the charging current is supplied through the single circuit breaker that just energized the line, and therefore, the charging current appears as a single-end feed. No restraining action is possible because there is no other current to use for restraining. Elevating the 87L element pickup, the classical solution to maintain security, reduces sensitivity.

Second, the line energization current has a transient inrush component in it, with peak values much higher than the steady-state charging current, calling for even higher pickup thresholds, at least temporarily until the capacitive inrush current subsides.

During symmetrical conditions, the line charging current is a positive-sequence current. This allows 87L elements that respond to negative- and/or zero-sequence differential signals to mitigate problems related to the line charging current. However, under unbalanced conditions, negative- or zero-sequence charging currents may appear in response to negative- or zero-sequence voltages. Good examples to consider are breaker pole scatter during line energization or external faults in very weak systems causing line voltage unbalance and making the line draw sequence charging currents.

2.3. SERIES-COMPENSATED LINES

Series-compensated lines create unique protection problems due to the capacitive reactance included in series with the protected line, potentially causing voltage and current inversion [1] [2]. In addition, the capacitor overvoltage protection makes the series capacitor circuit nonlinear, and unequal bypassing actions between the phases create series unbalance at the point of the capacitor installation. This series unbalance couples the sequence networks that represent the protected line, thus challenging traditional protection assumptions and relationships between sequence currents and voltages during both internal and external faults.

It is common knowledge that the differential principle is not affected by series compensation. This is only partially correct. Of course, the principle is not jeopardized from the security point of view, but current inversion and coupling between sequence networks create challenges from the dependability point of view. Series compensation may also delay 87L operation for internal faults [1] [3].

2.4. COMMUNICATIONS CHANNEL

Because lines span long distances, it is better to think of 87L protection as 87L schemes, rather than 87L relays. The 87L schemes comprise two or more relays that need to share their local currents measured in different substations located miles or even hundreds of miles apart. These separate relays therefore require a channel for exchanging current values as a part of the 87L scheme. In this respect, both analog and microprocessor-based implementations face considerable challenges, even though specific problems are different for the analog and microprocessor-based schemes.

Analog schemes using pilot wires can only be applied to very short lines because of signal attenuation due to the series resistance and shunt capacitance of the pilot wires. In order to reduce the number of pilot wires, these schemes often combine the phase currents into one signal instead of using the phase-segregated approach.

Microprocessor-based relays utilize long-haul digital communications to exchange the current signals, thus avoiding the limitation of the line length.

However, the following new challenges arise in microprocessor-based implementations:

- Because they work on digital data derived from current samples, these implementations require the means to align the local and remote current measurements so that currents taken at the same time are used in the differential calculations (see Section 2, Subsection 2.5).
- Long-haul channels, unless they use direct fiber, are often built with general purpose communications equipment. These networks are prone to various impairments that create both security and dependability problems for 87L schemes (see Section 2, Subsection 2.6).
- The available bandwidth (i.e., the amount of data that can be shared within any period of time) is limited, at least historically (see Section 2, Subsection 2.7).

2.5. ALIGNMENT OF DIGITAL CURRENT VALUES

Microprocessor-based relays using the differential principle need current data to have the same time reference. In bus, transformer, or generator protection, this is accomplished naturally by using a single protective device that directly receives all the required currents and samples them in a synchronized fashion. Microprocessor-based

87L schemes need an explicit method to synchronize or align the currents taken by separate 87L relays at various line terminals.

When using symmetrical channels (equal latencies in the transmitting and receiving directions), 87L schemes can align the data using the industry standard method known as the ping-pong algorithm. When the channel is not symmetrical, the ping-pong algorithm fails, yielding a current phase error proportional to the amount of asymmetry, which, in turn, creates a fictitious differential signal.

One solution is to use a common time reference to drive the current sampling (historically, Global Positioning System [GPS] clocks). However, reliance on GPS and associated devices for protection is not a commonly accepted solution.

In addition, channel latency may change in response to communications path switching when using multiplexed channels. This problem calls for proper data handling methods built in the 87L relays. In general, each relay needs to wait for the slowest channel to deliver the remote current data, but at the same time, the alignment delay needs to be as short as possible in order not to penalize the speed of operation.

2.6. CHANNEL IMPAIRMENTS

Bit errors, asymmetry, unintentional cross-connections between separate 87L schemes, path switching, accidental loopbacks, and frame slips are examples of impairments, or events in the long-haul communications network that may affect performance of 87L schemes.

Specific solutions are applied to each of these problems, such as disturbance detection supervision for undetected bit errors or relay addressing for unintended cross-connections and loopbacks [4]. Still, it is beneficial for the 87L operating characteristic itself to have a ride-through ability to prevent or mitigate the impact of channel impairments.

2.7. CHANNEL BANDWIDTH LIMITATION

Historically, microprocessor-based 87L schemes are required to work with 56 kbps or 64 kbps channels originally created by the telecommunications industry to carry voice data. A 64 kbps channel allows the clocking of about 260 bits of data in a quarter of a power cycle. Given the necessary overhead, such as packet framing, data integrity protection, and relay addressing, the room left to send current data is very limited, much lower than 260 bits every quarter of a power cycle. By comparison, bus, transformer, or generator differential relays have practically unlimited access (in terms of analog-to-digital converter resolution and sampling frequency) to all the protection zone boundary currents.

The channel bandwidth restriction is an important consideration because it limits the visibility of the local relay into the situation at the remote terminals. For example, in dual-breaker applications, the local relay ideally measures both breaker currents individually at the remote substation, but sending both current measurements doubles the packet payload.

The limited channel bandwidth makes the application of tried-and-true protection solutions and algorithms in 87L designs more challenging. The next subsection describes the most relevant example of this challenge.

2.8. CT SATURATION FOR EXTERNAL FAULTS

Because of its required sensitivity, differential protection must include countermeasures to CT errors, saturation during external faults in particular. External fault detection algorithms are known in the art of bus or transformer protection. These algorithms detect external fault events before any CT saturation occurs and engage extra security measures to prevent relay misoperation. These measures can include an increase in the restraining action and an extra intentional time delay, among others.

However, effective external fault detection algorithms require access to all the zone boundary currents with high fidelity (samples taken at relatively high sampling rates). This requirement may be challenging in 87L applications because of the channel bandwidth limitation. As a result, simplified external fault detection algorithms are often used, or the 87L operating characteristic is designed for better immunity to CT saturation at some expense of sensitivity.

2.9. PHASE AND SEQUENCE DIFFERENTIAL ELEMENTS

Phase differential (87LP) elements face two challenges in 87L applications. First, because they add the currents to create a differential signal, these elements are prone to misoperation for external faults if the currents were misaligned, such as when using asymmetrical channels in the ping-pong synchronization mode. Second, because they use the through currents (load or external fault currents) for restraining, these elements have limited sensitivity, despite the fact that their differential signals are not impacted by load. Setting the phase differential elements to be more sensitive only increases the danger of misoperation due to channel asymmetry, and the issues of immunity to alignment errors and sensitivity cannot be easily reconciled in phase differential element applications.

This observation inspired sequence differential elements–single-phase elements responding to the negative- or zero-sequence differential current (87LQ and 87LG, respectively) and stabilized with the corresponding sequence through current. This way, the load component is removed not only from the differential signal but also from the restraining action, thus allowing for much higher sensitivity. At the same

time, the standing sequence currents are very low (ideally zero) during normal system operation, which mitigates the effect of temporary current misalignment, such as that due to asymmetrical channels.

In addition, sequence networks are typically very homogeneous, which keeps the relative angles of the sequence currents of the line protection zone almost perfectly in phase for internal faults. This fact provides a good margin when balancing protection dependability and security. Relative immunity to line charging current is yet another advantage of sequence differential elements.

However, the high sensitivity of sequence differential elements makes them prone to misoperate on external faults accompanied with CT errors. Consider a three-phase balanced fault, such as when closing on safety grounds inadvertently left after equipment maintenance. True (primary) negative- and zero-sequence currents equal zero (or are very close to zero), but saturation of one or more CTs would generate fictitious negative- or zero-sequence components in the secondary currents. A negative- or zero-sequence differential scheme would experience security issues due to the fictitious differential signal. Restraining is very difficult because one of the line terminals would measure a fictitious non-zero sequence current, while the other terminals may correctly measure a zero value in the sequence current. A sequence differential scheme would not have any actual through negative- and zero-sequence current for restraining. Similar concerns apply to the zero-sequence current measurements during faults not involving ground.

These considerations make the external fault detection algorithms and channel bandwidth limitations even more relevant.

The challenges related to microprocessor-based multiterminal 87L protection described so far call for a multidimensional optimization of the relay design, involving protection algorithms, signal processing, communications issues, and so on. The 87L operating characteristic (the mapping of individual currents around the protection zone into a trip decision) plays an important role in addressing these problems. Different solutions have emerged since the introduction of microprocessor-based 87L relays.

In the remainder of this paper, we review details of some of the key solutions to the stated challenges.

3. PERCENTAGE DIFFERENTIAL CHARACTERISTIC

3.1. DIFFERENTIAL SIGNAL

A differential element responds to a differential (operating) signal. Equation (1) defines the differential signal i_{DIF} for a line bounded by N currents, i_1 through i_N.

$$i_{DIF} = i_1 + i_2 + ... + i_N \tag{1}$$

For example, a three-terminal line connected to a breaker-and-a-half bus at each terminal is bounded by six currents per phase.

The differential signal may be used in a number of ways by the differential element, but the primary purpose is to check the level of the differential signal to qualify an internal fault. For this reason, the differential signal is typically filtered for better accuracy, and its magnitude is derived:

$$I_{DIF} = \left| i_{DIF} \right| \tag{2}$$

| | denotes an operation of filtering and magnitude estimation.

Depending on the relay design and the particular processing of the differential signal in the relay algorithm, filtering and magnitude estimation can use a cosine or Fourier filter, or even absolute values of instantaneous samples. Filters may use half-cycle, full-cycle, or variable data windows. Moreover, a given relay may process the same differential signal (1) in multiple ways simultaneously, with resulting magnitudes (2) serving different parts of the differential element algorithm.

Designs that work on samples execute (1) first and follow with filtering and magnitude estimation per (2). Designs that work on phasors calculate phasors first, apply (1) to phasors, and follow with magnitude estimation per (2). The final outcome is the same, but there are significant differences between the two approaches (samples versus phasors) when it comes to the amount of data sent and amount of information available to remote relays. In general, 87L designs that work on samples are more potent because they have access to more information in the remote currents.

The phase differential (87LP) elements respond to the per-phase differential signals (1). The sequence differential (87LQ and 87LG) elements respond to the differential signal derived from the negative- or zero-sequence phasors calculated first from the phase currents. For example:

$$I_{DIF(Q)} = \left| \overline{I}_{1Q} + \overline{I}_{2Q} + ... + \overline{I}_{NQ} \right| \tag{3}$$

3.2. RESTRAINING SIGNAL

As explained in Section II, the differential signal can differ from zero for a number of events, not only for internal faults. Many of the sources of the fictitious differential signal depend on the magnitudes of the line currents (the greater the currents, the greater the fictitious differential signal). CT errors and current alignment errors are good examples of this relationship.

This observation led to the application of percentage differential elements [5]. The element develops a restraining signal and uses a portion of it (a percentage) to qualify the differential signal. Therefore, the function of the restraining signal is to reflect the overall current level for all the line currents (the through current). This function can be

fulfilled in a number of ways. Unlike the differential signal, which is created in the same universal way by all differential relays, the restraining signal is an arbitrary signal and, as such, is design-dependent.

Equations (4) and (5) describe typical restraining signals, I_{RST}, for multiterminal lines.

$$I_{RST} = |i_1| + |i_2| + ... + |i_N| \tag{4}$$

$$I_{RST} = \max\left(|i_1|, |i_2|, ..., |i_N|\right) \tag{5}$$

Most relays use one of these two expressions. Reference [6] provides more information on various ways of creating the restraining signal.

In general, the restraining signal alone can provide security only up to a certain degree of CT saturation, as we show in Section 7. As a result, advanced relays tend to rely on mechanisms other than a simple restraint during extreme CT saturation.

Combinations of the approaches (4) and (5) are possible. For example, the local currents at each terminal (in dual-breaker applications) can be treated using (4), and subsequently, the consolidated local and remote currents can be aggregated in the total restraining signal using (5).

Similar to the differential signal, the restraining signal can be processed using different filters of different window lengths or can use absolute values of instantaneous samples. Moreover, multiple restraining signals can be calculated for usage in different parts of the 87L algorithm. For example, using full-cycle cosine filtering in (2), (4), and (5) provides accurate differential and restraining signals, suitable for percentage differential characteristics. Using absolute values of samples in these operations provides faster, less accurate instantaneous differential and restraining signals, suitable for external fault detection algorithms.

The 87LP elements respond to the per-phase restraining signals. The 87LQ and 87LG elements respond to the restraining signal derived from the negative- or zero-sequence phasors calculated first from the phase currents. For example:

$$I_{RST(Q)} = \left|\overline{I}_{1Q}\right| + \left|\overline{I}_{2Q}\right| + ... + \left|\overline{I}_{NQ}\right| \tag{6}$$

During three-phase balanced faults, the restraining signals of the 87LQ and 87LG elements are zero, and during phase-to-phase faults, the restraining signal of the 87LG element is zero. Therefore, the restraining signal defined as (6) for these elements fails to meet its primary function of providing security for the mentioned fault types, and extra security measures are needed to secure the sequence elements for these fault types.

3.3. OPERATING CHARACTERISTIC

A percentage differential element operates when the differential signal is above a constant pickup value:

$$I_{DIF} > P \tag{7}$$

and above a percentage of the restraining signal:

$$I_{DIF} > K \cdot I_{RST} \tag{8}$$

Some relays may combine numerically, rather than logically, the pickup and restraining conditions:

$$I_{DIF} > P + K \cdot I_{RST} \tag{9}$$

The logic of (7) through (9) yields a characteristic on the differential-restraining plane in the form of a straight line with slope K (Fig. 1a). This characteristic handles errors that are proportional to the restraining signal, such as CT errors or current alignment errors.

For low fault currents, the CTs behave linearly and the error signal is a linear function of the restraining signal. For greater fault currents, the CTs saturate and cause a greater increase in the fictitious differential signal. This observation led to the application of dual-slope percentage differential characteristics (Fig. 1b). A dual-slope differential characteristic increases security for high-current external faults by applying greater restraint for greater currents to accommodate CT saturation errors, while allowing more sensitive operation for low-current internal faults.

Figure 1b shows that the second slope (K_2) line can either cross the origin or connect to the first slope (K_1) line at the break point (B). The former implementation creates a true percentage differential characteristic, meaning the amount of restraint is a constant percentage of the restraining signal, but adds discontinuity at the break point between the lower and higher slope lines. The latter implementation avoids discontinuity at the break point but constitutes a variable percentage restraint. Both approaches are valid as long as the fictitious differential signal is kept within the restraining region of the characteristic.

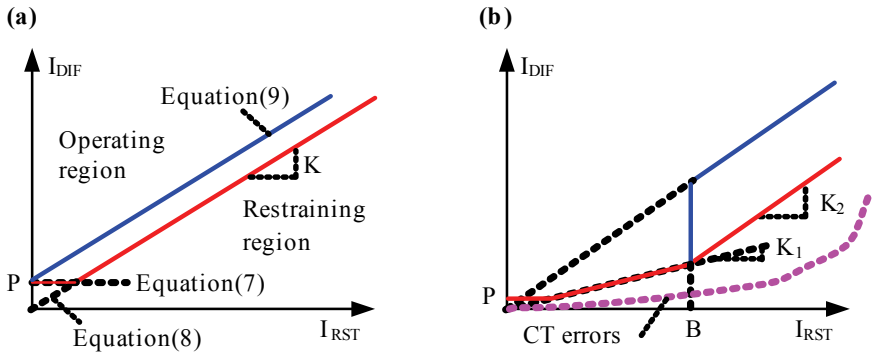

Fig. 1. Single-slope percentage differential characteristics (a); fictitious differential signal due to CT errors and dual-slope percentage differential characteristics (b)

3.4. ADAPTIVE PERCENTAGE DIFFERENTIAL CHARACTERISTIC

The single- and dual-slope characteristics need to be set to accommodate fictitious differential signals caused by CT errors, poor current alignment, line charging current, and so on, as explained in Section 2. As a result, low-sensitivity settings are applied permanently, even for internal faults, thus limiting sensitivity of the 87L element or even jeopardizing its dependability.

Adaptive differential elements control the restraining action dynamically using dedicated logic to detect conditions that require more security and engage the extra security only when required. This adaptive behavior can be achieved typically in two ways.

One solution uses two sets of settings (normal and extended security) and settings switchover logic to toggle between the normal and extended security. Normal security settings, in effect most of the time, provide high sensitivity. The adaptive element switches to the less-sensitive extended security settings only when required in response to rare or abnormal events. Settings switchover may be triggered by external fault detection (Section 7), poor data alignment (Section 8), loss of charging current compensation (Section 9), and so on.

Figure 2 illustrates the concept of adaptive percentage restraint settings. Typically, only the percentage restraint (slope) is increased, but increasing the pickup threshold is also an option.

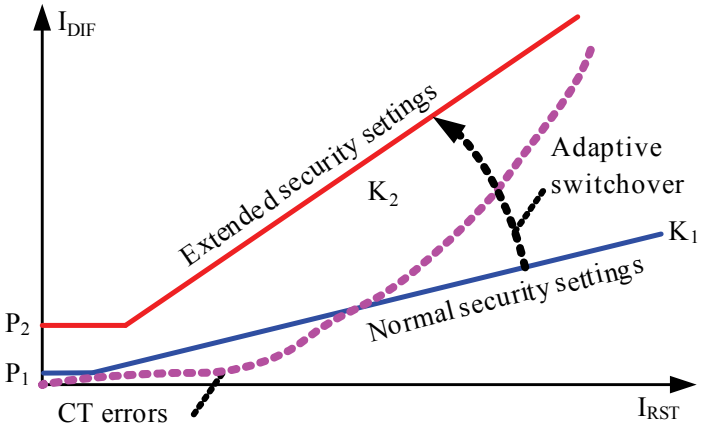

Fig. 2. Adaptive percentage differential characteristic

Another approach uses an adaptive restraining signal [7], [8]. As noted in Section 3, Subsection 3.2, the restraining signal is an arbitrary quantity, and as such, it can be augmented at will to provide extra restraint upon detection of a condition that requires extra security.

Section 5, Subsection 5.3 lists examples of extra terms that may be added adaptively to the restraining signal, while the following sections of the paper pro-

vide more details on conditions and detection methods to trigger the adaptive behavior.

4. ALPHA PLANE CHARACTERISTIC

4.1. ALPHA PLANE

The current-ratio complex plane, or Alpha Plane [9], provides a way to analyze the operation of a two-restraint differential element. In 87L protection, the Alpha Plane is a plot on a two-dimensional plane of the ratio of the remote current ($\bar{I}_R$) to the local current ($\bar{I}_L$):

$$\bar{k} = \frac{\bar{I}_R}{\bar{I}_L} \tag{10}$$

The 87L elements that operate based on the Alpha Plane principle continuously calculate the ratio (10) and compare this ratio with an operating characteristic defined on the Alpha Plane.

4.2. EVENTS RELEVANT TO 87L ELEMENTS ON THE ALPHA PLANE

The Alpha Plane approach resembles the analysis of distance element operation on the impedance plane. References [1] and [3] discuss the loci of various events on the Alpha Plane in detail. A short summary follows here.

1) Through-Current Conditions

For ideal through-current conditions (power flow or external faults with no CT or current alignment errors and without line charging current), the magnitudes of remote

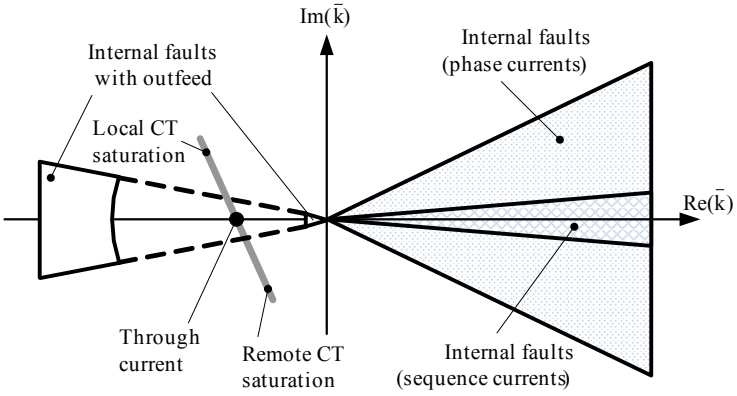

Fig. 3. Power system events on the Alpha Plane

and local currents are equal and their phases are 180 degrees apart. Hence, through-load and external fault conditions ideally plot at 1 ∠ 180° on the Alpha Plane (see Fig. 3). Logically, the restraining region of a differential element characteristic should include this ideal blocking point.

2) Internal Faults

For internal faults, the angles of the remote and local phase currents depend on the source voltage angles (prefault power flow) and the angles of the system impedances. Fig. 3 shows the internal fault region on the Alpha Plane as an angular sector that reflects variations in source voltage and impedance angles. This angular sector is narrower for sequence differential elements because, as explained in Section 2, Subsection 2.1, the angle difference between the local and remote sequence currents depends only on system nonhomogeneity, which is typically low for the negative- and zero-sequence networks. Logically, the restraining region of the operating characteristic should exclude the internal fault region.

3) Internal Faults with Outfeed

For some internal faults, the current flows out of the line at one terminal [3]. High-resistance internal faults with fault current less than load current cause outfeed conditions. In series-compensated lines, outfeed occurs when the reactance from one of the sources to the fault point is capacitive [2]. A line with a strong external parallel tie may experience outfeed at one terminal for some internal faults.

For internal faults with outfeed, the angle between the local and remote currents may be close to 180 degrees. However, the current magnitudes are very different. Therefore, these faults plot close to the negative real axis of the Alpha Plane, but away from the 1 ∠ 180° point (Fig. 3). Logically, the restraining region of the operating characteristic should exclude the regions corresponding to internal faults with outfeed.

4) CT Saturation During External Faults

When a CT saturates, the fundamental frequency component of the secondary current decreases in magnitude and advances in angle.

We consider the phase differential elements first. When the local CT saturates and the CT at the remote end of the protected line does not saturate, the current-ratio magnitude of the phase currents increases and its phase angle decreases, moving the operating point upward and to the left from the 1 ∠ 180° point (Fig. 3). When the remote CT saturates and the local CT does not saturate, the current-ratio magnitude decreases and its phase angle increases, moving the operating point downward and to the right. Because of the effect of the current dc offset on CT saturation and the relay filtering transients, the current ratio actually describes a time-dependent irregular trajectory. Section 7 provides more details and shows transient CT satu-

ration trajectories. Logically, the restraining region of the operating characteristic should include the current ratios corresponding to external faults with CT saturation.

The impact of CT saturation on the sequence current ratio is far more complex than just a relatively well-defined shift from the 1 ∠ 180° point. The sequence current ratio is a function of six phasors for a two-restraint differential zone and depends on the fault type and amount of CT saturation in any of the up to six CTs that may carry fault current. Section 7 further discusses this topic.

5) CT Saturation During Internal Faults

Similar phenomena take place during internal faults. CT saturation alters the phase current-ratio magnitude and angle, shifting the operating point from the expected internal fault position as defined by the source voltage angles and the system impedances. Logically, the restraining region of the operating characteristic should exclude the current ratios corresponding to internal faults with CT saturation.

6) Line Charging Current

As explained in Section 2, Subsection 2.2, the differential scheme measures the line charging current as a differential signal. Considering the charging current alone, the Alpha Plane element response to the charging current is very similar to that of internal faults. The current-ratio magnitude may vary considerably depending on the system impedances and reactive power sources in the vicinity of the line. This variation includes an ultimate case of an open breaker or a very weak system, leading to a current-ratio magnitude of zero or infinity. At the same time, the angles of the charging current contributions from both ends of the line are similar, placing the current ratio close to the positive real axis of the Alpha Plane.

When considering both the through current (load or external faults) and the charging current, the phase current ratio stays relatively close to the 1 ∠ 180° point, shifting more from this point when the charging current becomes a larger portion of the through current. The through current limits the impact of the charging current, providing the Alpha Plane elements with some security.

Sequence currents must be discussed separately, however. Under symmetrical conditions, there is no (or very small) standing sequence charging current. There is no (or very small) through sequence current either. Therefore, there is no stabilizing effect from the through current for the sequence current ratio, but that stabilizing effect is not required anyway.

However, sequence charging currents may appear under unbalanced conditions. Line energization (a single-end feed) creates challenges for any differential element. On the Alpha Plane, the single-end feed causes the current ratio to be zero or infinity, depending on if the local or remote terminal picks up the line.

Section 9 discusses solutions to the line charging current challenges.

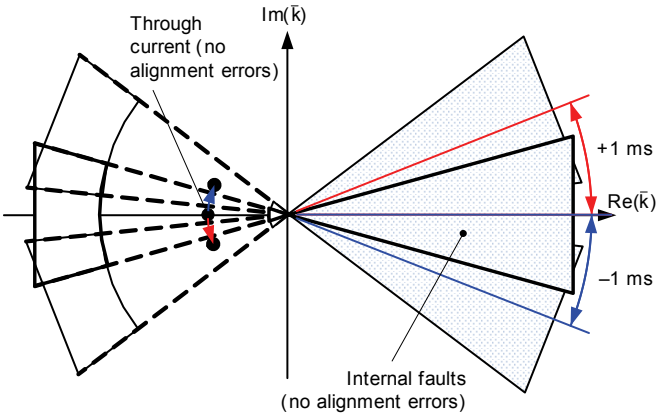

Fig. 4. Impact of current alignment errors on the Alpha Plane

7) Current Alignment Errors

Errors in alignment between the local and remote currents cause the current ratio to rotate around the origin on the Alpha Plane. The ratio magnitude is unchanged; the rotation angle equals the angle error caused by the amount of misalignment. For example, in a 60 Hz system, a 2-millisecond channel asymmetry causes the ping-pong algorithm to misalign the currents by $0.5 \cdot 2 = 1$ milliseconds, or 21.6 degrees, rotating the current ratio by 21.6 degrees. As a result of this rotation, the $1 \angle 180°$ point corresponding to load conditions or external faults becomes an arc and the internal fault areas effectively experience an angular expansion by rotating in either direction (Fig. 4).

4.3. ALPHA PLANE DIFFERENTIAL ELEMENT CHARACTERISTIC

With the current ratio regions mapped on the Alpha Plane for the relevant events (Fig. 3 and Fig. 4), it is straightforward to shape an optimum operating characteristic by dividing the Alpha Plane into blocking and operating regions, with the blocking region encompassing all the no-trip events and excluding all the trip events.

Figure 5a shows one such practical operating characteristic shaped with only two simple settings: the blocking radius, R, and the blocking angle, α [1] [3] [10]. The differential element operates when the current ratio leaves the restraining region and the differential signal magnitude is above a minimum pickup value.

Setting R determines the restraining region outer radius. The inner radius is the reciprocal of R.

Setting α determines the angular extent of the restraining region. The choice of using the angle to control the characteristic stems from the observation that many of the events of interest plot as angular sectors on the Alpha Plane (Fig. 3 and Fig. 4) and

therefore can be better accounted for with an angle setting than with a percentage slope setting.

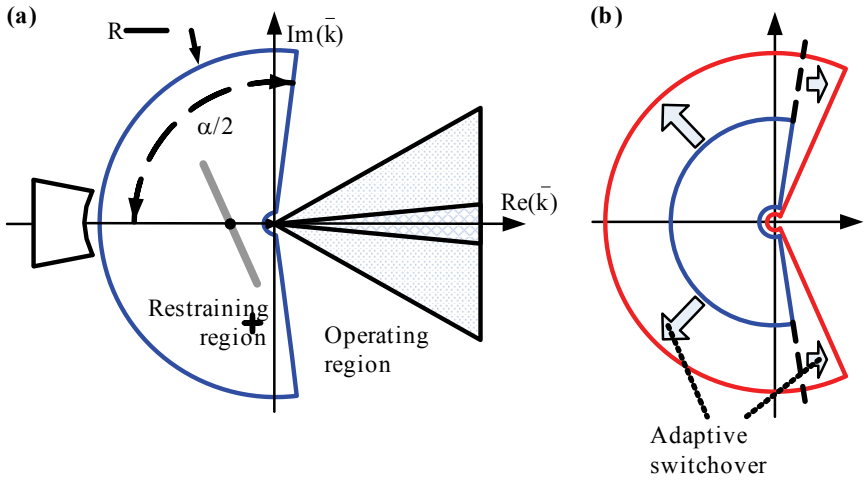

Fig. 5. Alpha Plane differential element operating characteristic (a);
adaptive Alpha Plane characteristic with normal and extended security settings (b)

In the Alpha Plane element, the angular setting α allows the accommodation of CT and current alignment errors without affecting sensitivity, while the radius setting *R* modifies sensitivity without penalizing tolerance to CT saturation and current alignment errors.

The phase and sequence elements may use the same settings for the Alpha Plane characteristic or separate settings, recognizing the different operating conditions and behavior of the phase and sequence elements.

4.4. ADAPTIVE ALPHA PLANE CHARACTERISTIC

The Alpha Plane characteristic accommodates many sources of errors in a very efficient way, allowing a good balance between security and sensitivity. In addition, the principle still can be made adaptive, providing extra advantages.

Figure 5b shows an adaptive Alpha Plane characteristic with a larger blocking region defined by extended security settings. As in the case of the percentage differential characteristic, the settings switchover logic may respond to external fault detection, poor data alignment, or loss of charging current compensation. Typically, both the blocking radius and angle are increased, but increasing the pickup threshold is also an option, as well as increasing only the blocking angle, for example, to accommodate larger data alignment errors.

5. COMPARING PERCENTAGE DIFFERENTIAL AND ALPHA PLANE CHARACTERISTICS

5.1. MAPPING CHARACTERISTICS INTO A COMMON PLANE

We continue to focus on two-restraint differential applications (zones bounded by two currents only). As phasors, the two currents of the differential zone have three degrees of freedom (two magnitudes and a relative angle); thus together, they constitute a three-dimensional space.

The percentage differential principle maps this space into a new two-dimensional space of the differential and restraining signals (both are magnitudes, or scalar values) and draws a boundary of operation as a line (not necessarily a straight line).

The Alpha Plane differential principle maps this three-dimensional space into a new two-dimensional space of real and imaginary parts of the ratio between the two currents and draws a boundary of the restraining region as an enclosed contour.

In order to better compare the two principles, we map the restraining and operating regions of one characteristic into the two-dimensional space of the other characteristic. References [3] and [11] offer information regarding the mapping process itself.

Figure 6 shows the mapping of the single-slope characteristic that uses (4) for restraint. The restraining region below the slope line of the percentage differential characteristic maps into the inside of a cardioid-like contour on the current-ratio plane (see the appendix). The greater the slope, the larger the restraining region inside the contour. The restraining and operating regions on the current-ratio plane do not overlap, meaning any single-slope characteristic can be represented exactly on the current-ratio plane.

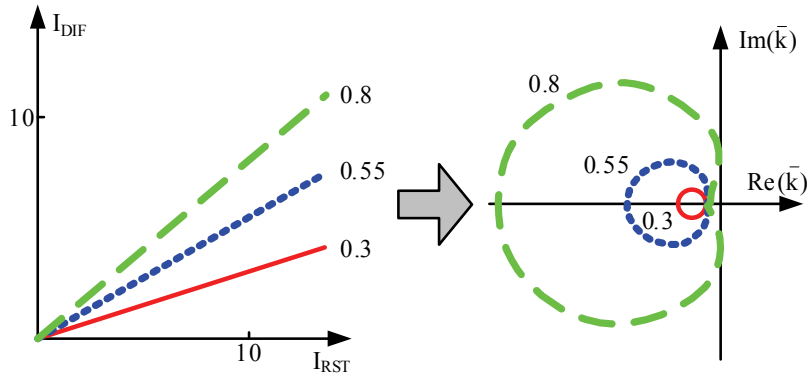

Fig. 6. Mapping a single-slope characteristic into the current-ratio plane

We now check if the Alpha Plane operating characteristic can be mapped exactly into the differential-restraining plane. Figure 7 shows the restraining and operating

regions of a sample Alpha Plane contour (radius of R = 3 and blocking angle of α = 240°). This mapping was obtained by computer simulations as follows. A large number of combinations of the two zone boundary currents were generated. Each combination falling into the operating region of the Alpha Plane was marked as a part of the operating region on the differential-restraining plane (contour *b*). Similarly, each combination falling into the restraining region of the Alpha Plane was marked as a part of the restraining region on the differential-restraining plane(contour *a*).

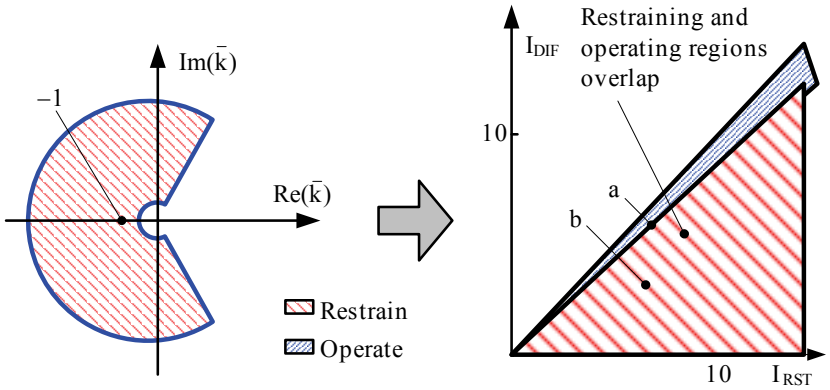

Fig. 7. Mapping an Alpha Plane characteristic into the differential-restraining plane. The operating and restraining regions overlap on the differential-restraining plane

Note that the restraining and operating regions (inside and outside of the Alpha Plane characteristic, respectively) overlap when mapped into the differential-restraining plane. The restraining region resembles that of a single-slope characteristic (line marked *a* with a slope of about 0.9 in this example), while the operating region resembles that of a dual-slope percentage differential characteristic (line marked *b* with slopes of about 0.5 and 0.9 and a break point of about 8 pu in this example). As expected and clearly visible in the percentage differential characteristic, the Alpha Plane characteristic is biased toward security.

The main point of Fig. 7, however, is that the percentage differential characteristic cannot emulate the Alpha Plane characteristic. In the area of overlap, the Alpha Plane characteristic restrains or operates based on the current ratio, while any percentage differential characteristic can either restrain or operate, but cannot do both. This can be easily understood by realizing that any given point on the differential-restraining plane can be created by multiple pairs of local and remote currents, with each pair having a different current ratio. To the percentage differential characteristic, all these current pairs appear the same, while the Alpha Plane characteristic can distinguish them based on their complex current ratio.

However, the percentage differential characteristic can mimic the Alpha Plane characteristic by switching adaptively between two characteristics as per Fig. 7 (i.e., between the slope characteristics marked *a* and *b*), using extra information derived from the zone boundary currents, such as phase difference or magnitude ratio. If a percentage differential element applied a characteristic similar to the one marked *a* during internal faults and a characteristic similar to the one marked *b* during external faults, this element would behave similarly to the Alpha Plane element.

Figure 7 illustrates the following about the Alpha Plane characteristic:

- The Alpha Plane characteristic is biased toward security (it maps into very high slopes).
- It allows more sensitivity based on the current ratio (the unconditional restraining region is a dual-slope line with reduced slope for smaller restraining signals).
- It is inherently similar to an adaptive percentage differential characteristic (compare the lines marked *a* and *b* in Fig. 7 with Fig. 1b, and assume a switchover takes place between the single- and dual-slope characteristics as per Fig. 2).

Next, we check if the dual-slope percentage differential characteristic can be mapped exactly into the current-ratio plane. The same technique of computer simulations has been used as when mapping the Alpha Plane characteristic into the differential-restraining plane. Figure 8 shows the restraining (shaded red) and operating (shaded blue) regions of a sample dual-slope characteristic (slopes of 0.5 and 0.7, break point of 6 pu). Because the two lines of the characteristic pass through the origin, the contours of the two regions in the Alpha Plane (operating region contour marked *a* and restraining region contour marked *b*) are effectively traced using the equation provided in the appendix.

Note that the restraining and operating regions (below and above the percentage differential characteristic, respectively) overlap when mapped into the current-ratio plane.

The main point of Fig. 8 is that the Alpha Plane characteristic cannot exactly replicate the dual-slope differential characteristic. In the area of overlap, the percentage differential characteristic restrains or operates based on the restraining signal level, while any Alpha Plane characteristic can either restrain or operate, but cannot do both. This can be easily understood by realizing that any given point on the current-ratio plane can be created by multiple pairs of local and remote currents, with each pair having a different current level. To the Alpha Plane characteristic, all these current pairs appear the same, while the dual-slope characteristic can distinguish them based on the current level (i.e., the value of the restraining signal).

However, the Alpha Plane differential characteristic can mimic the percentage differential characteristic by switching adaptively between multiple contours as per Fig. 8, using extra information derived from the zone boundary currents, such as the current magnitudes. If an Alpha Plane element applied a characteristic similar to the one

marked *a* during internal faults and a characteristic similar to the one marked *b* during external faults, this element would behave similarly to the dual-slope percentage differential element.

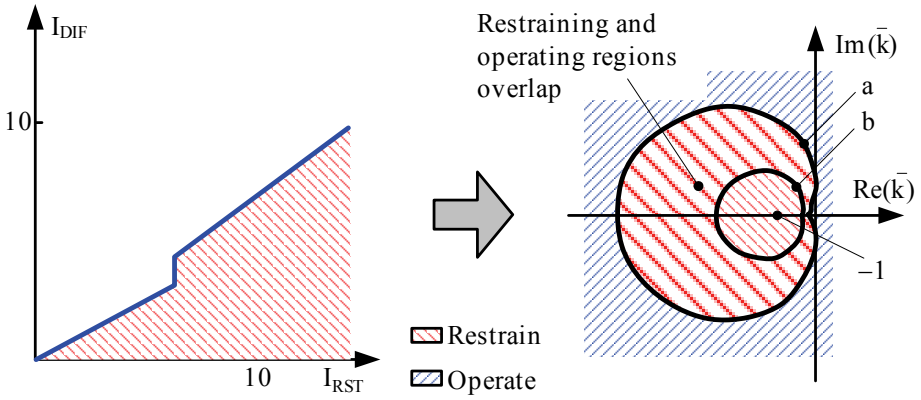

Fig. 8. Mapping a single-slope characteristic into the current-ratio plane

Figure 8 illustrates the following about the dual-slope percentage differential characteristic:

- The dual-slope percentage differential characteristic balances security and sensitivity based on the current level.

It is inherently similar to an adaptive Alpha Plane characteristic (compare the contours marked *a* and *b* in Fig. 8 with Fig. 5b, and assume a switchover takes place between the two Alpha Plane characteristics).

5.2. LIMITS OF COMPARISON

As illustrated previously, exact comparison of the two differential operating characteristics has its limits. Further, consider the following:

- For some combination of currents of the differential zone, one characteristic (percentage differential or Alpha Plane) cannot even be shown on the plane of the other characteristic (current-ratio or differential-restraining plane, respectively), preventing direct comparison.
- In the case of a single-slope characteristic, the two characteristics can be shown on a common plane (see Fig. 6), but the restraining and operating regions of the two characteristics are still very different.
- As a result, we cannot exactly emulate one principle with the other by applying settings.
- The differences between the two characteristics stem from the deeply diverse foundations of the two principles. The percentage differential principle blends

the magnitude and angle differences together and controls security based on the current level. The Alpha Plane ignores the current level and controls security by looking at the magnitude ratio and angle difference separately.

- In addition to using plain percentage differential or Alpha Plane comparators, actual 87L relays incorporate a number of supervisory conditions that may create more differences in the response of percentage differential and Alpha Plane elements.
- Last, but not least, the comparison is only possible for two-current differential zones and is not even applicable to multicurrent zones.

Interestingly, adaptive versions of the two principles tend to mimic each other to a degree. Consider external faults and CT saturation, for example. The dual-slope (or adaptive single-slope) characteristic provides security by relying on higher slopes when the current levels are high. The Alpha Plane characteristic relies on angle differences to provide security. Figure 7 shows how the Alpha Plane characteristic maps into a characteristic that resembles a dual-slope percentage characteristic with slope switchover logic. During high-current external faults with CT saturation, both the magnitudes are high and the angle differences are significant, allowing both principles to work well.

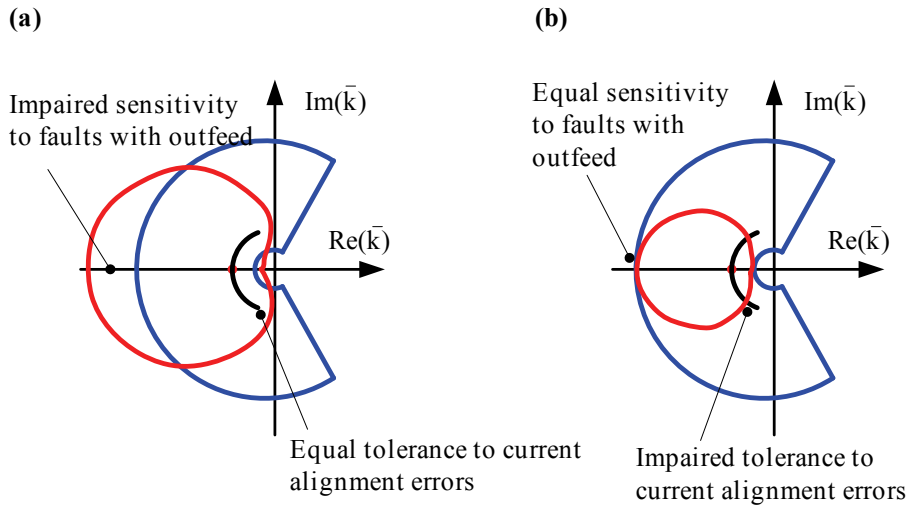

Fig. 9. Percentage differential and Alpha Plane characteristics set to provide similar tolerance to current alignment errors (a) and similar tolerance to internal faults with outfeed (b)

Tolerance to current alignment errors makes an important difference between the two principles in 87L applications. Alignment errors can occur irrespective of the current magnitude, which gives the Alpha Plane characteristic a relative advantage over the percentage differential characteristic. Figure 9 illustrates this fact further by

showing single-slope percentage differential and Alpha Plane characteristics set to provide similar tolerance to current alignment errors (Fig. 9a). As a result, the percentage differential characteristic is less sensitive to internal faults with outfeed. When both characteristics are set to provide similar sensitivity to internal faults with outfeed (Fig. 9b), the percentage differential characteristic is less tolerant to current alignment errors.

5.3. RELATIVE STRENGTHS

Historically, the percentage differential principle originated as a countermeasure to CT saturation with implementations often driven by a specific relay technology (electromechanical and static relays, carried forward toward microprocessor-based relays). The principle ignores phase errors individually, but blends them with magnitude errors, and therefore, it does not handle the current alignment errors peculiar to 87L applications well.

The Alpha Plane principle was conceived for 87L applications. Therefore, it responds better to phase (alignment) errors by explicitly looking at the angle difference between the two currents. However, this principle misses the opportunity of using the current level to control its security and sensitivity even better. In addition, the Alpha Plane principle as defined in Section 4 applies naturally only to two-current zones and is not easily expandable to multicurrent zones.

On the other hand, the percentage differential principle has been used for a long time; several relaying techniques have been developed to improve its performance. In particular, the restraining terms can be modified freely. For example, the following terms can be added to the restraining signal:

- Harmonics in the differential signal, because they indicate possible CT saturation under external faults. This increase can be in place permanently or engaged only upon detecting an external fault.
- A portion of the phase restraining signal added to the sequence restraining signal to provide proper restraint for three-phase and phase-to-phase faults. This increase can be in place permanently or engaged only upon detecting an external fault and/or the specific fault type.
- A factor proportional to the estimated error in data synchronization.
- The numerical difference between the samples of the actual differential signal and an ideal sine wave corresponding to the estimated phasor. This numerical difference may indicate transient errors in phasor estimation.
- High-frequency components in the differential signal when using charging current compensation, because they may indicate errors in compensation.

Finally, the percentage differential principle allows better utilization of the channel bandwidth in applications with multiple currents at each line terminal. Note that both the differential signal (1) and the restraining signal (4) are sums of all the zone bound-

ary currents. These sums can be created in two stages: adding all local terms before sending them and then adding the consolidated local terms and the received (and consolidated before sending) remote terms. This method allows the use of one data set in the communications packet irrespective of the number of local currents connected to each 87L relay.

It is thus appealing to combine the benefits of the two principles when designing the Alpha Plane operating characteristic for multicurrent zones. The next section introduces one such solution.

6. GENERALIZED ALPHA PLANE CHARACTERISTIC

The term *generalized Alpha Plane* refers to a differential protection principle that measures any number of currents that bound the differential zone, calculates and allows arbitrary manipulation of the differential and restraining auxiliary signals, and generates two equivalent currents yielding an operating point on an equivalent current-ratio plane. The equivalent operating point is further checked against a traditional Alpha Plane operating characteristic.

The primary drivers for the generalized Alpha Plane principle are to extend the well-proven Alpha Plane principle to multiterminal lines with each terminal having multiple local currents and to further enhance it by applying protection concepts that are more natural to the percentage differential principle.

6.1. GENERALIZED ALPHA PLANE ALGORITHM

In the following description of the generalized Alpha Plane algorithm, all the currents belong to the same phase of the 87LP element (A, B, or C) or are the negative- or zero-sequence currents for the 87LQ and 87LG elements, respectively. We use the following notation:

- $\bar{I}_1$, $\bar{I}_2$, ..., $\bar{I}_N$ are phasors of the partial differential terms formed from individual currents at each line terminal.
- I_{1RST}, I_{2RST}, ..., I_{NRST} are the partial restraining terms formed from individual current magnitudes at each line terminal.
- $\bar{I}_{DIF}$ is the phasor of the differential signal.
- I_{RST} is the restraining signal.
- $\bar{I}_{L(EQ)}$ is the phasor of the local equivalent current of the generalized Alpha Plane.
- $\bar{I}_{R(EQ)}$ is the phasor of the remote equivalent current of the generalized Alpha Plane.

The algorithm works in the following steps, each serving a purpose to address the challenges of multiterminal 87L protection:

1. All the local currents (samples or phasors) that belong to the 87L zone are aggregated into partial differential terms ($\bar{I}_1$, $\bar{I}_2$, ..., $\bar{I}_N$) by summing the locally measured currents before transmitting them to the remote relays. This approach reduces communications bandwidth requirements for the scheme (see Section 2, Subsection 2.7).
2. The magnitudes of all the local currents that belong to the 87L zone are aggregated into partial restraining terms (I_{1RST}, I_{2RST}, ..., I_{NRST}) by summing the magnitudes of the locally measured currents before transmitting them to the remote relays. Again, this approach optimizes the communications bandwidth (see Section 2, Subsection 2.7), while providing information to the 87L scheme on the level of currents at each terminal to address the problem of external faults with CT saturation (see Section 2, Subsection 2.8).
3. The local and remote partial differential and restraining terms are summed [per (1) through (4) and (4)] into the differential signal phasor ($\bar{I}_{DIF}$) and the restraining signal scalar (I_{RST}) for the complete N-terminal 87L protection zone.
4. The differential and restraining signals are modified at will using known protection techniques for better performance of the 87L scheme.
5. The equivalent local ($\bar{I}_{L(EQ)}$) and remote ($\bar{I}_{R(EQ)}$) currents are derived from the modified differential and restraining signals and used as inputs to the traditional Alpha Plane algorithm.

The first four steps are self-explanatory, while the fifth step is the cornerstone of this novel approach.

The algorithm determines the two equivalent currents that yield exactly the same differential signal phasor and the same restraining signal scalar in the equivalent two-current zone as in the original *N*-current zone. In other words, the algorithm design starts with the following question: Which are the two equivalent currents that yield exactly the same differential and restraining signals as the actual *N*-current zone? The problem is solved analytically during the algorithm design phase (as shown in the next paragraphs), and the resulting solution is programmed in a microprocessor-based relay and executed in real time during relay operation.

The algorithm design is constrained with three equations; the real and imaginary parts of the differential signal and the magnitude of the restraining signal from the two equivalent currents must match the actual values of the 87L zone. At the same time, the algorithm seeks to obtain four unknowns: the real and imaginary parts of the two equivalent currents. As a result, the problem has more variables than equations.

One specific approach avoids using a fourth equation by selecting the angular position of one of the equivalent currents to align the equivalent current with a specific actual zone boundary current [8]. That specific zone boundary current is the one that has the largest projection on the differential signal phasor.

The rationale supporting this solution is as follows. During external faults, it is preferable to select the current flowing out of the 87L zone as one of the equivalent

currents. Because of CT saturation, the highest current is not necessarily the current flowing out of the protection zone toward the external fault. However, CT saturation would yield an error signal in this current that is relatively in phase with the external fault current (angle difference up to 90 degrees in an ultimate case of extreme saturation). This error signal would demonstrate itself as a fictitious differential signal, assuming all other CTs work without saturation (the worst-case scenario). As a result, the secondary external fault current (including the effect of CT saturation) is relatively in phase with the differential signal in addition to being significant (unless extreme CT saturation brings the magnitude of the secondary current down). Therefore, looking at the angles between each of the zone boundary currents and the differential signal helps in identifying the external fault current.

To this end, the following auxiliary signals are calculated:

$$R_k = \mathrm{Re}\left(\bar{I}_k \cdot \bar{I}^*_{DIF} \right) \tag{11}$$

where:

* stands for a complex conjugate operation.

k is 1 ... N.

The zone boundary current $\bar{I}_k$ that yields the highest R_k value is selected as an angular reference for one of the two equivalent Alpha Plane currents:

$$\beta = \mathrm{Arg}\left(\bar{I}_k \right) \tag{12}$$

Next, an auxiliary phasor $\bar{I}_X$ is calculated by shifting the differential signal by the angle β:

$$\bar{I}_X = \bar{I}_{DIF} \cdot 1 \angle \left(-\beta \right) \tag{13}$$

Now, the following two equivalent currents can be calculated [8]:

$$\bar{I}_{L(EQ)} = \left(\frac{\mathrm{Im}\left(\bar{I}_X \right)^2 - \left(I_{RST} - \mathrm{Re}\left(\bar{I}_X \right) \right)^2}{2 \cdot \left(I_{RST} - \mathrm{Re}\left(\bar{I}_X \right) \right)} + j \cdot \mathrm{Im}\left(\bar{I}_X \right) \right) \cdot 1 \angle \beta \tag{14}$$

$$\bar{I}_{R(EQ)} = \left(I_{RST} - \left| \bar{I}_{L(EQ)} \right| \right) \cdot 1 \angle \beta \tag{15}$$

The generalized Alpha Plane algorithm derives the complex ratio of the two equivalent currents calculated per (14) and (15) and applies it to the operating characteristic. These internal calculations are performed independently for the A-phase, B-phase, C-phase, negative-sequence, and zero-sequence currents.

The following two examples illustrate the generalized Alpha Plane calculations using (11) through (15).

1) Example 1: Generalized Alpha Plane Calculations for a Three-Terminal Line with Single Breakers

Consider a three-terminal single-breaker 87L application.

First, we consider the 87LP element while assuming an external fault at Terminal 3. Assume the following phase currents of the 87L zone (in pu):

$$\bar{I}_1 = 10 \angle -95°, \quad \bar{I}_2 = 5 \angle -75°, \quad \bar{I}_3 = 8.88 \angle 131.6° \tag{16}$$

The third current is affected by CT saturation; its magnitude is reduced by 40 percent, and its angle is advanced by 40 degrees (the true value of this current is 14.8 ∠ 91.6°). Figure 10 plots the current phasors for better understanding.

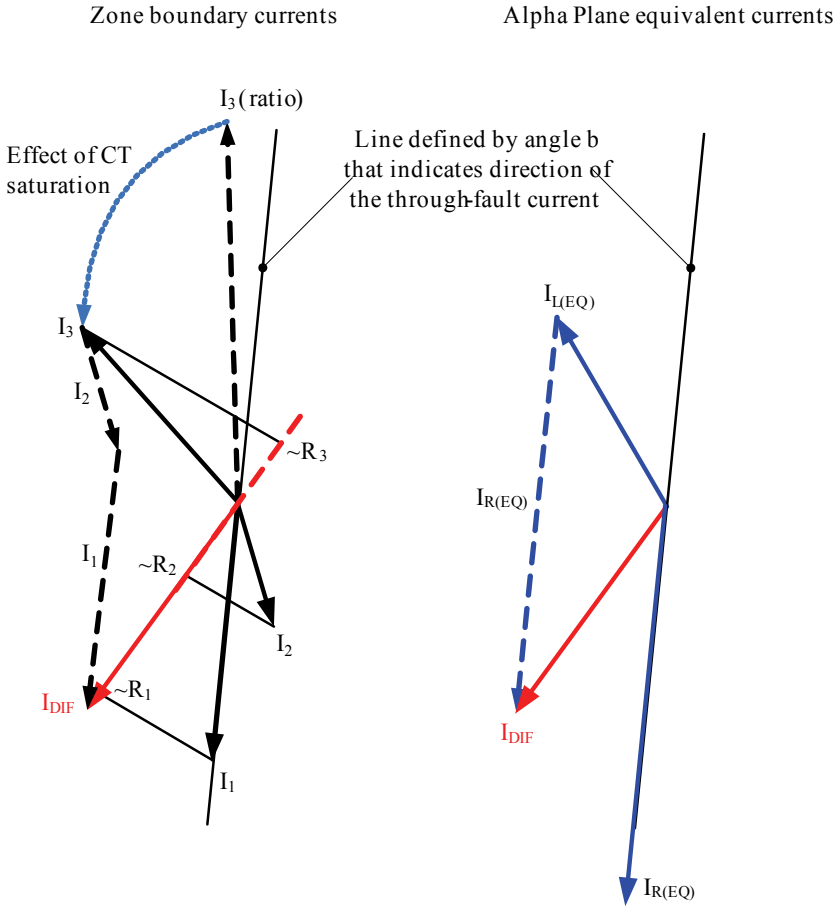

Fig. 10. Current phasors in Example 1

Given the values of the currents, the generalized Alpha Plane 87LP element works with the following quantities:

$$\bar{I}_{DIF} = 9.82 \angle -123.9° \text{ and } I_{RST} = 23.88 \tag{17}$$

The R_k values for the three currents as per (11) are 86.0, 32.3, and 21.8, respectively. The algorithm selects the Terminal 1 current $\bar{I}_1$ as the reference (the highest R_k). Therefore, β = –95° per (12). This selection is rational because, in this case, the bulk of the fault current flows between Terminals 1 and 3 (i.e., along the line of about ±90 degrees).

Using (14) and (15), the algorithm calculates:

$$\bar{I}_{L(EQ)} = 8.38 \angle 119.5° \text{ and } \bar{I}_{R(EQ)} = 15.5 \angle -95° \tag{18}$$

The complex ratio between the two equivalent currents is:

$$\bar{k} = 1.85 \angle 145° \tag{19}$$

An Alpha Plane characteristic with a blocking angle of at least 70 degrees (the typical setting is around 180 degrees) would qualify this condition as an external fault.

By comparison, the percentage differential characteristic would need a slope of at least 9.82/23.88, or 41.1 percent in order to remain secure for this external fault.

We now apply a traditional two-current Alpha Plane concept to this three-terminal line. In one approach [3], all possible fault locations are considered and a separate current ratio is derived for each of the combinations. In this example, the following ratios are checked:

- $\bar{I}_1$ versus $\bar{I}_2 + \bar{I}_3$, yielding the ratio of 2.02 ∠ 106.4° (assumes an external fault at Terminal 1).
- $\bar{I}_2$ versus $\bar{I}_1 + \bar{I}_3$, yielding the ratio of 1.51 ∠ –78.8° (assumes an external fault at Terminal 2).
- $\bar{I}_3$ versus $\bar{I}_1 + \bar{I}_2$, yielding the ratio of 1.66 ∠ 140° (assumes an external fault at Terminal 3).

Note that the blocking angle has the largest impact on security, and therefore, the third combination with the ratio of 1.66 ∠ 140° is the most appropriate. This result is expected because the external fault is truly at Terminal 3. The generalized Alpha Plane algorithm returned the ratio of 1.85 ∠ 145°. This value is a similar but slightly better value (considering protection security) and was obtained without exercising all possible fault locations.

Next, we consider the 87LQ element while assuming an internal fault. Assume the following negative-sequence currents (in pu):

$$\bar{I}_{1Q} = 2 \angle -87°, \quad \bar{I}_{2Q} = 3 \angle -85°, \quad \bar{I}_{3Q} = 1 \angle -82° \tag{20}$$

The currents have similar phase angles, which reflects the homogeneity of the negative-sequence network.

The generalized Alpha Plane 87LQ element works with the following quantities:

$$\bar{I}_{DIF} = 6 \angle -85.2° \text{ and } I_{RST} = 6 \tag{21}$$

The R_k values are 12.0, 18.0, and 6.0, respectively. The algorithm selects the Terminal 2 current $\bar{I}_{2Q}$ as the reference (the highest R_k). Therefore, β = –85°. This selection is of secondary importance as all the fault currents flow along the same line of about –85 degrees.

Using (14) and (15), the algorithm calculates:

$$\bar{I}_{L(EQ)} = 0.06 \angle -101.9° \text{ and } \bar{I}_{R(EQ)} = 5.94 \angle -85° \tag{22}$$

The complex ratio between the two equivalent currents is:

$$\bar{k} = 98.7 \angle 16.9° \tag{23}$$

Any Alpha Plane characteristic set rationally would qualify this condition as an internal fault.

When a given line terminal is a dual-breaker connection, the remote relays working with the partial differential and partial restraining terms do not have access to the individual phasors of the two currents, but only to their sums (partial terms). This is only a minor limitation to the effectiveness of the generalized Alpha Plane algorithm because its strength results from reflecting the differential and through currents of the zone and these two signals are always represented correctly. The following example illustrates this point better.

2) Example 2: Generalized Alpha Plane Calculations for a Two-Terminal Line with Dual Breakers

Consider a two-terminal dual-breaker application with currents labeled 1 and 2 at Terminal 1 and labeled 3 and 4 at Terminal 2.

We assume an external fault at Terminal 1 downstream from CT 2. Assume the following currents of the 87L zone (in pu):

$$\bar{I}_1 = 12 \angle -87°, \ \bar{I}_2 = 8.43 \angle 138.2°, \ \bar{I}_3 = 2 \angle -70°, \ \bar{I}_4 = 3 \angle -97° \tag{24}$$

Current $\bar{I}_2$ is affected by CT saturation; its magnitude is reduced by 50 percent and its angle advanced by 45 degrees (the true value of this current is 16.9 $\angle$ 93.2°). Figure 11 plots the current phasors for better understanding.

First, we consider 87L relays having single CT inputs and therefore wired to the two CTs at each terminal connected in parallel. These relays measure the following currents:

$$\begin{aligned} I_L &= \bar{I}_1 + \bar{I}_2 = 8.52 \angle -131.7° \quad \text{at Terminal 1;} \\ I_L &= \bar{I}_3 + \bar{I}_4 = 4.87 \angle -86.2° \quad \text{at Terminal 2.} \end{aligned} \tag{25}$$

The differential signal is:

$$\bar{I}_{DIF'} = 12.4 \angle -115.5° \tag{26}$$

The percentage differential element works with a restraining signal of I_{RST} = 8.52 + 4.87 = 13.4 and therefore requires a slope of at least 12.4/13.4, or 92.5 percent, for security.

The Alpha Plane element works with the complex current ratio of:

$$\bar{k} = \frac{\left(8.52 \angle -131.7°\right)}{\left(4.87 \angle -86.2°\right)} = 1.75 \angle -45.4° \tag{27}$$

and requires a blocking angle of at least 272 degrees for security.

Both the percentage differential and the Alpha Plane elements would have difficulties providing security in this case. The reason is that these elements are connected to the paralleled CTs and are not aware of the large through-fault current that flows in and out of the line protection zone at Terminal 1.

We now consider the generalized Alpha Plane elements in 87L relays with dual CT inputs that measure both currents at each line terminal. The partial terms are:

$$\begin{gathered} \text{Terminal 1, differential:} \\ \bar{I}_1 + \bar{I}_2 = 12 \angle -8.7° + 8.43 \angle 138.2° = 8.52 \angle -131.7°, \\ \text{Terminal 1, restraining:} \\ I_1 + I_2 = 12 + 8.43 = 20.43 \\ \text{Terminal 2, differential:} \\ \bar{I}_3 + \bar{I}_4 = 2 \angle -70° + 3 \angle -97° = 4.87 \angle -86.2°; \\ \text{Terminal 2, restraining:} \\ I_3 + I_4 = 2 + 3 = 5 \end{gathered} \tag{28}$$

The generalized Alpha Plane element works with the following quantities:

$$\bar{I}_{DIF} = 12.4 \angle -115.5° \text{ and } I_{RST} = 25.43 \tag{29}$$

The R_k values are 101.6 and 52.8, respectively. The algorithm selects the Terminal 1 current $\bar{I}_1$ as the reference (the highest R_k). Therefore, $\beta = -131.7°$.

Using (14) and (15), the algorithm calculates (30). See Fig. 12 for a graphical illustration.

$$\bar{I}_{L(EQ)} = 7.19 \angle 19.4° \text{ and } \bar{I}_{R(EQ)} = 18.23 \angle -131.7° \tag{30}$$

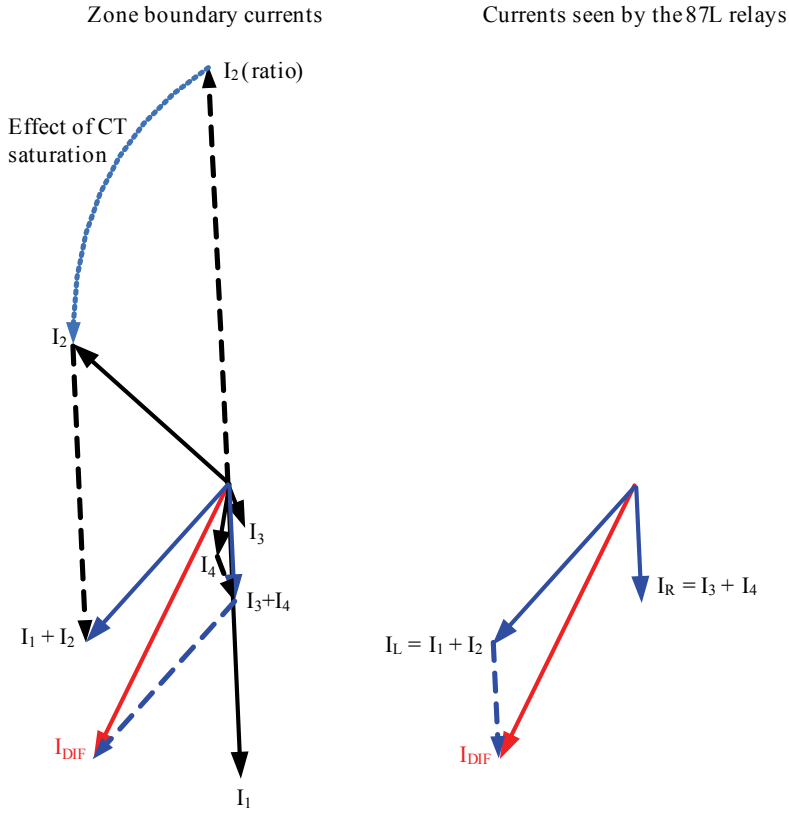

Fig. 12. Current phasors in Example 2, assuming the 87L scheme measures all zone boundary currents individually but the remote relay is provided with partial differential and partial restraining signals only, instead of individual local currents

The complex ratio between the two equivalent currents is:

$$\bar{k} = 2.53 \angle -151.2° \tag{31}$$

An Alpha Plane characteristic with the blocking angle of at least 59 degrees (the typical setting is around 180 degrees) would qualify this condition as an external fault.

In the above calculations, the selection of the reference current was limited to the two partial differential terms (sums of all local currents at each of the line terminals) because the algorithm does not have direct access to all four breaker currents.

For comparison, we assume that all four currents are communicated between the relays individually and the generalized Alpha Plane element selects the reference among all four currents (Fig. 13). If so, the R_k values are 131.1, 29.5, 17.4, and 35.4, respectively, and the algorithm selects the Terminal 1 current $\bar{I}_1$ as the reference. Therefore, $\beta = -87°$.

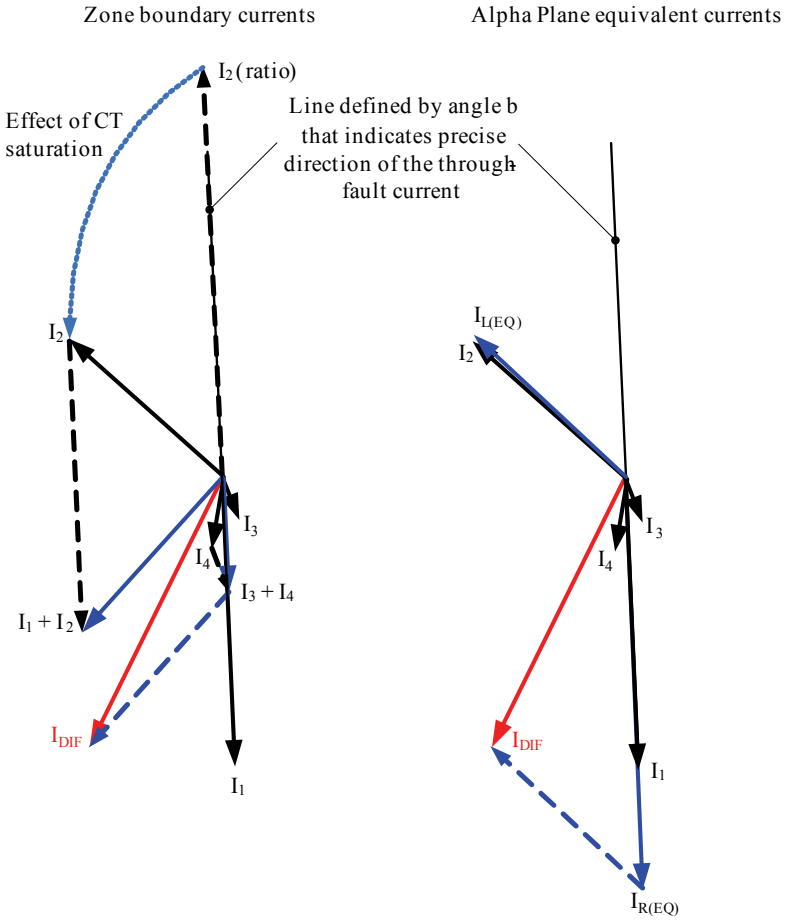

Fig. 13. Current phasors in Example 2, assuming the 87L scheme measures all zone boundary currents individually and both relays have individual access to all four zone boundary currents

Using (14) and (15), the algorithm calculates:

$$\bar{I}_{L(EQ)} = 8.46 \angle 137.4° \text{ and } \bar{I}_{R(EQ)} = 16.97 \angle -87° \tag{32}$$

The complex ratio between the two equivalent currents is:

$$\bar{k} = 2.0 \angle -135.4° \tag{33}$$

Note that the version working with the partial terms and the version working with all the currents of the 87L zone for selection of the reference current return very similar results ($2.53 \angle -151.2°$ and $2.00 \angle -135.4°$, respectively). Working with partial terms conserves the communications bandwidth and therefore is favored in practical implementations.

Next, we turn our attention back to the percentage differential characteristic, working with the restraining signal derived from all zone boundary currents (dual CT input relays). In this scenario, the percentage slope of 12.4/25.43, or 48.9 percent, ensures security (compared with 92.5 percent if the relay worked with externally paralleled CTs).

This numerical example illustrates that using true restraint derived from all 87L zone boundary currents improves security in dual-breaker applications – for both the generalized Alpha Plane and the percentage differential protection principles.

Reference [8] provides extra details on the generalized Alpha Plane concept and includes more numerical examples of (11) through (15).

6.2. BENEFITS OF THE GENERALIZED ALPHA PLANE ALGORITHM

1) Heuristic Manipulation of Differential and Restraining Signals

The differential and restraining signals are inputs to the generalized Alpha Plane calculations. They can be manipulated arbitrarily using the following concepts known in protective relaying, allowing the desired effects of such manipulation to propagate into the Alpha Plane:

- An external fault detection algorithm, upon detecting an external fault and in anticipation of possible CT saturation, can increase the level of phase restraining signals with the harmonics of the phase differential signals. The increase in the restraining signals shifts the operating point of the generalized Alpha Plane toward the ideal blocking point of $1 \angle 180°$ (see Example 4 in Section 7).
- An external fault detection algorithm, upon detecting an external fault and in anticipation of possible CT saturation, can increase the level of restraining signal for the 87LQ and 87LG elements with a portion of the maximum phase restraining signal in order to secure these functions in cases where they do not have any natural restraint. The increase in the restraining signal shifts the operating point of the generalized Alpha Plane toward the ideal blocking point of $1 \angle 180°$ (see Example 5 in Section 7).
- A line charging current compensation algorithm can reduce the amount of standing differential signal by calculating the actual present charging current and subtracting it from the measured differential signal. The reduction in the differential signal shifts the operating point of the generalized Alpha Plane toward the ideal blocking point of $1 \angle 180°$ (see Example 6 in Section 9).
- A magnetizing inrush restraining algorithm can increase the level of restraining signal with the harmonics of the differential signal in order to restrain the element under transformer inrush conditions (in applications with in-line transformers). The increase in the restraining signal shifts the operating point of

the generalized Alpha Plane toward the ideal blocking point of 1 ∠ 180° (see Example 3 that follows).

2) Example 3: Magnetizing Inrush and Harmonic Restraint

Consider an application with an in-line transformer and the case of line and transformer energization. The currents assumed are already compensated for the vector group, ratios, and zero sequence as per the art of transformer protection.

Assume the following fundamental frequency phase currents of the 87L zone (in pu):

$$\bar{I}_1 = 3 \angle -90°, \quad \bar{I}_2 = 0 \tag{34}$$

These values reflect the fact that transformer energization appears as a single-end feed.

The generalized Alpha Plane element works with the following quantities:

$$\bar{I}_{DIF'} = 3 \angle -90° \text{ and } I_{RST} = 3 \tag{35}$$

and operates in this case (single-end feed) unless harmonic blocking is in effect.

Assume harmonic restraint is used to prevent misoperation on transformer inrush – selected harmonics in the differential signal are added to the restraining signal. Assume the restraining signal is doubled as a result of the harmonic restraint. If so, the generalized Alpha Plane element with harmonic restraint for the in-line transformer works with these quantities:

$$\bar{I}_{DIF} = 3 \angle -90° \text{ and } I_{RST} = 6 \tag{36}$$

Using (14) and (15), the algorithm calculates:

$$\bar{I}_{L(EQ)} = 1.5 \angle 90° \text{ and } \bar{I}_{R(EQ)} = 4.5 \angle -90° \tag{37}$$

As a result of augmenting the restraining signal, both equivalent currents are not zero (unlike the actual currents), allowing the element to restrain. The complex ratio between the two equivalent currents is:

$$\bar{k} = 3 \angle 180° \tag{38}$$

This operating point is safely within the blocking region of a typical Alpha Plane characteristic, allowing the element to restrain properly.

In summary, having an intermediate layer of differential and restraining signals before transitioning into the Alpha Plane calculations allows the application of tried-and-true protection concepts and maximizes the advantages of both the traditional percentage differential and Alpha Plane principles.

7. ENHANCING DIFFERENTIAL ELEMENT SECURITY FOR CT SATURATION

Previous sections of this paper pointed out that CT saturation causes a fictitious differential signal and suggested methods for enhancing 87L element security. In this section, we further analyze this problem, describe various solutions in more detail, and illustrate the discussion with numerical examples, including transient simulation studies.

7.1. POWER SYSTEM SIMULATION CASES

Figure 14 shows a two-source power system that includes a short 120 kV power line. We use this elementary system to illustrate and evaluate the effect of CT saturation on a differential scheme protecting the line. We apply external (F2) and internal (F1) phase-to-ground faults close to Terminal *R* and perform steady-state and transient fault studies. For all faults, we assume the Terminal *L* CT behaves linearly. For external faults, we consider two cases for the Terminal *R* CT: linear behavior and saturation.

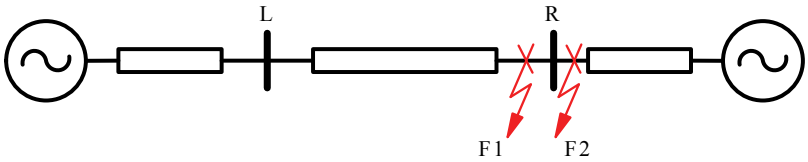

E	1 pu ∠ 0°		1 pu ∠ –4°
Z_1	0.021 ∠ 88°	0.021 pu ∠ 86°	0.021 pu ∠ 88°
Z_0	0.031 ∠ 88°	0.063 pu ∠ 75°	0.021 pu ∠ 88°

Fig. 14. Example power system

We used the Electromagnetic Transients Program (EMTP) to perform transient studies for the example power system. Fig.ure15 depicts the A-phase current waveform at Terminal R for an external A-phase-to-ground fault (F2). We use this waveform as an example to evaluate the performance of 87L schemes under transient conditions.

Table 1 lists the secondary steady-state currents measured at both line terminals by the differential scheme for the external fault. Two sets of currents are provided for Terminal *R* – assuming linear CT operation and CT saturation.

We used the concept of saturated current phasors proposed in [11] to determine the steady-state values of the secondary currents at Terminal R under CT saturation. In this concept, the secondary phasor is derived as the actual (ratio) phasor multiplied by

a complex number with a magnitude lower than 1 and a positive angle between 0 and 90 degrees to reflect saturation of the CT. This approach is justified because when a secondary current waveform of a saturated CT (such as the one in Fig. 15) is processed through a conventional filtering system, such as a full-cycle Fourier or cosine filter, the resulting current phasor has a smaller magnitude and a phase advance with respect to the actual current phasor. In order to evaluate the impact of saturation on a phasor-based protection element, the ratio current phasor can be replaced with a saturated current phasor that reflects the change in magnitude and phase angle.

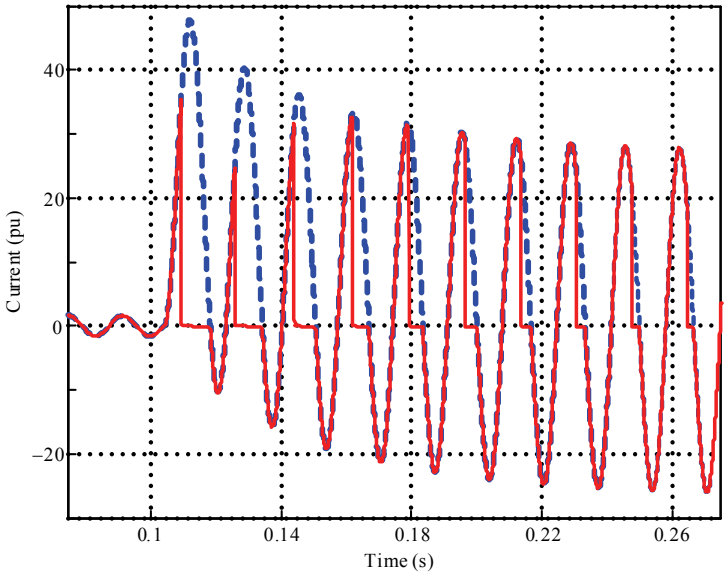

Fig. 15. A-phase CT saturation at Terminal R: ratio current (dashed line) and secondary CT current (solid line)

Table 1. Line Currents for an External Fault (F2) in Fig. 14

	Terminal *L* (pu)	Terminal *R* (pu)	
Current	Linear	Linear	Saturated
$\bar{I}_A$	19.03∠–84.4°	19.03∠95.4°	1.90∠–174.4°
$\bar{I}_B$	2.42∠93.2°	2.42∠–86.7°	2.42∠–86.7°
$\bar{I}_C$	4.36∠92.1°	4.36∠–87.8°	4.36∠–87.8°
$3\bar{I}_0$	12.26∠–82.7°	12.26∠97.2°	7.13∠–102.9°

As an example, in Table 1, we assume the A-phase current to have a magnitude equal to only 10 percent of the ratio current and a phase angle advance as high as 90 degrees. Using this saturated current phasor for A-phase, we calculate the zero-sequence current phasor shown in Table 1.

7.2. EFFECT OF CT SATURATION ON PERCENTAGE DIFFERENTIAL ELEMENTS

Consider a percentage differential element having the restraining signal (4) and the characteristic shown in Fig. 1b, with both slope lines passing through the origin (the blue characteristic).

For internal faults, the maximum possible differential signal value occurs when the terminal currents are in phase. This value equals the sum of the magnitudes of the Terminal *L* and Terminal *R* current phasors:

$$\max\left(\left|\bar{I}_{DIF}\right|\right)=\max\left(\left|\bar{I}_L+\bar{I}_R\right|\right)=\left|\bar{I}_L\right|+\left|\bar{I}_R\right| \tag{39}$$

This equation plots as a straight line of unity slope on the differential-restraining plane. Hence, the maximum allowable slope setting is 1 (100 percent). Higher values would ensure that the element would never operate for internal faults. In practice, the maximum allowable slope must be lower than 100 percent to maintain the dependability of protection because the two currents cannot be expected to be exactly in phase.

For external faults, the minimum second slope value K_2 that ensures security for CT saturation can be calculated from the differential and restraining signals obtained from the saturated phasor values. Using Table 1 data, the fictitious differential signal in the *A*-phase differential element is 19.1 pu while the restraining signal is 20.9 pu. Hence, the minimum K_2 value that would ensure security for the 87LP element in this case is:

$$K_{2(87LA)}=\frac{19.1}{20.9}=0.914 \text{ (or } 91.4\%) \tag{40}$$

For the zero-sequence differential element, the steady-state differential and restraining signals are 19.1 pu and 19.4 pu, respectively, which requires a minimum K_2 value of:

$$K_{2(87LG)}=\frac{19.1}{19.4}=0.985 \text{ (or } 98.5\%) \tag{41}$$

The K_2 values required to ensure security for the high level of CT saturation assumed in the example are very close to the maximum permissible slope value of 100 percent. Therefore, very little room is available for setting the K_2 value to maintain both security (>91.4 percent) and dependability (<100 percent). Reference [6] provides more information on balancing security and dependability in percentage differential elements.

Steady-state analysis provides a rule-of-thumb method for selecting percentage differential element settings. Transient studies are not an everyday engineering tool for settings selection, but they provide a more accurate evaluation in the context of this

paper. In the transient simulation examples that follow, we used EMTP to generate the current waveforms and processed these waveforms through a full-cycle cosine filter to obtain the current phasors.

Figure 16 shows the A-phase element transient differential signal trajectories for an internal fault without CT saturation (F1 in Fig. 14) and an external fault (F2) with CT saturation. For the external fault, the Terminal R secondary CT current waveform is that of Fig. 15. As expected, the internal fault trajectory is a straight line with a slope close to unity. It is obvious that there is not too much room to find a K_2 value that ensures sensitivity for internal faults and security for external faults with CT saturation.

Figure 17 shows the zero-sequence element transient differential signal trajectories for the same faults. In this case, it is not possible to ensure differential element sensitivity and security because the external fault trajectory transiently encroaches on the 100 percent line.

Applying an intentional time delay while using K_2 below 100 percent can provide a solution to this problem (note that the sequence elements can use high values of K_2 owing to the high homogeneity of the sequence network in the context of (39)).

These examples show that raising the characteristic slope value to cope with CT saturation has a limit, and if taken too far, it sacrifices sensitivity and, eventually, dependability.

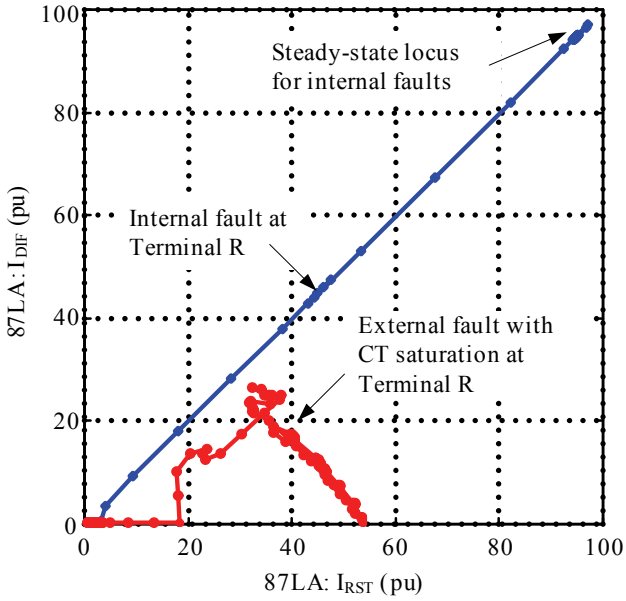

Fig. 16. A-phase element differential signal trajectories
for an internal fault and for an external fault with CT saturation

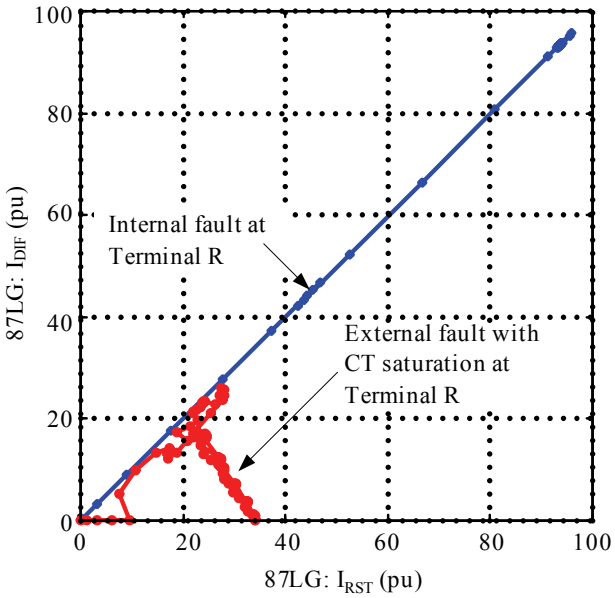

Fig. 17. Zero-sequence element differential signal trajectories
for an internal fault and for an external fault with CT saturation

7.3. EFFECT OF CT SATURATION ON ALPHA PLANE DIFFERENTIAL ELEMENTS

Consider now the Alpha Plane differential element described in Section 4, Subsection 4.3.

From the steady-state data of Table 1, the value of the current ratio as measured by the A-phase element for the external fault with CT saturation is:

$$\bar{k}_{(87LA)} = \frac{19.03 \angle -84.4°}{1.90 \angle -174.4°} = 10 \angle 90° \tag{42}$$

This complex value directly reflects the degree of saturation we assumed (tenfold reduction in the secondary current magnitude and 90-degree phase shift).

This equation indicates that the phase Alpha Plane element characteristic should have a minimum blocking radius of $R = 10$ and a minimum blocking angle of $\alpha = 180°$ to ensure security for this CT saturation case.

For the zero-sequence Alpha Plane element, the steady-state current ratio for the external fault with CT saturation is:

$$\bar{k}_{(87LG)} = \frac{12.26 \angle -82.7°}{7.13 \angle -102.9°} = 1.72 \angle 20.1° \tag{43}$$

The restraining region of the zero-sequence element characteristic cannot be enlarged to include the point corresponding to the steady-state current ratio given by (43) because this point is too close (in terms of the angle) to the internal fault region. The element would need to be set for dependability, and therefore, it may misoperate when this severe saturation occurs.

Figure 18 shows the A-phase current-ratio transient trajectory for an external fault (F2) with Terminal *R* CT saturation (using the CT waveform of Fig. 15). For this external fault, CT saturation shifts the current ratio from the ideal $1 \angle 180°$ value. Figure 18 confirms the well-established concept that enlarging the restraining area of phase element Alpha Plane characteristics provides security for CT saturation [1, 3, 10].

Figure 19 shows the zero-sequence current-ratio transient trajectory for an external fault (F2) with Terminal *R* CT saturation. Fig. 19 confirms that the angular expansion of the zero-sequence element characteristic required to avoid misoperation would make it encroach on the internal fault region shown in Fig. 3 through Fig. 5. Negative-sequence Alpha Plane elements have the same problem. In general, sequence Alpha Plane elements cannot be set to ensure security for external faults with heavy CT saturation [11] unless they incorporate extra security measures such as external fault detection or time delay, as explained later in this section.

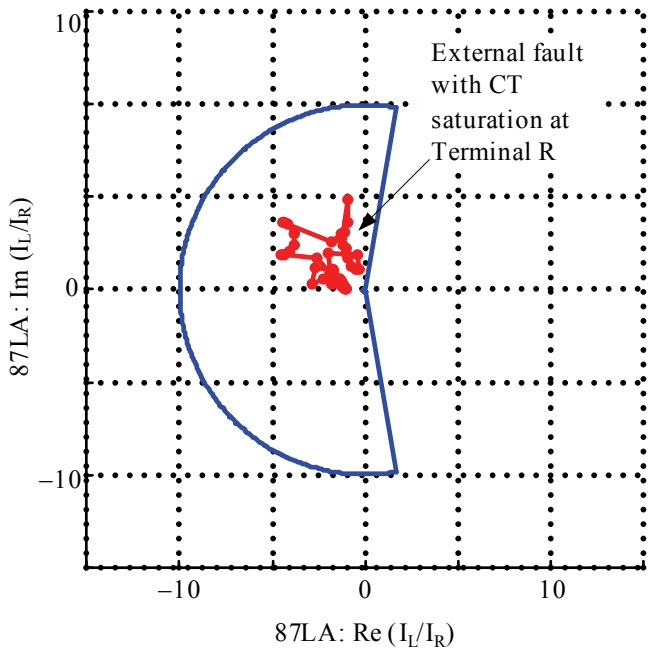

Fig. 18. A-phase current-ratio transient trajectory for an external fault with CT saturation

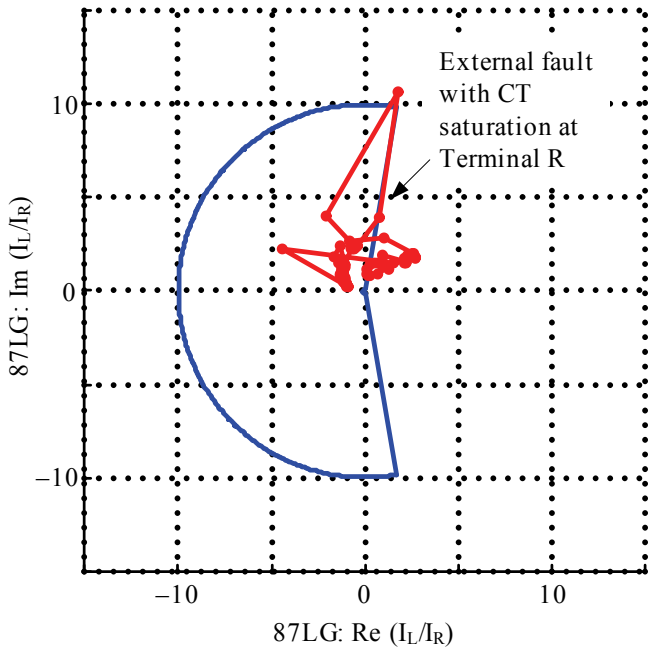

Fig. 19. Zero-sequence current-ratio transient trajectory for an external fault with CT saturation

7.4. EXTERNAL FAULT DETECTION ALGORITHMS

Section 7, Subsections 7.2 and 7.3 show that setting differential elements with fixed characteristics to ensure security for external faults with heavy CT saturation impairs element sensitivity. Moreover, percentage differential elements are difficult to set (and, in some cases, cannot be set) to ensure security for these faults. Phase Alpha Plane differential elements can be set to ensure security, but sequence Alpha Plane elements cannot be set for many CT saturation cases [11].

Section 3, Subsection D and Section IV, Subsection D suggest adaptive methods to accommodate CT saturation and other sources of fictitious differential signals without penalizing differential element sensitivity. These methods include modifying the element characteristic and adding terms to the restraining signal under the control of dedicated logic.

The logic for activating CT saturation countermeasures can be based on the following:

- Detecting external faults [1,8,12]. This method responds to the symptoms of external faults, operates on raw samples, and asserts before and regardless of CT saturation.
- Detecting CT saturation. This method is slower than the previous one because it is based on the symptoms of CT saturation and therefore needs to wait for CT

saturation to actually occur. Reference [11] describes a saturation detector that measures the levels of the dc component and the second harmonic of the phase currents.

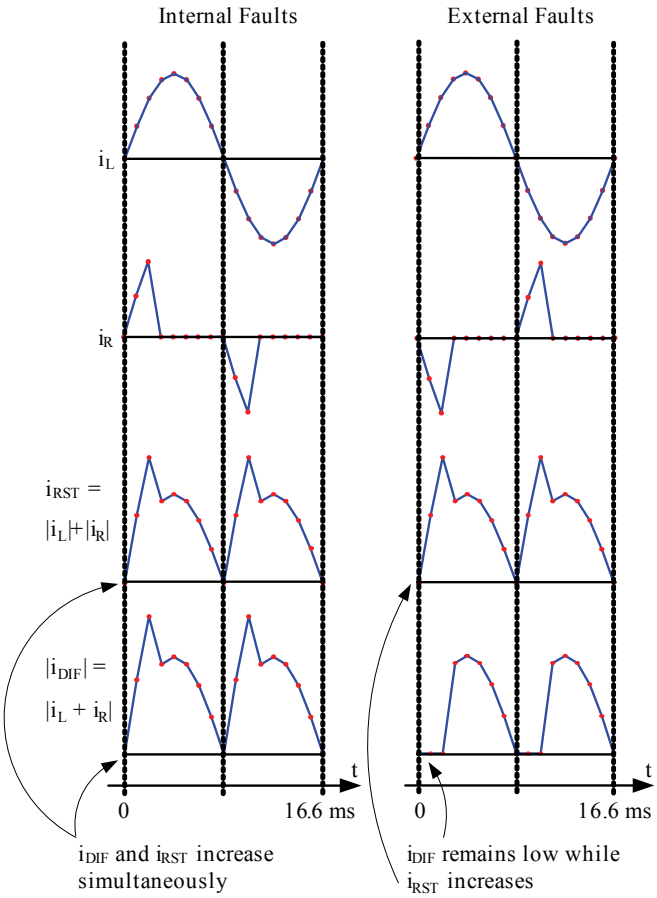

Fig. 20. External fault detection principle

Figure 20 illustrates the basic principle of a commonly used algorithm for detecting external faults. It shows the terminal (i_L and i_R), differential (i_{DIF}), and restraining (i_{RST}) signals for faults that cause saturation of the Terminal *R* CT. For internal and external faults, the Terminal *R* current i_R shows the typical CT saturation waveform – the CT reproduces the primary current well within the first few milliseconds after fault inception. The restraining and differential signals have the same behavior for internal faults; both signals grow in the first few milliseconds after fault inception when the CTs behave linearly. However, for external faults, the restraining signal grows, but the differ-

ential signal is practically zero in the first few milliseconds. The external fault detector (EFD) uses this information to discriminate between internal and external faults before and regardless of CT saturation. This means that the EFD asserts for all external faults even if CTs do not saturate and does not assert for internal faults even if CTs saturate. Figure 20 uses two currents for simplicity, but the principle works for any number of currents – the remote current in Fig. 20 can be understood as the external fault current, with the local current as the sum of all the other zone boundary currents.

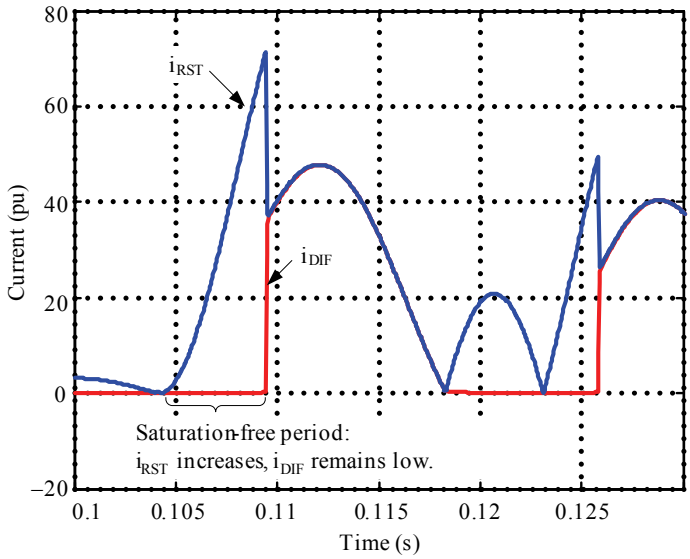

Fig. 21. Differential and restraining signals resulting from the current waveform shown in Fig. 15 for an external fault

Figure 21 shows the differential and restraining signals obtained from the raw samples of the saturated current shown in Fig. 15 for an external fault. The differential signal stays close to zero for 5 milliseconds, while the restraining signal rises immediately after the fault inception.

Figure 22 shows one possible logic implementation of the EFD that can use either instantaneous or phasor quantities. The logic uses incremental quantities (derived over a one cycle time span) to prevent the EFD from picking up on load currents [13]. The EFD asserts when the incremental restraining signal becomes greater than some threshold value P and, at the same time, the incremental differential signal remains smaller than a percentage (q factor) of the restraining signal during 3/16 of a cycle. Once the EFD picks up, it will remain in that state during the timer dropout time DPO.

The EFD logic is applicable to differential elements with any number of input currents.

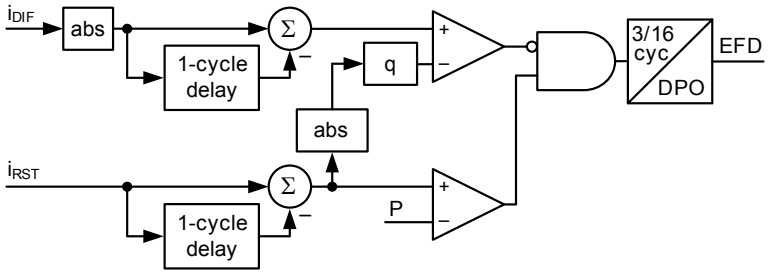

Fig. 22. External fault detector logic

7.5. ADAPTIVE PERCENTAGE DIFFERENTIAL ELEMENTS WITH EXTERNAL FAULT DETECTION

As mentioned previously, an adaptive differential element can use an EFD to trigger measures to mitigate the effect of CT saturation. In percentage differential elements, EFD assertion may increase the level of the restraining signal.

One approach is to apply factors greater than 1 (should the EFD assert) to the terminal currents used to calculate the restraining signal, as (44) shows for a two-restraint element.

$$I_{RST} = m_L \cdot \left|\bar{I}_L\right| + m_R \cdot \left|\bar{I}_R\right| \tag{44}$$

Figure 23 illustrates the effect of applying this method to the same A-phase percentage differential element as in Fig. 16. In this example, when creating the restraining signal, the element multiplies the currents when the EFD asserts. As a result, the trajectory moves to the right, which allows the use of a lower slope value to stabilize the element.

Another approach for increasing the restraining signal is to add terms given by the squared differences between the samples of the actual current waveform and the ideal sine wave (as estimated by the relay phasor estimator), summed over the length of the data window. When using half- or full-cycle Fourier filters, the said sum of the squared differences equals the difference between the root-mean-square (rms) value and the fundamental component magnitude of each terminal current:

$$I_{RST}^2 = \left|\bar{I}_L\right|^2 + m_L \cdot \left(I_{L(RMS)}^2 - \left|\bar{I}_L\right|^2\right) + \left|\bar{I}_R\right|^2 + m_R \cdot \left(I_{R(RMS)}^2 - \left|\bar{I}_R\right|^2\right) \tag{45}$$

The added terms reflect the amount of dc offset and harmonics present in the terminal currents in case of CT saturation. Figure 24 illustrates the effect of this compensation on the element of Fig. 16. Again, the trajectory moves to the right and allows the use of a smaller slope value.

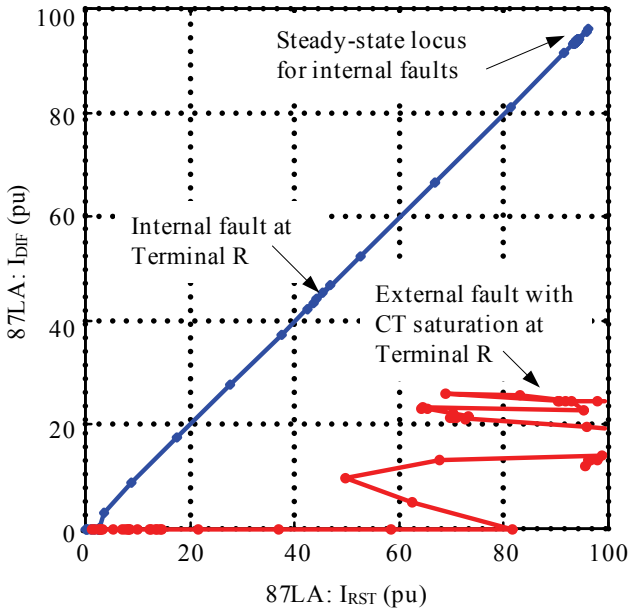

Fig. 23. Multiplying the current of the terminal with CT saturation by a factor enhances percentage differential element security

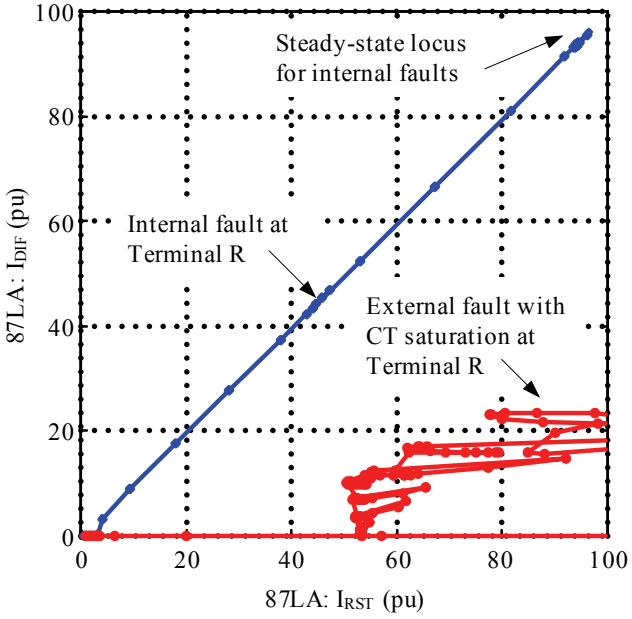

Fig. 24. Adding to the restraining signal terms corresponding to the difference between the rms and fundamental component currents enhances percentage differential element security

7.6. ADAPTIVE ALPHA PLANE DIFFERENTIAL ELEMENTS WITH EXTERNAL FAULT DETECTION

Differential elements based on the generalized Alpha Plane principle (Section 6) can apply the following measures upon assertion of the EFD:

- For phase and sequence elements, increasing the blocking radius, R, and/or the blocking angle, α, of the element characteristic.
- For phase elements, adding a percentage of the differential signal harmonics to increase the restraining signal that feeds the generalized Alpha Plane calculations (see Example 4 and Fig. 25).

For sequence elements, adding a fraction of the maximum phase restraining signal to increase the restraining signal that feeds the generalized Alpha Plane calculations (see Example 5 and Fig. 26).

The following two steady-state examples illustrate the methods for increasing security in adaptive Alpha Plane elements. Each example is followed by a corresponding transient simulation example.

1) Example 4: Using Harmonics to Increase Security of 87LP Elements During External Faults

Consider a two-terminal single-breaker line and an external fault with CT saturation at one terminal.

Assume the following phase currents of the 87L zone (in pu):

$$\bar{I}_1 = 20 \angle -85°, \;\; \bar{I}_2 = 10 \angle 135° \tag{46}$$

The second current is impacted by CT saturation; its magnitude is reduced by half and its angle advanced by 40 degrees.

The generalized Alpha Plane 87LP element works with the following quantities:

$$\bar{I}_{DIF} = 13.9 \angle -112.5° \;\text{ and }\; I_{RST} = 30 \tag{47}$$

Using (14) and (15), the algorithm calculates:

$$\bar{I}_{L(EQ)} = 10 \angle 135° \;\text{ and }\; \bar{I}_{R(EQ)} = 20 \angle -85° \tag{48}$$

As expected, the equivalent currents match the actual currents in this case of a zone bounded with two currents. The complex ratio between the two equivalent currents (or actual currents) is:

$$\bar{k} = 2 \angle 140° \tag{49}$$

The value of 2 reflects the 50 percent magnitude error due to CT saturation, and the angle of 140 degrees reflects the 40-degree phase error due to CT saturation (180° – 140° = 40°).

As expected, the generalized Alpha Plane element performs very well in this case because the zone is bounded by only two currents. Its performance can be further improved as follows.

Assume now that, upon detecting an external fault, the element adds harmonics from the differential signal to the restraining signal in order to increase security even more. Assume that, as a result of the adaptive addition of harmonics, the restraining signal is increased by 25 percent. If so, the generalized Alpha Plane element works with the following signals:

$$\bar{I}_{DIF} = 13.9 \angle -112.5° \text{ and } I_{RST} = 37.5 \tag{50}$$

Using (14) and (15), the algorithm calculates:

$$\bar{I}_{L(EQ)} = 13.4 \angle 123.7° \text{ and } \bar{I}_{R(EQ)} = 24.1 \angle -85° \tag{51}$$

The equivalent currents differ from the actual currents as a result of the arbitrary manipulation of the restraining signal. The complex ratio between the two equivalent currents is now:

$$\bar{k} = 1.80 \angle 151° \tag{52}$$

This operating point is located deeper within the blocking region of the Alpha Plane characteristic compared with the operating point of the traditional Alpha Plane characteristic (2.00 ∠ 140°), which provides even more security.

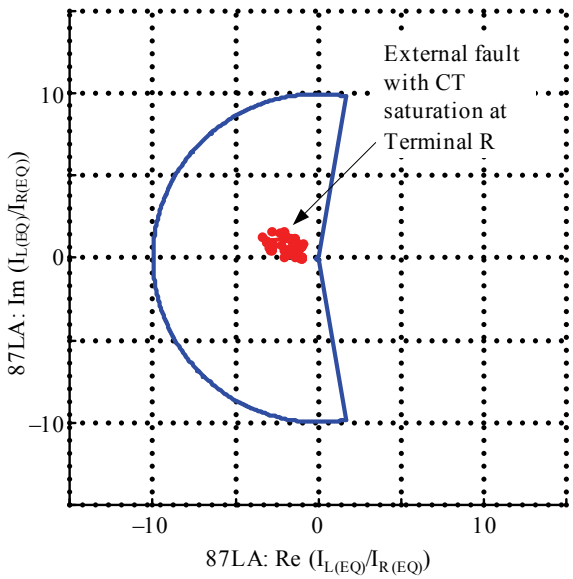

Fig. 25. Adding differential signal harmonics to the restraining signal improves the security for CT saturation of phase generalized Alpha Plane elements

Figure 25, obtained from a transient simulation of the Fig.14 system, also demonstrates the effect of adding harmonics to the phase element restraining signal. Figure 25 refers to the same A-phase Alpha Plane element as Fig. 18, but in this case, the element adds the magnitudes of selected harmonics of the differential signal to the restraining signal when the EFD asserts. The additional restraining action provided by harmonics concentrates the current-ratio trajectory much closer to the ideal $1 \angle 180°$ point than in the case of Fig. 18. Expanding the element characteristic as shown in Fig. 5b upon EFD assertion further improves element security.

2) Example 5: Using Cross-Phase Restraining to Increase Security of 87LQ Elements During External Faults

Consider a two-terminal single-breaker line and an external three-phase symmetrical fault with saturation of one of the CTs at Terminal 2. We analyze the impact on the 87LQ element.

Assume the following A-phase currents of the 87L zone (primary currents in pu):

$$\bar{I}_1 = 20 \angle -85°, \;\; \bar{I}_2 = 20 \angle 95° \tag{53}$$

The three-phase currents are balanced at Terminal 1, yielding a negative-sequence current equal to zero. However, as one of the CTs saturates at Terminal 2 (assume the A-phase CT saturates heavily, reducing the current magnitude to 10 percent of the actual value and advancing the angle by 80 degrees), the Terminal 2 relay receives a fictitious negative-sequence current, as follows:

$$\bar{I}_{1Q} = 0 \angle 0°, \quad \bar{I}_{2Q} = 6.58 \angle -91° \tag{54}$$

The generalized Alpha Plane 87LQ element works with the following quantities:

$$\bar{I}_{DIF} = 6.58 \angle -91° \text{ and } \; I_{RST} = 6.58 \tag{55}$$

These currents represent a single-end feed condition. Traditional Alpha Plane and percentage differential elements cannot be restrained for this condition.

Assume that, upon detecting an external fault, the 87LQ element adds 10 percent of the highest phase restraining signal to the negative-sequence restraining signal. If so, the generalized Alpha Plane 87LQ element works with the following quantities:

$$\bar{I}_{DIF} = 6.58 \angle -91° \text{ and } \; I_{RST} = 6.58 + 0.1 \cdot (20 + 20) = 10.58 \tag{56}$$

Using (14) and (15), the algorithm calculates:

$$\bar{I}_{L(EQ)} = 2 \angle 89° \text{ and } \; \bar{I}_{R(EQ)} = 8.58 \angle -91° \tag{57}$$

The complex ratio between the two equivalent currents is calculated as:

$$\bar{k} = 4.29 \angle 180° \tag{58}$$

This operating point is located within the blocking region of a typically set Alpha Plane characteristic, which provides security to the 87LQ element, despite the 90 percent magnitude and 80-degree phase error in the A-phase current and only 10 percent of extra restraining signal added from the phase currents.

Figure 26, obtained from a transient simulation of the Fig.14 system, also shows the effect of using the phase restraining signal to increase the zero-sequence element restraining signal. In this example, EFD assertion adds 100 percent of the maximum phase current to the restraining signal used for the generalized Alpha Plane calculations. Comparing Fig. 26 with Fig. 19, we conclude that the EFD logic enhances the zero-sequence Alpha Plane element security to the point of completely stabilizing it. The same method is applicable to negative-sequence Alpha Plane elements.

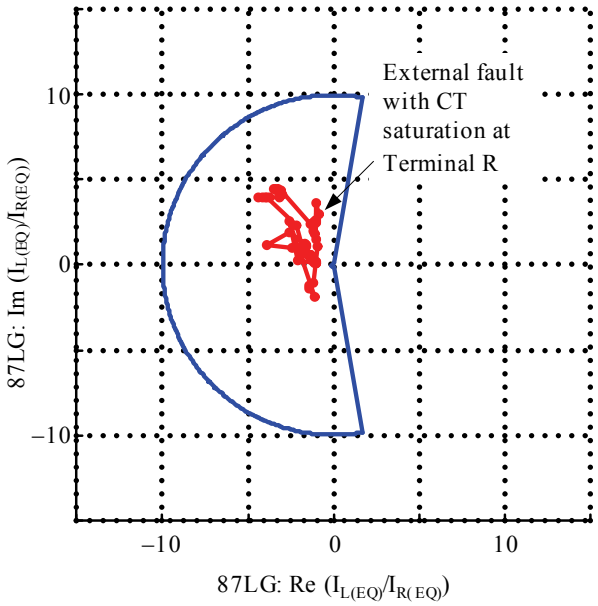

Fig. 26. Adding a fraction of the phase restraining signal to the sequence restraining signal improves the security for CT saturation of sequence generalized Alpha Plane elements

8. SECURITY UNDER CURRENT ALIGNMENT ERRORS

This section explains current alignment errors in more detail, reviews sources of alignment errors, and discusses possible countermeasures applied in 87L relays. These countermeasures often augment the operating characteristic of the 87L elements, making them unique compared with other differential elements. As we will see, the behavior of the 87L communications channel or external time sources can have an

impact on the restraining means applied and, as a result, on the security and sensitivity of the 87L protection elements.

8.1. UNDERSTANDING ALIGNMENT ERRORS

A current alignment error refers to a situation where the remote and local currents used in the differential calculations are misaligned (displaced by a non-zero time interval, ΔT). Normally, differential elements use aligned current data, meaning $\Delta T = 0$. By differential calculations, we mean operations that are sensitive to current sampling, such as deriving the differential current (instantaneous, phasor, or harmonic values) or executing the external fault detection logic.

Certain quantities are not subject to misalignment. For example, the two local currents measured by a single relay in dual-breaker applications are always aligned. In some cases, such as the restraining signal calculation, current misalignment has a very limited impact on 87L element performance.

To understand the issue of misalignment, it is convenient to consider the phasors of the local and remote currents. In this context, the timing error ΔT is equivalent to a fictitious phase shift $\Delta\Theta$ of one of the currents (assume the remote current) with respect to its true position by the equivalent portion of the signal period. Remember that a channel asymmetry of ΔT_A causes the ping-pong algorithm to misalign the data by half of ΔT_A. Therefore:

$$\Delta\Theta = 2\pi \cdot f \cdot \Delta T = \pi \cdot f \cdot \Delta T_A \tag{59}$$

For example, a channel asymmetry of 2 milliseconds causes the ping-pong algorithm to misalign the currents by 1 millisecond in a 60 Hz system, which is equivalent to a 21-degree fictitious angle shift of the 60 Hz phasor.

First, we consider the through-current case of Fig. 27a in the context of security. Applying basic trigonometry to the phasors of Fig. 27a allows us to estimate the fictitious differential signal:

$$I_{DIF} = 2 \cdot I \cdot \sin\left(\frac{\Delta\Theta}{2}\right) = 2 \cdot I \cdot \sin\left(\pi \cdot f \cdot \Delta T\right) \tag{60}$$

For example, in a two-terminal application with a load current of 1 pu and a misalignment of 2 milliseconds (4-millisecond channel asymmetry when using the ping-pong algorithm), the fictitious differential signal is 0.74 pu.

Equation (60) shows the following:

- The fictitious differential signal depends on the degree of misalignment. For example, in a 60 Hz system, 0.5 millisecond of timing error leads to a fictitious differential signal of 19 percent of the through current, 1 millisecond yields 38 percent, 1.5 milliseconds yields 56 percent, and 2 milliseconds yields 74 percent.

- The fictitious differential signal is proportional to the misaligned terminal current. In two-terminal applications, the error is proportional to the line load or external fault current. In multiterminal applications, the errors add (in the worst case) for all line terminal currents that are misaligned.

Equation (60) establishes an important between the phase and sequence differential elements. The 87LP elements respond to phase currents, and therefore, they measure the fictitious differential signal under normal load conditions. The 87LQ or 87LG elements only respond to sequence currents; misalignment during balanced load conditions does not expose these elements to any security concerns.

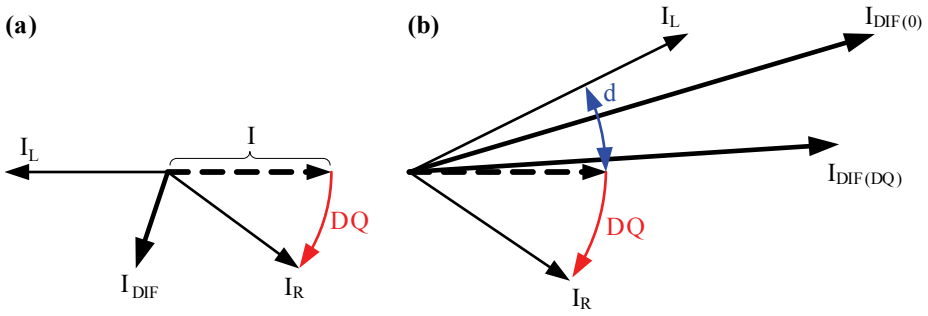

Fig. 27. Impact of misalignment for the through-current case (a) and the internal fault case (b)

Next, we consider the internal fault case of Fig. 27b in the context of dependability. We assume the currents have a phase shift δ. Applying basic trigonometry to the phasors of Fig. 27b allows us to estimate the impact of misalignment on the differential signal. We use the squared differential signal rather than the differential signal for the simplicity of the resulting equations.

The squared differential signal without any misalignment is a function of the magnitudes of the two currents and the angle δ between the two currents:

$$I_{DIF(0)}^2 = I_L^2 + I_R^2 + 2 \cdot I_L \cdot I_R \cdot \cos\delta \tag{61}$$

The squared differential signal with misalignment (in the worst-case scenario, when the phase shift $\Delta\Theta$ caused by misalignment adds to the δ phase shift) can be obtained by substituting δ with $\delta + \Delta\Theta$ in (61):

$$I_{DIF(\Delta\Theta)}^2 = I_L^2 + I_R^2 + 2 \cdot I_L \cdot I_R \cdot \cos(\delta + \Delta\Theta) \tag{62}$$

For example, in a two-terminal application with fault current contributions of 2 pu and 3 pu and a 60-degree phase shift between the two terminal currents, the actual differential signal is 4.36 pu, per (61). With a misalignment of 2 milliseconds (4-millisecond channel asymmetry when using the ping-pong algorithm) in the unfavorable direction, the differential signal only reaches 3.20 pu, per (62), a decrease

of 27 percent, which jeopardizes the percentage differential element sensitivity. In addition, the 2 milliseconds of misalignment (4 milliseconds of asymmetry) adds an extra phase shift of 42 degrees, making the two currents appear 102 degrees apart, which jeopardizes the Alpha Plane element sensitivity.

The impact of misalignment can be evaluated as the difference between the squared differential signals without misalignment (61) and with misalignment (62):

$$I_{DIF(0)}^2 - I_{DIF(\Delta\Theta)}^2 = 2 \cdot I_L \cdot I_R \cdot \left(\cos\delta - \cos\left(\delta + \Delta\Theta\right)\right) \tag{63}$$

Equation (63) shows the following:

- The impact of misalignment depends on the magnitudes of the local and remote currents. Therefore, the impact is greater when the two currents are large and lower if one or both of the currents are small. This fact agrees with the intuitive observation that single-end-feed internal faults are not impacted by misalignment.
- The differential signal decreases as a result of misalignment. This is because the cosine function decreases when its argument increases (Fig. 28). Therefore, $\cos(\delta + \Delta\Theta) < \cos\delta$, and consequently, $I_{DIF(0)}^2 - I_{DIF(\Delta\Theta)}^2 > 0$. This differential signal decrease affects 87L element sensitivity.
- The impact of misalignment increases when the fictitious angle shift $\Delta\Theta$ increases (Fig. 28a).
- The impact of misalignment is greater when the two currents are more phase-shifted (higher values of δ). This is because the steepness of the cosine function increases when its argument increases, departing from zero (Fig. 28b).

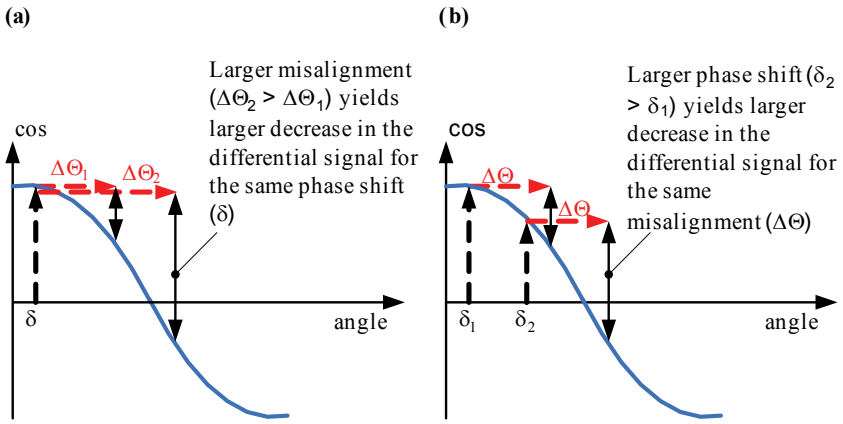

Fig. 28. Impact of misalignment for the through-current case (a) and the internal fault case (b)

Equation (63) establishes an important difference between the phase and sequence differential elements. The 87LP elements respond to internal fault currents that are

shifted by potentially considerable angles because of the prefault power flow. The 87LQ or 87LG elements respond to internal currents that are almost perfectly in phase and therefore are impacted much less than 87LP elements by misalignment during internal faults (refer to Fig. 28b, and assume $\delta_1 \approx 0$ for sequence elements and $\delta_2 \gg 0$ for phase elements).

Finally, we look at applications with in-line transformers, which require calculating the harmonics of the differential current for blocking or restraining. Equation (59) applies not only to the fundamental frequency phasors but also to harmonics. A misalignment of 1.66 milliseconds creates a 36-degree fictitious shift in a 60 Hz component. The same 1.66 milliseconds of misalignment shifts the second-harmonic phasor by 72 degrees and the fifth-harmonic phasor by 180 degrees. Having shorter periods, harmonics are more sensitive to misalignment.

Consider the fifth-harmonic blocking method to prevent misoperation during transformer overexcitation conditions. The fifth harmonics supplied from transformer windings naturally add up, giving a solid base for blocking. However, a 180-degree error in the angle of the fifth harmonic, caused by an alignment error of 1.66 milliseconds, would make the winding fifth harmonics effectively subtract, resulting in low fifth-harmonic measurements and a loss of security.

Similar considerations apply to external fault detection logic. Some algorithms require tight timing relationships between signals to distinguish between internal and external faults. A misalignment in the order of 2 or 3 milliseconds can challenge such algorithms (see Section 7 for more information).

In summary, consider the following points:

- Misalignment increases the differential signal during through-current conditions, jeopardizing protection security. Misalignment can decrease the differential signal during internal faults, reducing protection sensitivity, regardless of any settings selection already in place to maintain security.
- The impact of misalignment on the current ratio of the Alpha Plane characteristic is a simple angle shift that creates a circular locus that crosses by the $1 \angle 180°$ point (Fig. 4).
- The impact of misalignment on the operating point of the percentage differential characteristic is a straight line with a considerable slope that depends on the degree of misalignment.
- Sequence differential elements are less impacted by misalignment than phase differential elements.
- In multiterminal applications, the effects for all terminals add up and depend on the magnitudes and degrees of misalignment of the terminal currents.

Certain functions, such as harmonic blocking or external fault detection, can be more sensitive to current alignment errors than functions based on fundamental frequency components.

8.2. SOURCES OF ALIGNMENT ERRORS

The most common sources of current misalignment are the following [4]:

- Channel asymmetry when using the channel-based (ping-pong) synchronization method. This is the most common source of misalignment, calling for symmetrical channels or external time-based synchronization. It must be emphasized that, if a fairly symmetrical channel is not consistently available or the application does not allow the use of external time sources for protection, the 87L principle cannot be reliably applied. The Alpha Plane characteristic has better tolerance than the percentage differential characteristic of alignment errors, but both characteristics reach their limits when the fictitious angle shift approaches 90 degrees, equivalent to a quarter of a power cycle in terms of timing error and half a cycle in terms of channel asymmetry when using the ping-pong algorithm. Other algorithms that respond to smaller time differences, such as harmonic calculations or external fault detection, are even more sensitive to misalignment. Note that two relays working over a given channel and connected to the same time reference (historically, GPS clocks) can measure channel asymmetry and use it for alarming or securing the 87L scheme when the channel (which was procured, engineered, and commissioned as symmetrical) is no longer symmetrical.
- Time source errors when using the external time-based synchronization method. In the external time-based synchronization mode, 87L schemes use time as served by time sources connected to the relays (historically, GPS clocks). If these sources are not accurate, such as upon loss of GPS reception or GPS jamming or spoofing [14], the data are likely to be misaligned. A terrestrial time-distribution system recently developed alleviates some of the disadvantages of using GPS timing for protection applications [14]. Time sources following the IEEE C37.118 time-quality bit extension of the IRIG-B signal inform the application in the end device about the estimated worst-case timing error. Typically, 87L relays examine the time-quality bits and apply extra security measures should any time source report degraded time quality. In addition, the relays monitor the consistency of the timing signal in general.
- Transients in the internal alignment algorithms. Often, 87L relays apply a certain degree of intentional inertia when deriving the timing information for current aligning. The methods, which include averaging or phase-lock looping, allow relays to ride through temporary loss of timing signals or switching events in communications networks. The dynamic behavior associated with the internal inertia may create transient alignment errors until the averaging filters settle or phase-lock loops converge. This is typically the case when the relay is powered up or when it recovers from a communications failure or a major communications network path switching event. These errors can be estimated and

accounted for by the 87L relays because the inner workings of the relays create them in the first place.

- Misbehavior of the communications equipment. Variability in the channel propagation time, frequent path switching as a result of a failing component or other problems, and other similar events can lead to errors in channel-based alignment algorithms. The intentional inertia applied when deriving timing information is a mitigating factor, but a drastic misbehavior of the communications channel can lead to alignment errors. The 87L relay can watch the consistency of the raw timing measurements and use the measures of spread or variation as an indication of a potential timing error (for example, a variation in the round-trip channel time can indicate channel timing problems).

8.3. COUNTERMEASURES TO ALIGNMENT ERRORS

It is possible for an 87L relay to estimate the amount of potential misalignment, as explained when we discussed the sources of alignment errors in the previous subsection. The relay can use this information to adaptively increase security.

1) Alpha Plane Characteristic

The Alpha Plane characteristic is designed to tolerate large phase errors (Fig. 9), making the 87LP elements secure and intentionally less sensitive, while relying on the 87LQ and 87LG elements for sensitivity.

In addition to this inherent immunity, adaptive Alpha Plane 87L elements can engage more secure settings upon suspecting increased alignment errors (Fig. 5b).

2) Percentage Differential Characteristic

The percentage differential characteristics can be severely impacted by alignment errors and would require high slope settings values to retain security. Some implementations [15] rely on increasing the restraining signal proportionally to the product of the suspected alignment error and the associated current in order to match the nature of the fictitious differential signal per (60):

$$I_{RST} = I_{RST(CURRENTS)} + \varepsilon(\Delta\Theta) \cdot I_{RST(REM)} \tag{64}$$

where:

I_{RST} is the effective restraining signal.

$I_{RST(CURRENTS)}$ is the traditional restraining signal derived from the 87L zone boundary currents using, for example, (4) though (6).

$\varepsilon(\Delta\Theta)$ is an arbitrary measure of potential misalignment of data from a given remote 87L relay.

$I_{RST(REM)}$ is the contribution to the restraining signal from the said remote 87L relay. Multiterminal applications can add the $\varepsilon(\Delta\Theta) \cdot I_{(RST(REM))}$ terms for all remote relays.

Another approach is to use a simplified version of (64) without making a distinction between the various line terminals:

$$I_{RST} = I_{RST(CURRENTS)} + \varepsilon(\Delta\Theta) \cdot I_{RST(CURRENTS)} \tag{65}$$

Equation (65) simply adds an adaptive multiplier to the traditional restraining signal:

$$I_{RST} = (1 + \varepsilon(\Delta\Theta)) \cdot I_{RST(CURRENTS)} \tag{66}$$

Combined with the percentage slope characteristic (8), the adaptive multiplier translates into an adaptive slope:

$$I_{DIF} = K \cdot (1 + \varepsilon(\Delta\Theta)) \cdot I_{RST(CURRENTS)} \tag{67}$$

Equation (67) is equivalent to dynamically increasing the slope based on the suspected alignment error. Alternatively, the percentage differential element can just switch between two or more slope values based on the estimated alignment error (Fig. 2).

9. LINE CHARGING CURRENT COMPENSATION

As mentioned in Section 2, Subsection 2.2, the line charging current appears to the 87L elements as a fictitious differential signal and jeopardizes security. Under balanced conditions, the line charging current only affects phase differential elements. However, under unbalanced conditions (open-phase conditions, for example), the line charging current also affects sequence differential elements.

Three possible approaches to mitigate the impact of the line charging current on 87L elements are as follows:

- Setting the differential element pickup value above the charging current with margin. This approach is simple to apply and does not require relays with built-in charging current compensation. However, it limits sensitivity, especially for the phase elements in applications with long lines and cables. The addition of sequence differential elements significantly improves 87L sensitivity when using this approach – the pickup value of these elements needs to be set only above the small, normal system unbalance. This pickup value should be raised during open-phase conditions (in single-pole tripping applications, for example), which cause a significant level of sequence charging currents, with the consequence that the sensitivity will be further reduced.
- Subtracting a standing value in the differential signal from the measured differential signal. In one implementation for phase 87L elements [16], the relay stores steady-state differential signal values, averages them over a number of

power cycles, and uses this value as the presumed line charging current. This method does not require voltage information and provides higher sensitivity than the previous method. However, the standing differential signal does not match the transient inrush component caused by line energization. Increasing the differential element pickup value to avoid misoperation for line energization limits 87L sensitivity. In addition, when de-energizing the line (i.e., when opening the last breaker), the standing differential signal subtracted from the zero differential signal after line de-energization would make the 87L elements operate and generate confusing targets for the system operators.

- Calculating the phase charging currents using the measured voltages and an adequately accurate line model and subtracting the calculated currents from the measured phase currents [8]. This method provides the most accurate compensation and works well under unbalanced and transient conditions. However, the method requires voltage information.

9.1. PRINCIPLE OF VOLTAGE-BASED COMPENSATION

Figure 29 shows the distributed capacitance model of a three-terminal line that we will use to explain the principle of line charging current compensation using measured voltage information. Figure 30 depicts the line lumped parameter model. The line draws a charging current component at each terminal. The current distribution depends on the line and system parameters, as well as on the voltage profile along the line. However, for charging current compensation, we only need information on the total charging current. The current distribution among the terminals is not relevant. The total line charging current can be well approximated as the current drawn by the total line capacitance (a relay setting) under the average line voltage (calculated from the measured line terminal voltages), as (68) shows.

$$i_{C\_TOTAL} = C_{TOTAL} \cdot \frac{d}{dt} v_{AVERAGE} \tag{68}$$

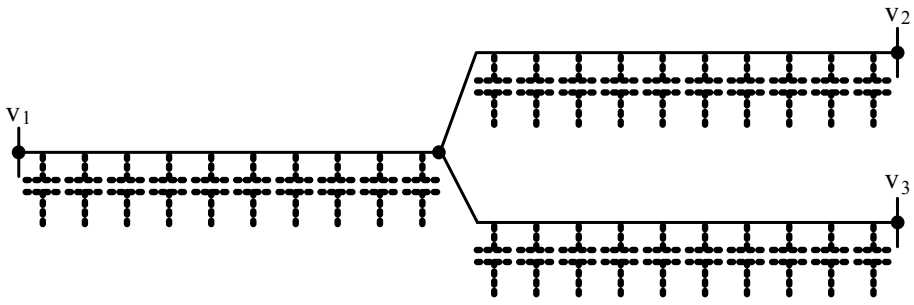

Fig. 29. Distributed capacitance three-terminal line model

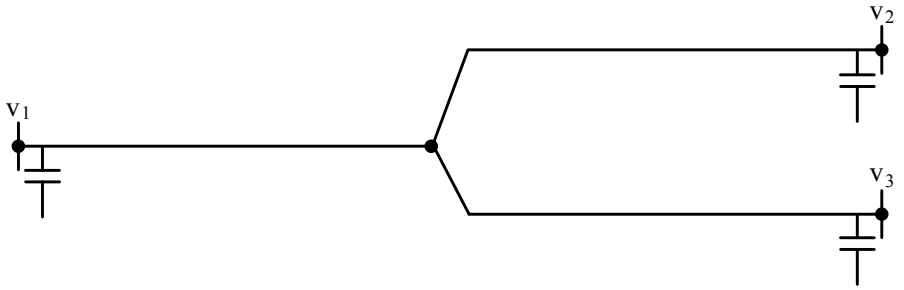

Fig. 30. Lumped parameter three-terminal line model

The average line voltage can be approximated by the average terminal voltage (assuming there is no fault on the protected line):

$$i_{C\_TOTAL} = C_{TOTAL} \cdot \frac{1}{3} \cdot \frac{d}{dt}\left(v_1 + v_2 + v_3\right) \tag{69}$$

Rearranging further:

$$i_{C\_TOTAL} = \frac{1}{3} \cdot C_{TOTAL} \cdot \frac{d}{dt} v_1 + \frac{1}{3} \cdot C_{TOTAL} \cdot \frac{d}{dt} v_2 + \frac{1}{3} \cdot C_{TOTAL} \cdot \frac{d}{dt} v_3 \tag{70}$$

In other words, the total charging current is the sum of three components:

$$i_{C\_TOTAL} = i_{C1} + i_{C2} + i_{C3} \tag{71}$$

each derived from a single line terminal voltage:

$$i_{C1} = \frac{1}{3} \cdot C_{TOTAL} \cdot \frac{d}{dt} v_1 \tag{72}$$

$$i_{C2} = \frac{1}{3} \cdot C_{TOTAL} \cdot \frac{d}{dt} v_2 \tag{73}$$

$$i_{C3} = \frac{1}{3} \cdot C_{TOTAL} \cdot \frac{d}{dt} v_3 \tag{74}$$

Equations (72) through (74) show that each terminal can calculate a share of the total charging current based on local voltage and a portion of the total line capacitance. This portion is inversely proportional to the number of relays located at different line terminals that perform the compensation at any given time. In general, for a line with N terminals, each relay with access to voltage uses $1/N$ of the total line capacitance and its own voltage to estimate its share of the charging current. The share of the charging current estimated at a given terminal may not equal the actual charging current supplied by this terminal.

However, adding up the estimated terminal charging currents gives the total line charging current. Each terminal subtracts its share of the charging current from the measured current per (75) and sends the resulting current i_{TX} to its peers.

$$i_{TX} = i_{MEASURED} - i_C \tag{75}$$

Then each terminal adds the compensated local current (i_{TX}) and the received remote currents (i_{RX}) per (76) to calculate the line differential signal, which becomes free from the charging current.

$$\begin{aligned} i_{DIF} &= i_{TX} + \sum_{REMOTE} i_{RX} = \sum_{ALL} \left(i_{MEASURED} - i_C \right) = \sum_{ALL} i_{MEASURED} - \sum_{ALL} i_C \\ &= i_{C\_TOTAL\_ACTUAL} - i_{C\_TOTAL\_CALCULATED} \cong 0 \end{aligned} \tag{76}$$

In this way, the method does not require sending voltage values.

The three-phase implementation uses (77) to calculate the phase charging currents. These charging currents are valid for open-phase and line energization conditions as long as the voltage transformers are installed on the line side. The symmetrical components of the charging current are compensated for automatically by compensating the phase currents using (77).

$$\begin{bmatrix} i_A \\ i_B \\ i_C \end{bmatrix} = \begin{bmatrix} C_{AA} & C_{AB} & C_{AC} \\ C_{BA} & C_{BB} & C_{BC} \\ C_{CA} & C_{CB} & C_{CC} \end{bmatrix} \cdot \frac{d}{dt} \begin{bmatrix} v_A \\ v_B \\ v_C \end{bmatrix} \tag{77}$$

For fully transposed lines, the matrix is near symmetrical [17] and is composed of the self-capacitance and mutual capacitance calculated from the positive-sequence (C_1) and zero-sequence (C_0) capacitances of the line, as (78) shows.

$$\begin{bmatrix} i_A \\ i_B \\ i_C \end{bmatrix}_{\mathrm{C}} = \begin{bmatrix} \frac{2C_1 + C_0}{3} & \frac{C_0 - C_1}{3} & \frac{C_0 - C_1}{3} \\ \frac{C_0 - C_1}{3} & \frac{2C_1 + C_0}{3} & \frac{C_0 - C_1}{3} \\ \frac{C_0 - C_1}{3} & \frac{C_0 - C_1}{3} & \frac{2C_1 + C_0}{3} \end{bmatrix} \cdot \frac{d}{dt} \begin{bmatrix} v_A \\ v_B \\ v_C \end{bmatrix} \tag{78}$$

Figure 31 illustrates the effectiveness of the described charging current compensation technique when applied to a three-terminal 275 kV line with a total length of 186 miles (300 kilometers) and a steady-state positive-sequence charging current of 230 A. This example is the transient simulation of a line energization. In Fig. 31, the differential signal without compensation is the current measured at the energizing terminal. The differential signal with compensation is the signal calculated per (76). Note that a vast portion of the charging current is removed from the differential signal.

Equations (77) and (78) are the time-domain implementation of the method. Not only the fundamental frequency component but also the instantaneous values of the differential signal are compensated. This allows various algorithms that respond to instantaneous values (such as external fault detection and harmonics calculations for blocking or restraining) to work well.

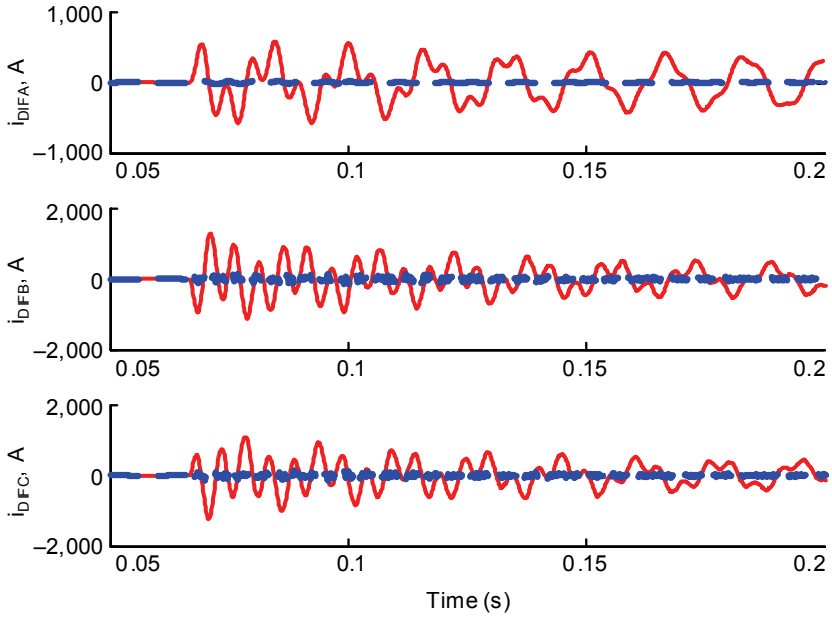

Fig. 31. Line energization example: phase differential signals without (red solid line) and with (blue dashed line) charging current compensation

The method can also be implemented using phasor quantities, as (79) shows.

$$\begin{bmatrix} \overline{I}_A \\ \overline{I}_B \\ \overline{I}_C \end{bmatrix}_{\mathrm{C}} = j\omega \cdot \begin{bmatrix} \frac{2C_1 + C_0}{3} & \frac{C_0 - C_1}{3} & \frac{C_0 - C_1}{3} \\ \frac{C_0 - C_1}{3} & \frac{2C_1 + C_0}{3} & \frac{C_0 - C_1}{3} \\ \frac{C_0 - C_1}{3} & \frac{C_0 - C_1}{3} & \frac{2C_1 + C_0}{3} \end{bmatrix} \cdot \begin{bmatrix} \overline{V}_A \\ \overline{V}_B \\ \overline{V}_C \end{bmatrix} \tag{79}$$

Charging current compensation requires voltage measurements, which may not be available at all line terminals. A solution to this problem is for each line terminal to inform the other terminals whether it is performing the charging current compensation. Each terminal receiving this information knows how many terminals actually subtract their share of the charging current and can calculate its own share of compensation in order to make up for the full charging current of the line.

For example, when all three voltage measurements are available in a three-terminal line, each terminal applies a 1/3 multiplier in the equation to calculate its share of the charging current. When one voltage measurement is not available, the other two terminals use a 1/2 multiplier and the compensation uses the two voltages that are representative of the line voltage profile.

9.2. ACCURACY OF VOLTAGE-BASED COMPENSATION

By using the lumped parameter model to represent the actual (typically long) line, the compensation method accuracy degrades for frequencies in the order of a few hundred hertz and above. The lumped parameter model can undercompensate or overcompensate the charging current, depending on the frequency of a given charging current component. This phenomenon results in a high-frequency component left in the compensated differential signal (inspect Fig. 31 closely). Using a more accurate (distributed) line model would solve this problem, but this is neither practical nor necessary.

To use a more accurate model, the relay would need more information about the line in the form of settings, making the application more complicated from the user perspective.

The higher-frequency signals are of secondary importance anyway and are suppressed by the relay filters.

One solution to this problem measures the high-frequency components in the differential signal and adds them to the restraining signal of the 87L elements [8]. This way, the degraded compensation accuracy is counterbalanced by an intentional adaptive elevation of the restraining means.

9.3. CHARGING CURRENT COMPENSATION IN ALPHA PLANE ELEMENTS

1) The Principle of Compensation

In a traditional Alpha Plane element, compensating the differential signal alone would not be sufficient and compensating each line terminal current individually would be required (which would be complicated).

The generalized Alpha Plane element incorporates the charging current compensation in the following natural way:

- Removing the charging current from the differential signal brings the operating point on the complex current-ratio plane close to the ideal blocking point.
- Increasing the restraining signal with high-frequency components to deal with the finite accuracy of the lumped parameter model used by the compensation algorithm brings the operating point on the complex current-ratio plane even closer to the ideal blocking point.

The following example illustrates the effect of line charging current compensation in Alpha Plane 87L elements.

2) Example 6: Line Charging Current Compensation

Consider a long, lightly loaded two-terminal line carrying a purely resistive load current of 0.25 pu and drawing considerable charging current that divides between the two terminals unevenly in the 0.8 to 0.2 pu proportion.

The phase currents of the 87L zone are (in pu):

$$\bar{I}_1 = 0.838 \angle 107.3°, \;\; \bar{I}_2 = 0.320 \angle 38.7° \tag{80}$$

The generalized Alpha Plane element works with the following quantities:

$$\bar{I}_{DIF} = 1 \angle 90° \text{ and } I_{RST} = 1.158 \tag{81}$$

and derives:

$$\bar{I}_{L(EQ)} = 0.32 \angle 38.7° \text{ and } \bar{I}_{R(EQ)} = 0.838 \angle 107.3° \tag{82}$$

As expected, the equivalent currents match the actual currents in this case of a zone bounded with two currents. The complex ratio between the two equivalent currents (or actual currents) is:

$$\bar{k} = 2.62 \angle 68.7° \tag{83}$$

In order to ensure security in this situation, the Alpha Plane characteristic would have to have a blocking angle of at least 222 degrees.

Assume now that a charging current compensation algorithm is applied and reduces the standing differential signal by 80 percent, changing the differential signal to 0.2 pu.

The generalized Alpha Plane element now works with the following quantities:

$$\bar{I}_{DIF} = 0.2 \angle 90° \text{ and } I_{RST} = 1.158 \tag{84}$$

Using (14) and (15), the algorithm calculates:

$$\bar{I}_{L(EQ)} = 0.486 \angle -65.6° \text{ and } \bar{I}_{R(EQ)} = 0.673 \angle 107.3° \tag{85}$$

As a result of modifying the differential signal, the two equivalent currents now differ from the actual currents. The complex ratio between the two equivalent currents is:

$$\bar{k} = 1.39 \angle 172.9° \tag{86}$$

This operating point is safely within the blocking region of a typically set Alpha Plane characteristic.

9.4. CHARGING CURRENT COMPENSATION AND INTERNAL FAULTS

The average voltage among all line terminals reflects the average line voltage profile as long as there is no fault on the line. During internal faults, the average terminal

voltage is higher than the average line voltage because the fault brings the voltage down at the fault point.

As a result, the algorithm may overcompensate for the charging current during internal faults. However, this is not a significant concern because of the following:

- The difference between the average terminal voltage and the average line voltage is large only when the system is strong (Fig. 32a). In strong systems, the 87L elements operate with large margin and the slight inaccuracy of compensation does not have any real impact.
- When the system is weak, the 87L elements may not have much margin to operate for an internal fault. However, in weak systems, the difference between the average terminal voltage and the average line voltage is small because all voltages are small (Fig. 32b).

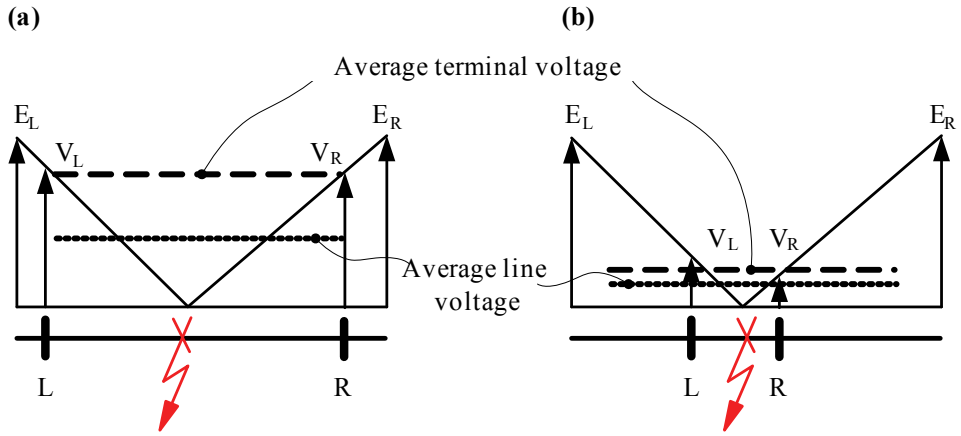

Fig. 32. Difference between the average line voltage (dotted line) and average terminal voltage (dashed line) during an internal fault in strong (a) and weak (b) systems

The other two methods for mitigating the impact of the line charging current described previously would face issues during internal faults as well. The elevated pickup approach penalizes sensitivity on a permanent basis. The approach of subtracting the standing value from the differential signal does not recognize that the charging current changes during an internal fault.

9.5. CHARGING CURRENT COMPENSATION AND EXTERNAL FAULTS

During external faults, the average voltage among all line terminals reflects the average line voltage profile (Fig. 33). As a result, the voltage-based compensation method performs very well. The other methods are less accurate, at least in theory, because they do not reflect the changes in the charging current due to changes in line

voltages caused by external faults. However, during external faults, the elements are restrained by the fault current. Therefore, they naturally tolerate the extra error in the differential signal caused by the lack of charging current compensation or inaccurate compensation. Weak systems are exceptions – the charging current can be high while the through-fault current can be low, producing only a small restraining action.

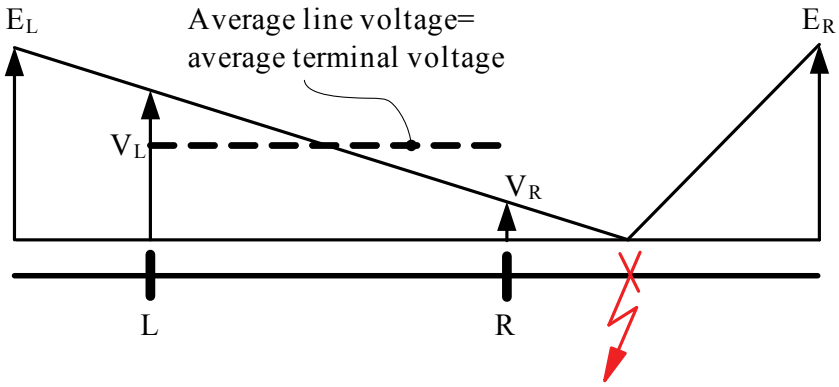

Fig. 33. During external faults, the average terminal voltage and the average line voltage are the same

10. ADAPTIVE BEHAVIOR OF 87L ELEMENTS

As explained and illustrated previously in this paper, 87L elements in present microprocessor-based relays are adaptive. In this section, we summarize the purpose, form, and consequences of the adaptive nature of practical 87L elements.

10.1. PURPOSE FOR 87L ADAPTIVITY

The general reason for the highly adaptive nature of the present 87L elements is to balance protection security with dependability and sensitivity, given the unique challenges and requirements of 87L protection.

Current alignment errors, possible data corruption in communications, misbehavior of the channel, misbehavior of timing sources if used for data alignment, line charging current, and CT saturation threaten the security of 87L elements.

Limited communications bandwidth between relays in the 87L scheme precludes direct application of some of the tried and true relay design algorithms and logic, which calls for more sophisticated versions of the known solutions. Moreover, some crude ways to address security challenges, such as sacrificing the sensitivity of protection, are not acceptable (but sometimes unavoidable) in 87L protection due to the requirement of detecting high-resistance faults on transmission lines.

As a result, the majority of available 87L relays are highly adaptive. This adaptivity allows them to maintain all the advantages of the differential principle while addressing the challenges of a distributed scheme that uses long-haul communications.

10.2. FORMS OF 87L ADAPTIVITY

In general, 87L elements adapt in response to one or more of the following events:

- Startup of an 87L relay in the scheme.
- External faults with CT saturation.
- Suspected or detected data alignment problems.
- Suspected or detected problems with external time sources, if used for data alignment.
- Suspected or detected problems with voltage sources, if used for charging current compensation.
- Communications problems, such as failed data integrity check or channel interruption.
- Line energization.

The adaptive behavior can include one or more of the following responses:

- Increasing restraining means to maintain security at the expense of a temporary decrease in sensitivity.
- Switching between normal and extended security 87L settings.

Adding extra intentional delay to 87L outputs to maintain security at the expense of temporarily slowing down operation, particularly for sensitive sequence differential elements.

10.3. CONSEQUENCES OF 87L ADAPTIVITY

Because of the highly adaptive nature of 87L elements, they respond simultaneously to quantities and events from diverse domains. These domains, which are normally separated in other types of protection, include the following:

- Power system (faults, line energization).
- Communication (channel asymmetry, data corruption, channel interruption and recovery).
- Time-distribution networks, if used (IRIG-B signal loss or excessive jitter, GPS clock reporting loss of satellite lock).

As a result, testing of practical 87L schemes requires knowledge of the 87L element algorithms and logic. The response of the 87L elements to power system faults is not controlled only by the pickup and restraining levels defined by the settings and does not depend only on the currents applied to the 87L relays; but in addition, it depends on events and quantities in communications and data alignment.

11. SETTINGS AND TESTING CONSIDERATIONS

11.1. SETTINGS

Adaptive 87L elements may appear difficult to set because of their changing operating characteristics in response to a variety of events. In reality, however, these elements do not require much engineering to select their basic settings. The following three factors contribute to the simplicity of settings selection:

- Typically, only three settings are required: the pickup threshold and the restraining settings, such as the slope (or slopes and the break point) for percentage differential elements or the blocking angle and radius for Alpha Plane elements.
- The differential principle itself makes the settings selection easier by alleviating issues like infeed effect for distance functions, impact of weak terminals, impact of series compensation, current reversal when clearing external faults on parallel lines, or power swings.
- The internal sophistication of present 87L elements allows them to perform very well based on built-in adaptivity. The user-selected basic settings only provide the general boundaries for the balance between sensitivity and security.

In summary, adaptive 87L elements rely on built-in algorithms and logic as much as on user settings. As a result, the differences in the nature of their settings (slopes versus blocking angle or radius) should not be overstated.

11.2. TESTING

The adaptive nature of 87L relays increases the complexity of 87L scheme testing. Reference [18] reviews the many aspects of testing 87L schemes with a focus on field testing (commissioning testing, maintenance testing, and troubleshooting). The following three aspects are worth emphasizing:

- Testing the operating characteristic (with the basic settings of pickup and restraining) confirms the integrity of the scheme and verifies that the intended settings are applied in the relays. This testing is valuable in commissioning. Simple steady-state input signals generated by standard test set software are typically sufficient for these tests. This type of testing, however, does not provide much information related to the actual performance of the 87L element during power system faults.
- When testing for performance as a part of product certification or development, we should apply as realistic inputs to the relays as possible, instead of applying input signals generated by simple means. This procedure verifies that the relay algorithms respond correctly for real power system patterns. Testing with waveforms generated by electromagnetic transient programs, either in closed-loop

mode (Real Time Digital Simulator) or in playback mode (output files from EMTP), is recommended when probing the relays for performance.

- When testing for performance, we should simulate events in all three domains to which the elements respond: power system, communications, and timing. This is most conveniently done in closed-loop simulation environments using scripts to coordinate events in all the domains involved (e.g., an external fault followed by a communications path switching 10 milliseconds after the fault inception and before the fault clearance).

12. CONCLUSION

This paper provides a wealth of information on the algorithms and logic of 87L protection elements available in present microprocessor-based 87L relays.

Unique challenges for 87L schemes, as compared with other types of differential protection, are reviewed in great detail because they are the key driving forces for the internal sophistication and adaptivity of 87L elements.

This paper focuses on percentage differential and Alpha Plane operating characteristics because these two characteristics dominate the actual implementations presently available. Their similarities and differences are reviewed, as well as the relative strengths of each.

The Alpha Plane operating characteristic is able to tolerate greater phase angle errors that may result from current misalignment in 87L applications. On the other hand, the percentage differential operating characteristic allows the manipulation of the differential and restraining signals for the benefit of charging current compensation, cross-phase restraining of sequence differential elements, harmonic restraint in applications with in-line transformers, and so on.

This paper describes a generalized Alpha Plane element. This new technique applies the concept of the restraining signal before transitioning to an equivalent current ratio, thus benefiting from the relative strengths of both the percentage differential principle and the Alpha Plane principle.

Solutions to key challenges in 87L protection, applicable to either percentage differential or Alpha Plane elements, are reviewed in great detail. These challenges include security under external faults with CT saturation, security under current alignment errors, and line charging current. To address these unique challenges of 87L protection, the 87L elements are sophisticated and highly adaptive. The impact of adaptivity on settings selection and testing is also reviewed in this paper.

The 87L elements found in present microprocessor-based relays are optimized for performance rather than built to follow a simple operating characteristic. They perform very well without relying on fine-tuned settings to suit any particular application.

As a matter of fact, the performance of 87L elements depends as much on the algorithms and logic as on user settings. Therefore, knowledge of the algorithms and logic allows for a better grasp of the operating limits of any given 87L element in terms of security and sensitivity, as well as creating better certification programs for new relays.

13. APPENDIX

The single-slope percentage differential characteristic with a slope of K ($0 < K < 1$) passing through the origin and corresponding to (4) and (8) can be unambiguously mapped into the Alpha Plane. Equation (87) provides the limiting contour of the restraining region in polar coordinates $\bar{k} = k \angle \theta$.

$$k^2 = \frac{2k}{1-K^2}\left(\cos\theta - K^2\right) + 1 = 0 \tag{87}$$

REFERENCES

[1] ALTUVE H.J., SCHWEITZER E.O., III (eds.), *Modern Solutions for Protection, Control, and Monitoring of Electric Power Systems*, Schweitzer Engineering Laboratories, Inc., Pullman, WA, 2010.

[2] ALTUVE H.J., MOONEY J.B., ALEXANDER G. E., *Advances in Series-Compensated Line Protection*. Proceedings of the 35th Annual Western Protective Relay Conference, Spokane, WA, October 2008.

[3] ROBERTS J., TZIOUVARAS D., BENMOUYAL G., ALTUVE H. J., *The Effect of Multiprinciple Line Protection on Dependability and Security*. Proceedings of the 55th Annual Georgia Tech Protective Relaying Conference, Atlanta, GA, May 2001.

[4] KASZTENNY B., FISCHER N., FODERO K., ZVARYCH A., *Communications and Data Synchronization for Line Current Differential Schemes*. Proceedings of the 38th Annual Western Protective Relay Conference, Spokane, WA, October 2011.

[5] SLEEPER H.P., *Ratio Differential Relay Protection*, Electrical World, October 1927, pp. 827–831.

[6] THOMPSON M.J., *Percentage Restrained Differential, Percentage of What?* Proceedings of the 64th Annual Conference for Protective Relay Engineers, College Station, TX, April 2011.

[7] ZIEGLER G., *Numerical Differential Protection: Principles and Applications*, Publicis Corporate Publishing, Erlangen, Germany, 2005.

[8] MILLER H., BURGER J., FISCHER N., KASZTENNY B., *Modern Line Current Differential Protection Solutions*, proceedings of the 63rd Annual Conference for Protective Relay Engineers, College Station, TX, March 2010.

[9] WARRINGTON A.R. van C., *Protective Relays: Their Theory and Practice*. Vol. 1. Chapman and Hall, Ltd., London, England, 1962.

[10] TZIOUVARAS D.A., ALTUVE H., BENMOUYAL G., ROBERTS J., *Line Differential Protection With an Enhanced Characteristic*. Proceedings of Med. Power 2002, Athens, Greece, November 2002.

[11] BENMOUYAL G., LEE T., *Securing Sequence-Current Differential Elements*, proceedings of the 31st Annual Western Protective Relay Conference, Spokane, WA, October 2004.

[12] GUZMÁN A., LABUSCHAGNE C., QIN B.L., *Reliable Busbar and Breaker Failure Protection With Advanced Zone Selection*. Proceedings of the 31st Annual Western Protective Relay Conference, Spokane, WA, October 2004.

[13] BENMOUYAL G., ROBERTS J., *Superimposed Quantities: Their True Nature and Application in Relays*. Proceedings of the 26th Annual Western Protective Relay Conference, Spokane, WA, October 1999.

[14] FODERO K., HUNTLEY C., WHITEHEAD D., *Secure, Wide-Area Time Synchronization*. Proceedings of the 12th Annual Western Power Delivery Automation Conference, Spokane, WA, April 2010.

[15] ADAMIAK M.G., ALEXANDER G.E., PREMERLANI W., *A New Approach to Current Differential Protection for Transmission Lines*. Proceedings of the 53rd Annual Georgia Tech Protective Relaying Conference, Atlanta, GA, May 1999.

[16] GAJIC Z., BRNCIC I., RIOS F., *Multi-Terminal Line Differential Protection With Innovative Charging Current Compensation Algorithm*. Proceedings of the 10th Developments in Power System Protection Conference, March 2010.

[17] SCHWEITZER E.O., III, FISCHER N., KASZTENNY B., *A Fresh Look at Limits to the Sensitivity of Line Protection*. Proceedings of the 37th Annual Western Protective Relay Conference, Spokane, WA, October 2010.

[18] FINNEY D., FISCHER N., KASZTENNY B., LEE K., *Testing Considerations for Line Current Differential Schemes*. Proceedings of the 38th Annual Western Protective Relay Conference, Spokane, WA, October 2011.

voltage stability margin,
Thevenin equivalent,
accuracy analysis

Bartosz BRUSIŁOWICZ*, Janusz SZAFRAN*

A NEW METHOD OF THE STABILITY MARGIN DETERMINATION OF A RECEIVING NODE

The paper concerns the problem of local voltage instability of the power system receiving node. There were presented bases of analysis of stability margin determination using Thevenin equivalent model. Basing on Thevenin model new method of stability margin calculation was developed. The method has been described in the article. Contrary to well known methods, presented algorithm does not use a derivates of measured parameters. The algorithm uses only the measured values of steady working points. The last part of paper contains an analysis of potential errors.

1. INTRODUCTION

It is well known that in the analysis of work and control of power system there are important two pairs of values: active power–frequency P–f and reactive power–voltage Q–V [1]. The first of these pairs is global. The frequency of the entire power system should be constant. This corresponds to the balance of generated and received active power. It is different with the voltage and reactive power. In some of the power system nodes voltage can be close to the nominal value and in others differ quite significantly. Therefore voltage is the local parameter and can be controlled, changed and stabilized according to the requirements. This task must be realized in on-line mode to ensure suitable quality of energy. The reasons of voltage changes are normal operation of power system where configuration changes and temporary, daily and seasonal load changes occur. The system can be designed to maintain the value of voltage in acceptable limits despite of load changes. However, randomly situations and system configuration changes where these limits are exceeded (most of decrease of voltage to low value) can occur. In such situation there is a need to use different voltage control

* Institute of Electrical Power Engineering, Wrocław University of Technology, Wrocław, Poland.

methods. The simplest but the most severe for customer is undervoltage load shedding. In the nodes where such situations occur regularly, voltage regulation using the transformer tap changer (under load) should be performed. When the tap changer is used, problem of stability margin decreases along with the voltage increase occurs. This may cause tap changer blocking in some positions. This shows, that analysis of node working point requires, beyond the voltage measuring and undervoltage criterion formulating, stability margin studies. Moreover, similar case can occur when reactive power compensation is used. Using this method of voltage regulation can lead to a situation when changing the load impedance argument causes the possibility of local instability even when the node voltage is close to the nominal value. This might mean that undervoltage load shedding should be performed despite of voltage near or even greater than the nominal. This also shows that it is not only reasonable to measure the voltage, as it is done in most cases, but also there is a need to calculate the stability margin.

Paper presents a new method of local stability margin calculation. In literature a lot of stability margin determination methods can be found [2–5], including work of the authors [6]. Most of these methods use derivatives of voltage or apparent power against the load impedance changes. Ensuring adequate accuracy is possible for linear load impedances. The non-linear models require appropriate adjustments. Presented method does not use these derivatives. Therefore, the method may be freely used for any load model, assuming that parameters of steady working point are used.

2. THE RECEIVING NODE AND ITS THEVENIN EQUIVALENT

Figure 1 shows scheme of Thevenin equivalent calculation. Because of using off-line modelling in suitable digital environment it is possible to determine all values of parameters of Thevenin model. The parameters are real and imaginary parts of voltage, current and impedance: E, Z_S, Z_L, V, I or their amplitudes and angles. According to the initial power system model, parameters of Thevenin equivalent are calculated as follows [1, 2, 4, 7]: ideal voltage source E parameters are calculated basing on voltage phasor measured at idle node, parameters of series impedance Z_S are determined by short-circuit all voltage sources and calculating impedance seen from considerate node.

Unfortunately, according to the protection devices operating or processes of power system configuration switching, values of E and Z_S are changing. These parameters do not physically exist; they are only parameters of section of power system virtual model. In the node directly measurable are current I and voltage V (Fig. 1) and derived values e.g. load impedance Z_L. Other parameters, including value of ideal voltage source E and series system impedance Z_S, which affect the stability of the power system, must be calculated indirectly in on-line mode and updated in the measurement

process. It may be noted that, range of changes of E and Z_S can be determined in off-line mode according to the switching processes that may occur.

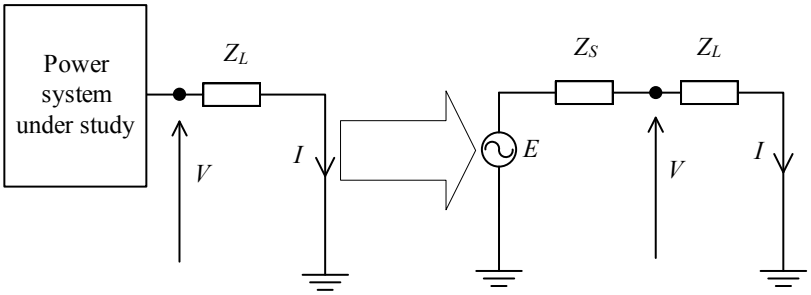

Fig. 1. Thevenin model calculation scheme

Determination of those indirect parameters can be made basing on two fundamental values that can be described by the following equations [3]:

$$V = \frac{E}{\sqrt{1 + W^2 + 2W\cos\beta}}, \tag{1}$$

$$S = \frac{E^2 W}{Z_S(1 + W^2 + 2W\cos\beta)}. \tag{2}$$

where: $W = Z_S/Z_L = Z_S{*}Y_L$ and $\beta = \varphi_S - \varphi_L$.

Common curve that corresponds to equations (1) and (2) changes its shape according to the variations of parameters e.g., Z_S and β. Also the load curve can have different shapes because the active and reactive power characteristics may depend on various factors. In general it can be written that both parameters $W = f(V)$ and $\beta = f(V)$ depend on the voltage

It can be calculated that the maximum of receiving power occurs when $W = 1$ that is when series and load impedance are equal $Z_S = Z_L$ [4]. On the other hand it can be noticed in equation (2) that when impedance Z_S is larger the value of maximum received power is lower.

Therefore, with the increase of system impedance Z_S or decrease of load impedance Z_L value of W increases. This causes the node voltage drop. When the constant impedance load model is used, changes of node voltage results in received power change and when constant power load model is used, there is only the voltage change and the received power remains constant. It can be noted that the decrease of voltage in this model is much higher because the value of W is greater. This is caused by increase of system impedance Z_S as well as the decrease of load impedance Z_L (or increase of load admittance Y_L) with change of node voltage.

Equations (1) and (2) are valid in steady-state either for the constant impedance load model (not depending on the voltage) and constant power load model or any other load model.

As Figure 2 shows, for impedance Z_S change occurrence identification following condition can be used:

$$\frac{\Delta S}{\Delta V} \geq 0 \,. \tag{3}$$

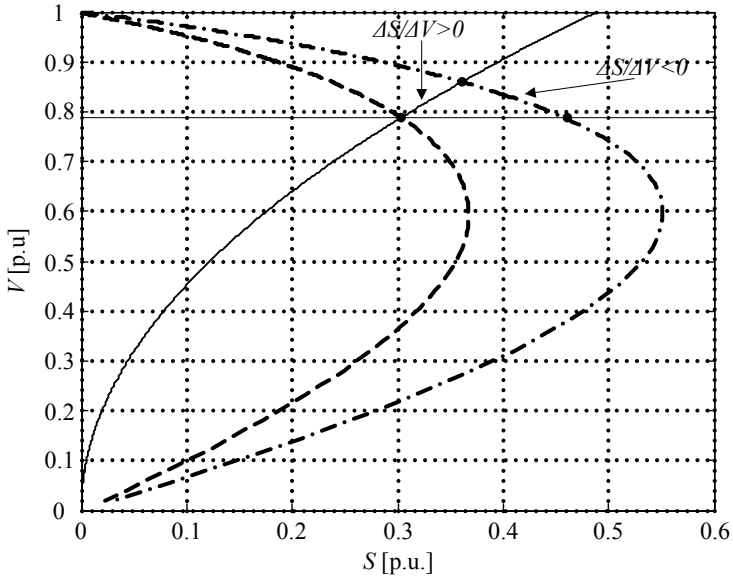

Fig. 2. Nose curves for different value of impedance Z_S and load curve

This condition can indicate the need of starting the procedure of calculating the new value of impedance Z_S and voltage measuring for the changed value of load impedance Z_L and/or β. The value of angle needed for the calculation can be taken as the average value $0{,}5(\varphi_{S\max} + \varphi_{S\min})$. Changes of this argument are not large, and extreme values can be obtained from off-line simulation studies of considered power system section.

In contrast to this, changes of load impedance argument, the second component of β angle can be significant, especially when load model is highly non-linear or when the node voltage regulation is performed. However, even large changes of load impedance argument do not have a significant impact on the stability margin estimation results because they are directly measurable in considered node, as well as other needed parameters obtained based on the measurements of currents and voltages.

3. A NEW METHOD OF STABILITY MARGIN ASSESMENT

Taking into account the assumptions presented in previous paragraph and assuming that the stability margin identification based on changes of node voltage is carried out when these changes are caused by load impedance module or argument changes, the following equation for two steady working points can be obtained:

$$V_1 = \frac{E}{\sqrt{1 + W_1^2 + 2W_1 \cos \beta_1}}, \tag{4}$$

$$V_2 = \frac{E}{\sqrt{1 + W_2^2 + 2W_2 \cos \beta_2}}, \tag{5}$$

where: $W_1 = Z_S{*}Y_{L1}$, $W_2 = Z_S{*}Y_{L2}$, $\beta_1 = \varphi_S - \varphi_{L1}$, $\beta_2 = \varphi_S - \varphi_{L2}$, E = const.

After squaring both sides of equations (4) and (5), dividing and transforming the quadratic equation is obtained:

$$aZ_S^2 + bZ_S + c = 0 . \tag{6}$$

This has the following solution:

$$Z_{S1,2} = \frac{-b \pm \sqrt{b^2 - 4ac}}{2a}, \tag{7}$$

where: $a = Y_{L2}{}^2(g^2h - 1)$, $b = 2Y_{L2}[gh\cos\beta_1 - \cos\beta_2]$, $c = h - 1$ and $g = Y_{L1}/Y_{L2}$, $h = (V_1/V_2)^2$.

Basing on the calculated value of system impedance Z_S and measured impedance Z_L stability margin can be determined. Limit of local stability occurs when:

$$Z_S Y_L = 1 . \tag{8}$$

So stability margin is equal to:

$$\Delta_{stab} = 1 - Z_S Y_L . \tag{9}$$

4. ANALYSIS OF ERRORS COMING FROM UNMEASURABLE VALUES

In presented method of stability margin determination unknown value of voltage source E is simplified. The only unknown parameter is β angle (or cosine of this angle $\cos \beta$) – equations (4) and (5). However, considering the derivation of equation (4) and (5) it can be noticed that, due to possibility of load impedance argument φ_L measuring, the only unknown is actual value of system impedance argument φ_S. Range of

system impedance Z_S changes in equivalent Thevenin model can be estimated on the basis of off-line studies of power system model according to the particular connections – especially close power lines. It can be expected that the difference of maximum and minimum values of the argument generally does not exceed ten to twenty degrees. Assuming an average value obtained from off-line studies, errors of stability margin estimation basing on the average value and the expected changes can be calculated as follows:

$$\arg Z_S = 0{,}5\left[\varphi_{S\max} + \varphi_{S\min}\right] + \Delta\varphi_S, \tag{10}$$

where

$$\Delta \arg Z_S = 0{,}5\left[\varphi_{S\max} - \varphi_{S\min}\right]. \tag{11}$$

Arising errors can be considered basing on the Figure 3. This figure shows curve of the value of V/E as a function of the β angle (in range 0°–140°) for various values of W (0,1; 0,5; 1) or alternatively various stability margin Δ_{stab} (0,9; 0,5; 0) (equation (9)). Obviously, the minimum values of voltage occur for the smallest voltage stability margin and these values are growing with the increase of β angle. The observed increase of steepness of the V/E curve indicates also that in the area of larger value of β there will be greater sensitivity to errors in the β angle determination.

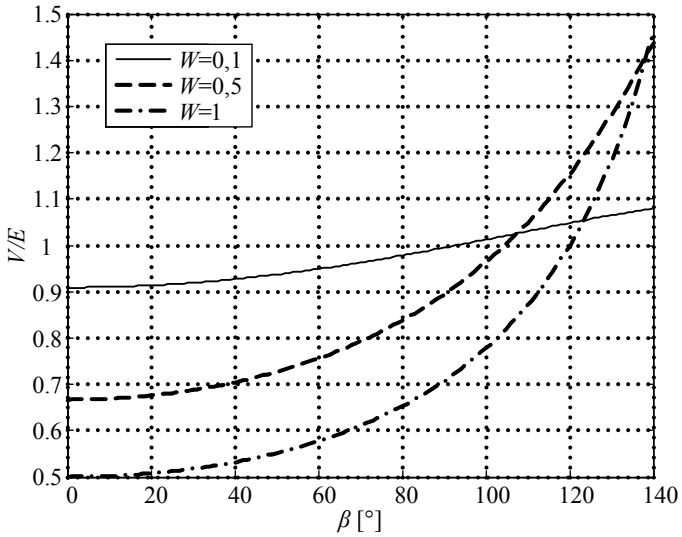

Fig. 3. Value of V/E as a function of β curve for different value of W

Details of these errors which confirm previous considerations are shown in Figure 4. This Figure shows curves of errors as a function of β angle for different W values. For a given value of W and β angle, errors obtained by inaccurate estimation of

the β were calculated. Changes of β angle have amounted ±5°. It can be seen that errors rise when β parameter increases. It is obvious because the steepness of voltage changes (Fig. 3) rises with increasing β. The specific curves are plotted for different values of W. The lowest errors are for $W = 0.1$ and the largest for $W = 1$ which is the voltage stability limit.

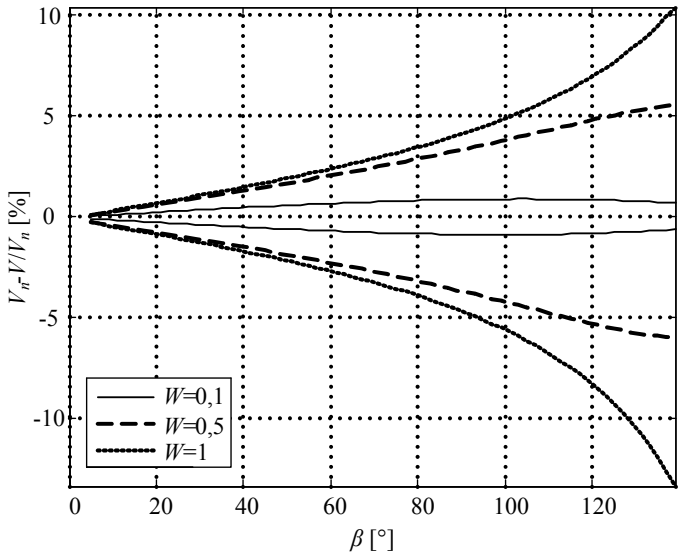

Fig. 4. Value of $V_n - V/V_n$ error for +/–5° β deviation as a function of β for different value of W

Figure 3 also shows that the large changes of β value, according to the non-linear load model or using of reactive power compensation, can cause changes of critical value of voltage of stability limit in a wide range. In this range values of voltage may differ significantly from the nominal value but also these differences can be very small. This means that the application of the voltage stabilization or undervoltage load shedding requires consideration of current voltage stability margin or/and load impedance angle calculation. Such extend of information can greatly improved quality and reliability of the decisions about the undervoltage load shedding.

5. CONCLUSIONS

1. The paper presents a simple method of voltage stability margin assessment of the receiving node based on the Thevenin model equivalent. The method uses locally measurable parameters of stable working point in two different moments of time.

2. Discussed algorithm ensures good accuracy of stability margin estimation and can be used for any non-linear load impedance model. The method is insensitive to small deviations of impedances arguments β. For standard values of the β angle relative voltage measurements differ by a few percent when the angle deviations amount ±5°. It is worth noting that the source of errors is an unknown argument of system impedance which changes slightly.
3. Undervoltage load shedding should be used when the node voltage decrease below an acceptable value and there is no voltage control or range of this regulation is exceeded.
4. Using reactive power compensation to regulate or stabilize node voltage can cause closing of voltage value to the nominal even when the node working point is near or at the local stability limit. Therefore, for load shedding additional criteria, beyond undervoltage, should be use. These criteria can be: value of voltage and/or stability margin or value of voltage and/or difference of arguments of series and load impedance. It is also possible to use the hierarchy of this criteria or assign them specific weights.

REFERENCES

[1] KREMENS Z., SOBIERAJSKI M., *Analiza systemów elektroenergetycznych*, WNT, Warszawa, 1996 (in Polish).
[2] MACHOWSKI J., BIALEK J.W., BUMBY J.R., *Power System Dynamics – Stability and Control* (2nd Edition), Wiley – IEEE Press, 2008.
[3] WISZNIEWSKI A., *New Criteria of Voltage Stability Margin for the Purpose of Load Shedding*, [in:] IEEE Transactions on Power Delivery, Vol. 22, No. 3, July 2007, pp. 1367–1371.
[4] KHOI V., BEGOVIC M.M., NOVOSEL D., SAHA M.M., *Use of Local Measurements to Estimate Voltage Stability Margin*, [in:] IEEE Transactions on Power Systems, Vol. 14, No. 3, August 1999, pp. 1029–1035.
[5] WISZNIEWSKI A., REBIZANT W., KLIMEK A., *A method of Accurate Determination of Voltage Stability Margin*. Proceedings of the CIGRE Canada Conference on Power Systems, Winnipeg, Canada, October 19–31, paper C4-109, 2008.
[6] BRUSIŁOWICZ B., REBIZANT W., SZAFRAN J., *A new method of voltage stability margin estimation based on local measurements*, APAP 2011 Conference, Beijing, No. 1790, 2011, pp. 2443–2447.
[7] CORSI S., TARANTO G.N., GUERRA L.N.A., *New Real-Time Voltage Stability Indicators Based on Phasor Measurement Unit Data*. Proceedings of the CIGRE session, 2008, paper C4-109.

Dynamic Thermal Line Rating,
distance protection,
power swing, third zone

Łukasz STASZEWSKI*, Waldemar REBIZANT*

THERMAL CALCULATION FOR DISTANCE PROTECTION ENHANCEMENT

Worldwide analysis of recent wide area cascading failures has shown that very often their main cause was the mal-operation of the distance protection relay third zone. The load encroachment and power swing phenomena are the two dire problems to solve when dealing with the third zone of distance protection. The vast number of blackouts could have been avoided or the consequences lowered if the distance relay had not operated due to impedance encroachment while there was no risk of further, continuous operation.

This paper proposes a way to improve operation of the distance protection relay by introducing a new blocking algorithm that uses the Dynamic Thermal Line Rating (DTLR) to restrain relay from tripping when conditions in electrical power system allow for it.

1. DISTANCE PROTECTION RELAY

A high speed protection for transmission and distribution circuits is under continuous development. It considers the most important fact for protection devices that is to meet the requirements of combining fast fault clearance with selective tripping. Thus for many years distance protection relay has been one of the most commonly used devices amongst electrical protection equipment. Distance protection is comparatively simple to apply and can be fast in operation for faults located along the majority of protected circuit. It can also provide both primary and remote back-up functions in a single device [1].

The basic principle of operation of the distance protection relay is based on impedance calculation seen by the relay. Since the impedance of a transmission line is proportional to its length, for distance measurement it is appropriate to use a relay able to

* Wrocław University of Technology, Institute of Electrical Power Engineering, Wybrzeże Wyspiańskiego 27, 50-370 Wrocław, Poland.

measure the transmission line impedance to a predetermined point. Such a relay is designed to operate only for faults occurring between the relay location and the selected reach point, thus giving discrimination for faults that may occur in different line sections. The ratio between voltage and current phasors measured at the relay installation point is calculated. The impedance calculations are based upon the following relationship:

$$\overline{Z}_R = \frac{\overline{V}_R}{\overline{I}_R} \tag{1}$$

with: $\overline{Z}_R$, $\overline{V}_R$ and $\overline{I}_R$ being impedance, voltage and current phasors, respectively, whereas the detailed algorithms can be found in [2, 3].

The reach point of a relay is the point along the line impedance that corresponds to a certain distance from the relay. As this is dependent on the ratio of voltage and current and the phase angle between them, it may be plotted on an R/X diagram as in figure 1b) below.

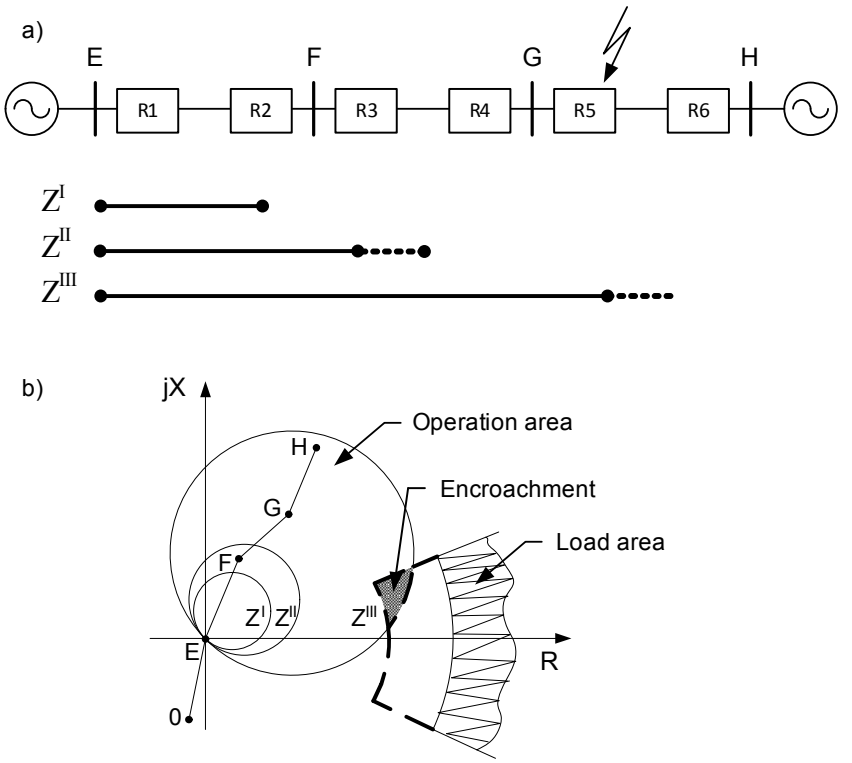

Fig. 1. a) Structure of a test transmission network,
b) distance relay zones 1, 2 and 3 vs. load area

The EF, FG and GH sections in figure 1a correspond to respective impedances of line sections seen by relay R1. The position of power system impedances as seen by the relay during faults, power swings and load variations may be plotted on the same diagram. In this manner the performance of the relay in the presence of system faults and other disturbances may be studied. This fact will be used in this paper for Zone 3 operation investigation of distance relay. Especially the third zone encroachment phenomena will be shown in situations of high load and power swing and its influence on the distance relay operation.

Careful selection of the reach settings and tripping times for the various zones of protection enables correct co-ordination of the distance relays in a power system. Main distance protection will comprise instantaneous directional Zone 1 and one or more time-delayed zones. Typical settings for three forward zones are given as follows.

Zone 1 is set up to 85% of the protected line impedance, Zone 2 must cover the remaining 15% of the first line section and, to ensure full coverage of the line, is set to cover 120% of the protected line or the protected line section +50% of the shortest adjacent line [4]. Remote back-up protection for all faults on adjacent lines can be provided by a third zone that is time delayed to discriminate with Zone 2 protection plus circuit breaker trip time for the adjacent line. Zone 3 reach should be set to at least 120% of the impedance presented to the relay for a fault at the remote end of the second line section (Fig. 1a) [5]. However due to the effect of interconnected power systems (Fig. 2), the effect of fault current infeed at the remote busbars will cause the impedance seen by the relay to be much greater than the actual impedance to the fault and this needs to be taken into account when setting Zone 3 like in equation (2). As the third zone of impedance relays with mho-characteristic covers significant part of the network and thus the impedance characteristic area is big, it is the most vulnerable to abnormal conditions zone in the electrical power system configuration and operation.

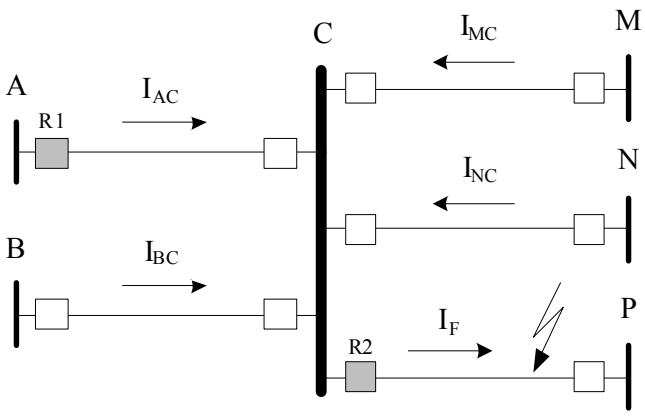

Fig. 2. Sample structure of an interconnected transmission network

Considering the problem of backing up the protection system of line CP (relay R2, Fig. 2) by the distance relay R1 it must be taken into account that because of the currents contributions from the lines BC, CM and CN, the third zone setting will be equal to:

$$Z^{III} = Z_{AC} + 1.2Z_{CP}\left(1\frac{I_{BC} + I_{MC} + I_{NC}}{I_{AC}}\right) \tag{2}$$

where: Z^{III} is apparent impedance seen by the relay R1 in case of the other lines current contribution.

In case of an extreme situation of equal contribution to the fault current from all the remaining lines the third zone relay setting will be:

$$Z^{III} = Z_{AC} + 4.8Z_{CP} \tag{3}$$

Therefore the third zone is especially exposed to load encroachment and power swing – all these situations can lead to the measured impedance encroachment into the Zone 3 area. This results in relay mal-operation and can be a leading factor to a large scale blackout occurrence, as it was seen, e.g. in Germany on November 4th, 2006 [5].

Despite the fact of Zone 3 setting encroachment, the system operational conditions may not be dangerous and in case of load encroachment the load may be permissible due to the transmission lines temporary loadability. In case of stable power swing, after some time the system recovers to its normal operation conditions. The important issue is to distinguish whether the third zone area encroachment is a result of fault and the relay should operate, or it is one from above-mentioned situations and the relay decision about tripping should be restrained.

There are various ways to avoid over-tripping due to unwanted impedance encroachment, both at the level of protection designing (characteristic shape shifting, adding restrictions) and during the relay operation (measuring additional criteria signals, e.g. zero sequence currents) [1–3]. However, it is very difficult to predict all possible situations in power system and all possible operating conditions, thus none of them is perfect. This paper is focused on the possibility of Dynamic Thermal Line Rating usage to prevent distance protection relay from tripping in situations of extreme load conditions and power swing by introducing an additional blocking signal into the standard distance relay. The blocking signal is based on the DTLR technique monitoring weather conditions and calculating the overhead conductor temperature and actual for ambient weather conditions conductor current limit as well as the time left to reach this thermal limit.

2. DYNAMIC THERMAL LINE RATING BASICS

The Dynamic Thermal Line Rating technique aims at real time calculation of an overhead bare conductor ampacity dependent on the ambient weather conditions. The DTLR algorithm cooperates with standard distance protection devices to fully utilize the transmission line by calculation of temporary current-carrying capability.

The conductor temperature is calculated from the heat balance equation [6, 7]:

$$q_c + q_r = q_s + q_i \tag{4}$$

where: q_c, q_r are heats dissipated due to convection and radiation and q_s, q_i are heat gain due to solar radiation and heating due to Joule's law, respectively.

Each of above heat balance components are calculated in numerical way. Specific formulas the calculations are based on can be found in [6]. However, at this point, it is worth mentioning that the most significant factors for the heat balance are the convective cooling (due to wind) and Joule's heating (due to current flow and conductor resistance change).

Basing on the heat balance it is possible, using numerical solutions, to compute the current conductor temperature as well as the time needed for the conductor to reach its thermal limit according to the actual current value and ambient weather conditions. The solution is given by the following:

$$\frac{dT_C}{dt} = \frac{1}{mC_p}[R(T_C)I^2 + q_s - q_c - q_r] \tag{5}$$

where m is mass of conductor and C_p is specific heat of conductor material.

3. ENHANCED DISTANCE PROTECTION SCHEME

During the high load and power swing phenomena there is a high risk of the measured impedance encroachment into the Zone 3 area. Both these situations correspond to current values higher than the values during the normal operating conditions thus the measured impedance is sometimes even much lower than during the normal operating conditions (Eq. 1). The standard way of designing protection devices usually does not take into consideration the Joule's law, i.e. the fact that higher currents evoke higher conductor temperatures and each conductor has its thermal limit that due to the safety reasons cannot be exceeded.

The Dynamic Thermal Line Rating application introduces an additional algorithm into a standard distance relay, that is based on real-time conductor temperature calcu-

lation. The aim is to restrain the relay from tripping until the conductor temperature reaches its thermal limit. The block scheme of DTLR supported distance relay operation is presented in figure 3 below:

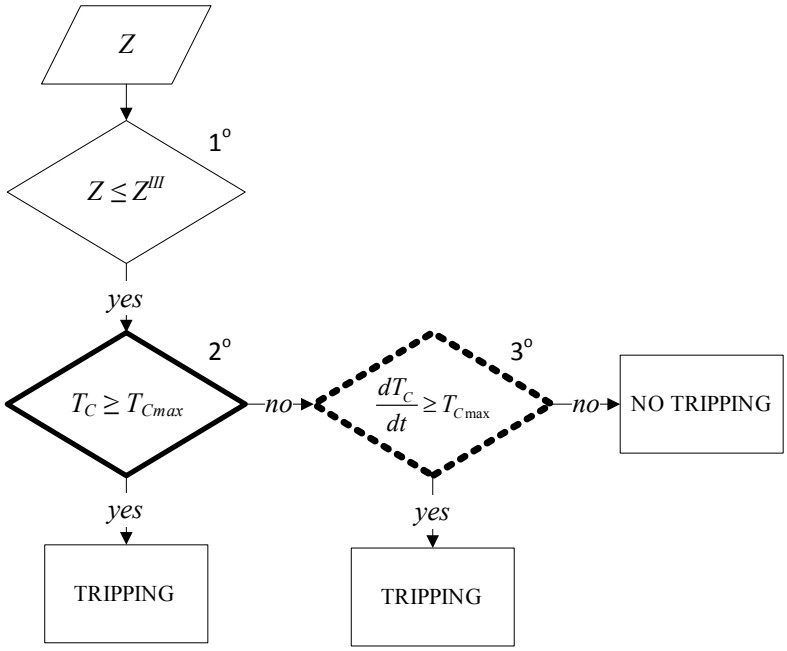

Fig. 3. Block diagram of a distance relay with new blocking algorithms

The block diagram above presents the idea of a standard distance relay enhancement based on temperature calculation. The relay acquires current samples and then using standard Fast Fourier Transform (FFT) computes the magnitudes of phase current signals, which is followed by computation of the conductor temperature [8].

Block 1 of the new protection scheme is a standard solution applied commonly in impedance relays. Its task is to compare the measured (seen by the relay) impedance with Zone 3 setting and operate if the impedance encroaches on the operation area (Fig. 1b). However, as it was mentioned earlier, there are some possible situations during which impedance encroachment occurs when the relay decision of tripping is unnecessary and even highly unwanted. Therefore there is a need for introducing additional blocks 2 and 3 to the relay logic, as described below.

Block 2, presented in figure 3, is responsible for the conductor temperature monitoring and ensures that it will not exceed the designed, for particular conductor, maximum operating temperature. Thus in case of heavy load and power swing it allows the transmission line to be operated safely, without tripping, when sufficient cooling conditions are met.

However as in some cases the temperature itself is not a sufficient factor to decide an additional algorithm (Block 3) is needed. Here a ratio of a conductor temperature change is observed. As the fault causes faster change in current magnitudes than power swings or heavy load situations, it is reasonable to use the information about the speed of change to determine whether the situation met is safe for further operation or if it should be stopped.

Figures 4a and 4b below show the impedances seen by the relay in case of some faults and power swing conditions. From the relay point of view there is no difference between these two phenomena. In each of presented situations the third zone setting area was encroached. The standard relay would operate in all five situations and that is why the additional algorithms, based on the Dynamic Thermal Line Rating, are proposed to be implemented into a distance relay. If introduced, a hope is justified that the relay would restrain itself from tripping in Power Swing situations, when it is not desired.

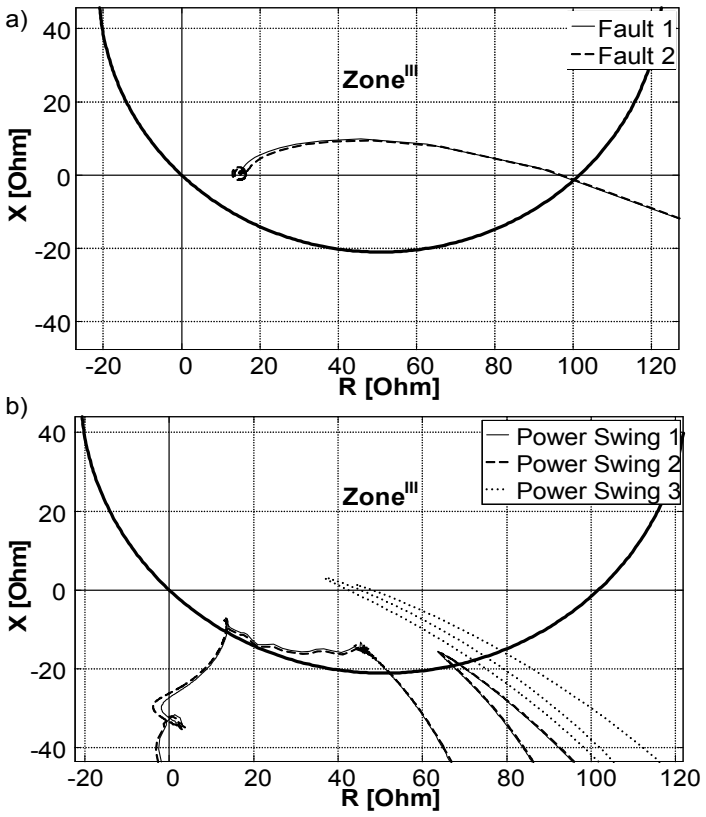

Fig. 4. Impedance trajectory encroaching third zone of a distance relay (circle char.) during: a) faults, b) power swing situations

4. PROTECTION TESTING RESULTS

During the tests AFL 6 240 conductor with rated current of 645 [A] and its thermal limit of 60 [°C] was used at nominal transmission line voltage of 110 [kV], protected line length was 70 [km] which corresponds to 29.96 [Ω]. Fault and power swing situations were simulated and examined and the testing results will be presented below. The most important signals from the point of view of introducing the new algorithm were taken into account. Thus the current magnitude (as a factor highly responsible for the conductor temperature), the conductor temperature (as in the Block 2) and the ratio of change of the conductor temperature were examined (as in the Block 3).

During the simulated situations the current flowing throughout the conductor in cases of faults and power swings was as presented in figure 5 below.

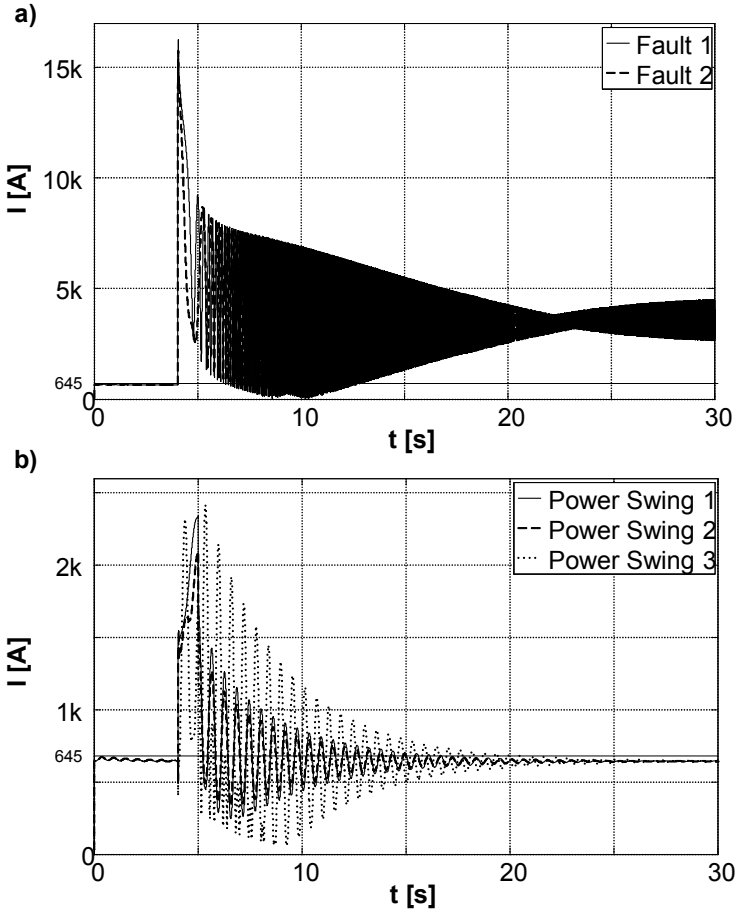

Fig. 5. Current magnitudes during a) faults, b) power swing situations

As it can be noticed in figure 5a the current magnitudes in both fault and power swing cases were much higher than the nominal conductor rating value of 645 [A]. In fault causes the values were of course much higher, momentarily over 15 [kA], than in cases of power swings were the values not even reached 2.5 [kA]. However in all the power swing situations the current magnitudes returned to their normal values after the time from 15 to 20 seconds and in both fault situations currents stabilized over 4 [kA]. Of course the thermal impact on the conductor in so different situations was also altered. The conductor thermal behaviour is presented in figure 6 below.

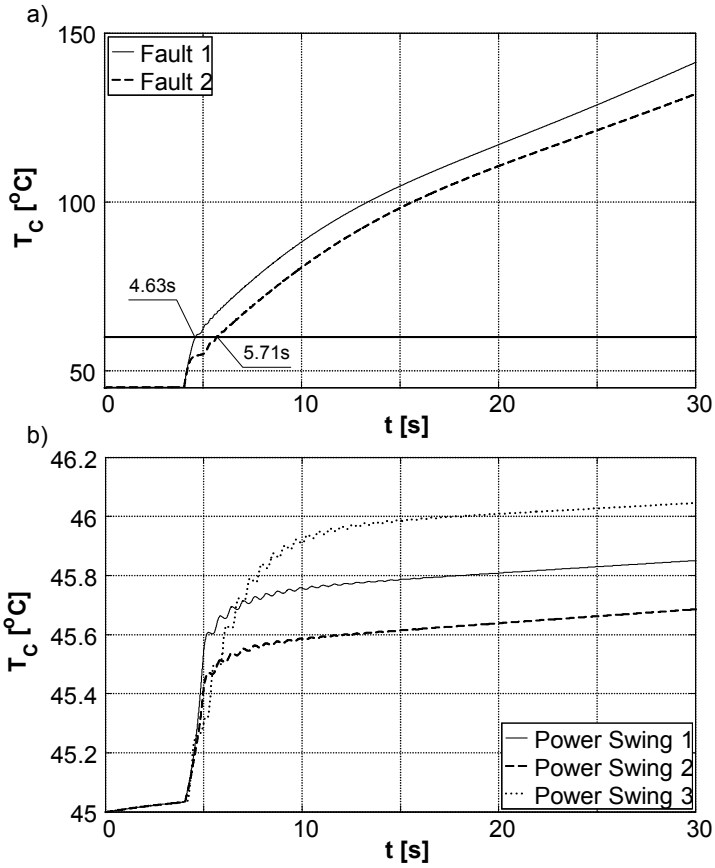

Fig. 6. The conductor temperatures during a) faults, b) power swing situations

As seen in figure 6a, much higher and longer lasting current magnitudes in case of faults cased much faster and higher temperature exceeding the conductor thermal limit at 4.63 [s] and 5.71 [s] of simulation which is respectively 0.595 [s] and 1.675 [s] after

the fault happened. This situation highlights the need for fast protection because less than two seconds are enough for the fault currents to permanently destroy the conductor. However, all three situations of power swing phenomena proven the fact, that during sufficient weather conditions the continuous transmission line operation is safe and allowable.

Despite the fact, that the temperature monitoring is usually a sufficient factor to determine whether the situation met by the relay is a fault or a power swing the decision time can still be shortened by additional algorithm (Block 3 in Fig. 3). The conductor temperature change ratio (calculated as a derivative of conductor temperature over time) limit value was determined experimentally as 1, however was set to 2 due to safety reasons. The results of the ratio values examinations can be seen in figure 7 below.

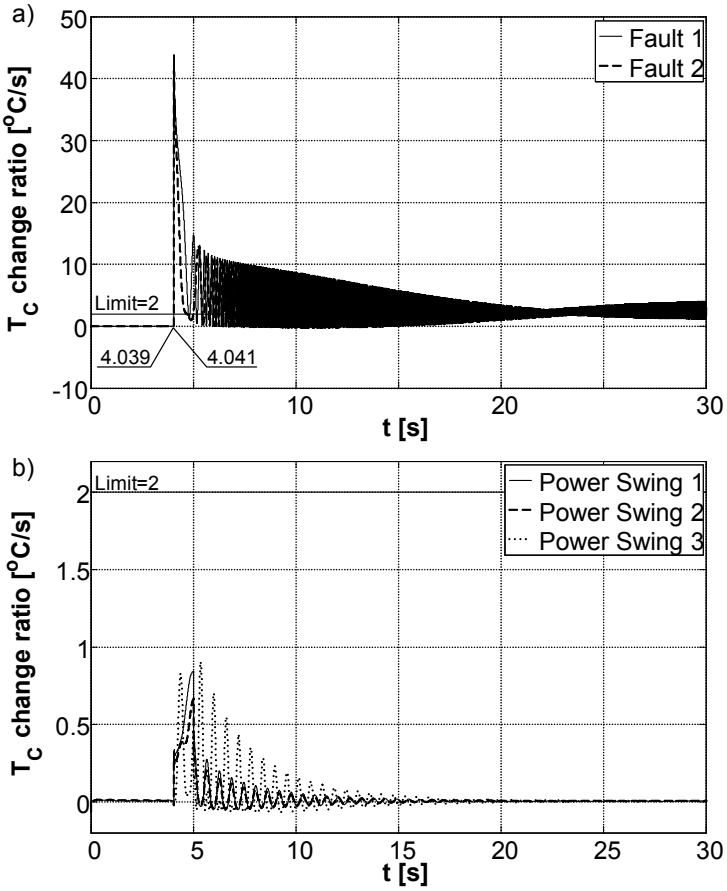

Fig. 7. The conductor temperature change ratios during a) faults, b) power swing situations

As it was seen in figure 7, the additional algorithm responsible for conductor temperature change ratio monitoring also perfectly determined between the fault and power swing situations and as expected operated much faster than the algorithm monitoring the conductor temperature. The reaction time for the Block 3 was 0.004 [s] and 0.006 [s] instead of the longer Block 2 reaction times of 0.595 [s] and 1.675 [s] respectively. The Block 3 reaction times are shorter by the time the conductor needed to reach the temperature of its thermal limit.

Despite the fact that the Block 3 presented reaction times are shorter than in case of Block 2, there is a risk that during unstable power swing situation or long-lasting ones the conductor limit temperature can be exceeded with simultaneously low ratio of temperature increase causing the conductor damage. That is why for the best performance both Block 2 and 3 should co-operate with standard protection relay.

5. CONCLUSIONS

This paper presented the examination of a standard distance protection relay enhanced with two additional algorithms based on the Dynamic Thermal Line Rating. The examination, considering the most important factors: current magnitudes, conductor temperature and conductor temperature change ratio has proven that the proposed algorithms improved the distance relay operation reaction times and reliability.

Despite the Dynamic Thermal Line Rating application high weather dependency, in vast number of cases it is very efficient and reliable tool making it worth considering for the standard distance protection improvements.

The DTLR can also introduce much better transmission line utilization and increase of the transmission system efficiency, bringing additional profits for operators. It can also improve the system reliability and safety avoiding unnecessary relay operations.

REFERENCES

[1] WISZNIEWSKI A., UNGRAD H., WINKLER W., *Protection techniques in electrical energy systems*, New York 1995.

[2] REBIZANT W., SZAFRAN J., WISZNIEWSKI A., *Digital Signal Processing in Power System Protection and Control*, Springer Verlag, Series: Signals and Communication Technology, London 2011.

[3] SZAFRAN J., WISZNIEWSKI A., *Algorytmy pomiarowe i decyzyjne cyfrowej automatyki elektroenergetycznej*, 2001.

[4] HOROWITZ S.H., PHADKE A.G., *Third zone revisited*, IEEE Transactions on Power Delivery, Vol. 21, January 2006, pp. 23–29.

[5] YAMASHITA K., LI J., ZHANG P., LIU C.-C., *Analysis and Control of Major Blackout Events*, IEEE, 2009.
[6] *IEEE Standard for Calculating the Current-Temperature of Bare Overhead Conductors*, IEEE Std. 738-2006 (Revision of IEEE Std. 738-1993).
[7] SAMANMIT U., CHUSANAPIPUTT S., PUNGPRASERT V., *Increasing of Dynamic Thermal Rating of Transmission Line*, International Conference on Power System Technology, 1–4, 2006.
[8] SMITH S.W., *Digital signal processing: A practical guide for engineers and scientists*, 2003.

arc fault,
fault location,
signal processing

Mateusz PUSTUŁKA*, Jan IŻYKOWSKI*,
Mirosław ŁUKOWICZ*

LOCATION OF ARC FAULTS ON POWER TRANSMISSION LINES

This paper presents a fault location algorithm, which allows to determine the distance to a fault and fault resistance, as a result of considering natural fault loops. It is assumed that three-phase voltages and currents from both ends of the line measured asynchronously are the input signals of the fault locator. In case of the availability of synchronized measurements the elements associated with the determination of the synchronization angle should be omitted. In addition to natural fault loop signals also use of symmetrical components (positive and negative or incremental positive sequence components) to fault location were considered as well.

1. INTRODUCTION

The reliable operation of the electric power grid is one of the main goals of power system operators. Reduction of the duration of outages is one of the key requirements. There are many different ways that this goal can be achieved, with accurate fault location for an inspection-repair purpose [1]–[4] being one of them.

Algorithms for accurate location of faults on power lines have been a subject of great interest of researchers since the power system reliability became an important factor for network operators and customers [3]. Among the known methods, the approach based on an impedance principle is the most popular and most frequently implemented into protective relays or stand alone fault locators. In particular, the algorithms utilizing one-end current and voltage measurements have been introduced at the beginning [4]. Then two-end fault location principle [1]–[3] has been extensively explored. This principle is considered in the paper.

* Institute of Electrical Power Engineering, Wrocław University of Technology, Wrocław, Poland.

2. FAULT LOCATION ALGORITHM

Natural fault loops, identical as for a distance protection [2], are considered. For this purpose, the relaying signals (both voltage and current fault loop signals) are formed accordingly to the fault type. Table 1 defines those signals to any consideration of fault loops seen from the S end of the line for a single-circuit line (Fig. 1). Signals for fault loop seen from the R end are composed analogously.

In a case of phase-to-earth fault the voltage and current of a given faulted phase are taken, but the component associated with the zero-sequence component: zero-sequence current ($\underline{I}_{S0}$) multiplied by the factor: $k_0 = (\underline{Z}_{0L} - \underline{Z}_{1L})/\underline{Z}_{1L}$ is added to the phase current. This results from the fact that the impedances of the line for the positive sequence ($\underline{Z}_{1L}$) and zero sequence ($\underline{Z}_{0L}$) are not identical, and the impedance of the line section between the measuring point (S) and the fault point (F) for the positive sequence ($d\underline{Z}_{1L}$) is a measure of the distance to fault (d (p.u.)) – Fig. 1.

For a fault loop phase$_1$-to-phase$_2$, the differences of voltages and currents from the phases involved in the fault, respectively, are taken as the fault loop signals. As a result of the subtraction, the zero sequence component is eliminated and there is no compensation due to different line impedances for the positive and zero sequences.

Figure 1 shows the models of the considered fault loops (Fig. 1a, b) and the aggregated model (Fig. 1c).

Table 1. Composition of fault loop voltage and current signals for single-circuit line

Fault type	Fault loop voltage	Fault loop current
L1–E	$\underline{V}_{S\_L1}$	$\underline{I}_{S\_L1} + \underline{k}_0\underline{I}_{S0}$
L2–E	$\underline{V}_{S\_L2}$	$\underline{I}_{S\_L2} + \underline{k}_0\underline{I}_{S0}$
L3–E	$\underline{V}_{S\_L3}$	$\underline{I}_{S\_L3} + \underline{k}_0\underline{I}_{S0}$
L1–L2, L1–L2–E, (L1–L2–L3, L1–L2–L3–E)*	$\underline{V}_{S\_L1} - \underline{V}_{S\_L2}$	$\underline{I}_{S\_L1} - \underline{I}_{S\_L2}$
L2–L3, L2–L3–E	$\underline{V}_{S\_L2} - \underline{V}_{S\_L3}$	$\underline{I}_{S\_L2} - \underline{I}_{S\_L3}$
L3–L1, L3–L1–E	$\underline{V}_{S\_L3} - \underline{V}_{S\_L1}$	$\underline{I}_{S\_L3} - \underline{I}_{S\_L1}$
* – includes loop L1–L2, but also loops L2–L3, L3–L1 can be analyzed, $\underline{k}_0 = \dfrac{\underline{Z}_{0L} - \underline{Z}_{1L}}{\underline{Z}_{1L}}$.		

Fault loop seen from the S end (Fig. 1a) consists of a line section of the positive sequence impedance: $d\underline{Z}_{1L}$ and the transverse branch that represents a fault (resistance: R_{arc}). In case of the fault loop seen from the R end (Fig. 1b) impedance of the line section for the positive sequence is: $(1 - d)\underline{Z}_{1L}$ and the transverse branch is as in the previous fault loop (Fig. 1a).

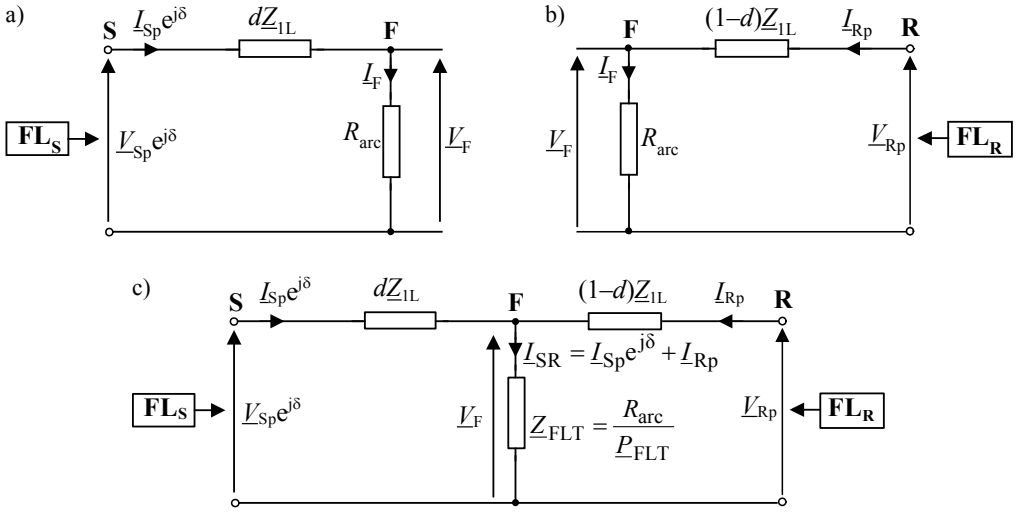

Fig. 1. Models of fault loop measurement for:
a) relay at bus S, b) relay at bus R, c) aggregated model

Use of unsynchronized measurements from both ends of the line is considered and the measurements from the R end (fault loop voltage and current: $\underline{V}_{Rp}$, $\underline{I}_{Rp}$) are assumed as a reference base. Therefore, the measurements from the S end (fault loop voltage and current: $\underline{V}_{Sp}$, $\underline{I}_{Sp}$) are synchronized analytically with use of the synchronization operator: $e^{j\delta}$, where δ – unknown synchronization angle. This is achieved by multiplying the phasors of the original fault loop signals of the bus S by this operator.

Aggregating both fault loop models from Fig. 1a and b leads to the model as shown in Fig. 1c [2]. There is a fictitious transverse branch, through which flows the total current ($\underline{I}_{Sp}\, e^{j\delta} + \underline{I}_{Rp}$) and not, as in reality: $\underline{I}_F$. Therefore, to provide the voltage in this branch: $\underline{V}_F$, as it is present in reality, the impedance of this fictitious branch ($\underline{Z}_{FLT}$) is not equal to the fault path resistance (R_{arc}). This impedance ($\underline{Z}_{FLT}$) matches the arc resistance (R_{arc}) divided by the complex factor: $\underline{P}_{FLT}$, which depends on the type of a fault (Table 2) [2].

Table 2. Coefficient $\underline{P}_{FLT}$ for different fault types

Fault type	$\underline{P}_{FLT}$
L1–E, L2–E, L3–E	$\frac{2\underline{Z}_{1L} + \underline{Z}_{0L}}{3\underline{Z}_{1L}}$
L1–L2, L2–L3, L3–L1	2
L1–L2–E, L2–L3–E, L3–L1–E, L1–L2–L3, L1–L2–L3–E	1

Comparison of voltage on the transverse branch, i.e. at the fault point (F) – determined from the S and R line ends (Fig. 1), respectively, yields:

$$\underline{V}_{\mathrm{Sp}}\mathrm{e}^{j\delta} - d\,\underline{Z}_{1\mathrm{L}}\,\underline{I}_{\mathrm{Sp}}\mathrm{e}^{j\delta} = \underline{V}_{\mathrm{Rp}} - (1-d)\underline{Z}_{1\mathrm{L}}\,\underline{I}_{\mathrm{Rp}} \tag{1}$$

Equation (1) can be written separately for the real and imaginary parts. This gives a system of two equations with two unknowns: d – fault distance (p.u.), δ – synchronization angle. It can be solved using very well-known numerical procedures. However, one may face problems with obtaining a correct solution. In fact, the unknowns are: d, $\sin(\delta)$, $\cos(\delta)$ while the synchronization angle δ can be positive or negative, i.e. in the following range: $-\pi <= \delta <= \pi$. Only one solution, out of two, is a correct one.

In order to avoid iterative calculations it is proposed to specify the modulus (absolute value) for the synchronization operator $\mathrm{e}^{j\delta}$ determined from (1) as follow:

$$\left|\mathrm{e}^{j\delta}\right| = \left|\frac{\underline{V}_{\mathrm{Rp}} - \underline{Z}_{1\mathrm{L}}\,\underline{I}_{\mathrm{Rp}} + d\,\underline{Z}_{1\mathrm{L}}\,\underline{I}_{\mathrm{Rp}}}{\underline{V}_{\mathrm{Sp}} - d\,\underline{Z}_{1\mathrm{L}}\,\underline{I}_{\mathrm{Sp}}}\right| \tag{2}$$

This gives:

$$\left|\underline{V}_{\mathrm{Rp}} - \underline{Z}_{1\mathrm{L}}\,\underline{I}_{\mathrm{Rp}} + d\,\underline{Z}_{1\mathrm{L}}\,\underline{I}_{\mathrm{Rp}}\right| = \left|\underline{V}_{\mathrm{Sp}} - d\,\underline{Z}_{1\mathrm{L}}\,\underline{I}_{\mathrm{Sp}}\right| \tag{3}$$

After tedious manipulations on (3) the following quadratic equation for the sought distance to fault is obtained:

$$A_2 d^2 + A_1 d + A_0 = 0 \tag{4}$$

where: A_2, A_1, A_0 – coefficients (real numbers) specified by the phasors of fault loop signals: ($\underline{V}_{\mathrm{Sp}}$, $\underline{I}_{\mathrm{Sp}}$) and ($\underline{V}_{\mathrm{Rp}}$, $\underline{I}_{\mathrm{Rp}}$), obtained with unsynchronized measurements at both ends of the line, and by the impedance of the line for the positive sequence ($\underline{Z}_{1\mathrm{L}}$), as follows:

$$A_2 = \left|\underline{Z}_{1\mathrm{L}}\,\underline{I}_{\mathrm{Sp}}\right|^2 - \left|\underline{Z}_{1\mathrm{L}}\,\underline{I}_{\mathrm{Rp}}\right|^2 \tag{5}$$

$$A_1 = -2\mathrm{real}[\underline{V}_{\mathrm{Sp}}(\underline{Z}_{1\mathrm{L}}\,\underline{I}_{\mathrm{Sp}})^* + (\underline{V}_{\mathrm{Rp}} - \underline{Z}_{1\mathrm{L}}\,\underline{I}_{\mathrm{Rp}})(\underline{Z}_{1\mathrm{L}}\,\underline{I}_{\mathrm{Rp}})^*] \tag{6}$$

$$A_0 = \left|\underline{V}_{\mathrm{Sp}}\right|^2 - \left|\underline{V}_{\mathrm{Rp}} - \underline{Z}_{1\mathrm{L}}\,\underline{I}_{\mathrm{Rp}}\right|^2 \tag{7}$$

where: $\underline{X}$* denotes conjugate of $\underline{X}$.

The solution of (4) gives two results for the sought fault distance (d_1, d_2). At least one of them indicates a detected fault in the line. If only one solution is such that it is satisfied: $0 < (d_1 \text{ or } d_2) < 1$, then in a natural way this solution is taken as the correct (valid). On the other hand, if it is obtained that the two solutions indicate a fault in the line: $0 < (d_1 \text{ and } d_2) < 1$, an additional selection of a solution that is correct has to be performed. Determination of the correct solution, which corresponds to the actual fault, can be determined by analyzing the estimated fault path resistance (in a general case it is obtained as the complex impedance). For the correct solution it should be very close to a pure resistance i.e. containing the smallest possible imaginary part.

As the input signals of the fault locator also symmetrical components of voltages and currents from both ends of the lines can be used:

- positive and negative – for asymmetrical faults,
- positive and incremental positive – for symmetrical three-phase faults.

In this case one needs replacing the fault loop signals in the derived equations (4)–(7) by the corresponding symmetrical components.

3. ARC FAULT LOCATION ANALYSIS

Fault location algorithm was performed using the signals generated by simulating arc faults [1] on the transmission line: 400 kV, 50 km with the aid of ATP-EMTP software. The representative results for the single-phase arc fault: *L*1–*E* are presented further.

Table 3 presents results when the fault loop signals are taken as the input signals, and Table 4 while positive and negative sequence components of voltages and currents from both ends of the line are applied. Both cases include the measurements acquired asynchronously – phasors of signals from the S end were software delayed by 15°, and thus the sought synchronization angle was $\delta = 15°$.

Standard full-cycle Fourier filtration was used as the basic in the considered location algorithms. It has been found that in some cases (rows in Table 3 marked with a shading), the applied filtering alone appears as insufficient due to a severe distortion of the processed signals. This is particularly in relation to the synchronization angle which is determined inaccurately. It was shown that performing the averaging of the results of the location in the fourth cycle after the fault, instead of averaging in the third cycle, significantly improves accuracy. Of course, this is possible only if the fault is not switched off earlier. An alternative approach to this is based on introducing

an additional pre-filtering, leaving the averaging within the 3rd cycle – as was assumed at the beginning of the study. Additional pre-filtration was used with half-cycle sine filter. It has been found that such extra pre-filtering contributes to a significant improvement of the fault location accuracy.

Selection of the correct solution out of the two obtained from the quadratic equation (4) was performed as follows: Table 3 – the correct solution is determined by taking the solution for which the estimated fault-path impedance has less imaginary part; Table 4 – only one of the solutions for the fault distance indicates a fault in the line and it is naturally assumed to be the correct solution.

Table 3. Arc location using fault loop signals

Accurate fault distance [km]	d_1 [km]	R_{arc1} [Ω]	δ_1 [°]	d_2 [km]	R_{arc2} [Ω]	δ_2 [°]	Error [%]
Full-cycle Fourier filtering Averaging within the third period after fault							
5.06	5.12	0.60 + 0.13i	17.41	6.30	0.59 + 0.22i	81.06	0.12
10.11	9.59	0.72 + 0.21i	–2.62	14.15	0.56 + 1.21i	137.50	1.04
17.52	17.36	0.96 + 0.25i	15.55	22.32	0.80 + 1.27i	139.63	0.32
22.22	22.12	0.69 + 0.18i	10.27	12.32	0.167 – 2.85i	–140.22	0.20
28.03	28.04	0.67 + 0.17i	16.66	31.68	0.71 + 0.90i	142.52	0.03
30.43	29.95	0.66 + 0.21i	–4.35	32.49	0.57 + 0.66i	113.53	0.95
35.59	35.65	1.60 + 0.39i	15.18	21.22	1.31 – 4.40i	–102.78	0.13
40.44	40.51	1.01 + 0.27i	16.38	27.96	1.23 – 3.85i	–105.03	0.14
45.75	45.74	0.36 + 0.08i	14.36	45.04	0.31 – 0.26i	–41.49	0.02
Full-cycle Fourier filtering Averaging within the fourth period after fault							
10.11	10.07	0.57 + 0.15i	14.87	13.63	0.59 + 0.91i	144.48	0.09
30.43	30.54	0.55 + 0.10i	21.38	31.98	0.56 + 0.30i	99.69	0.23
(Full-cycle Fourier filtering) + (Pre-filtration: sine half-period), Averaging within the third period after fault							
10.11	10.14	0.52 + 0.14i	17.19	13.57	0.59 + 0.87i	148.32	0.06
30.43	30.48	0.53 + 0.16i	12.69	32.14	0.49 + 0.38i	108.20	0.10

Table 4. Arc fault location using symmetrical component signals

Accurate fault distance [km]	Location for positive sequence		Location for negative sequence	
	d [km]	Error [%]	*d* [km]	Error [%]
5.06	4.86	3.88	5.15	1.76
10.11	9.94	1.68	9.80	3.11
17.52	17.40	0.69	17.16	2.03
22.22	22.16	0.25	22.14	0.38
28.03	28.04	0.03	28.04	0.02
30.43	30.48	0.17	30.24	0.64
35.59	35.88	0.81	34.78	2.27
40.44	40.71	0.67	40.32	0.30
45.75	45.85	0.23	46.17	0.91

Better accuracy was achieved by using fault loop signals and it is slightly better than the location with using of the measured data from one end of the line (Takagi algorithm [4]). This is the effect that in case of measurements at one end only (Takagi algorithm [4]), as a result of insufficient information there is a need for introducing simplifying assumptions.

4. CONCLUSION

Arc fault location on transmission lines with use of voltage and current measurements from both ends of the line acquired asynchronously has been considered. The derived algorithm applies the fault loop signals from the two ends of the line as the fault locator inputs. Quadratic equation for the sought distance to fault, whose coefficients are expressed in the most compact form, has been obtained. The selection of the correct solution (out of the two) is obtained by taking the solution for which the estimated impedance of the fault path has less imaginary part.

The derived algorithm can also be applied when symmetrical components of measured voltages and currents are applied as the locator input signals. One should then use: positive and negative sequence components for asymmetrical faults and positive and incremental positive sequence for three-phase symmetrical faults. For a correct solution there is a coincidence of the results obtained for two different components, which in practice means that they are very close to each other, while for the other solution (to be rejected) there are significant differences.

The results of the study indicate the important role of digital filtering of the processed signals that are severely distorted under arc faults. It is reasonable to take a direct result of the calculations or results averaged – as late as possible after fault incipience, but before its elimination. It has been shown that using the standard full-cycle Fourier filtering combined with the pre-filtering in the form of a half-cycle sine filter

improves considerably the accuracy of the calculation results. In particular, this relates to determining the synchronization angle.

Analyzed application of measurements from both sides of the line to fault location does not require introducing the simplifying assumptions, which are necessary if the location is performed with only the local measurements. As a result, better accuracy is obtained. Further improvement of fault location accuracy can be achieved by taking into account the distributed-parameter line model for lines of considerable length. Another means could be related to developing more effective filtering of distorted signals, and it seems that this task can be done with a well-designed neural network.

REFERENCES

[1] JOHNS A.T., AGGARWAL R.K., SONG Y.H., *Improved techniques for modelling fault arcs an faulted EHV transmission systems*, Generation, Transmission and Distribution, IEE Proceedings, Vol. 141 , No. 2, Mar. 1994, pp. 148–154.

[2] SAHA M.M., IŻYKOWSKI J., ROSOŁOWSKI E., *Fault Location on Power Networks*, Springer, London 2010.

[3] SAHA M.M., ROSOŁOWSKI E., IŻYKOWSKI J., *New Fault Location Method*, PACWorld, Vol. 21, September 2012.

[4] TAKAGI T., YAMAKOSHI Y., YAMAURA M., KONDOU R, MATSUSHIMA T., *Development of a new type fault locator using the one-terminal voltage and current data*, IEEE Trans. on Power Apparatus and Systems, Vol. 101, No. 8, Aug. 1982, pp. 2892–2898.